MODELING THE EFFECT OF CURING ON EARLY AGE DISTRESS POTENTIAL OF CONCRETE PAVEMENT

A Dissertation

by

MUHAMMAD EHSANUL BARI

Submitted to the Office of Graduate and Professional Studies of
Texas A&M University
in partial fulfillment of the requirements for the degree of

DOCTOR OF PHILOSOPHY

Chair of Committee,	Dan Zollinger
Committee Members,	Robert L. Lytton
	Dallas Little
	Thomas Wehrly
Head of Department,	Robin Autenrieth

May 2014

Major Subject: Civil Engineering

ABSTRACT

Understanding the early age behavior of concrete is an important issue in construction of concrete structures since different factors during construction, such as design consideration, material usage, and environmental influence, can alter the original configuration of the structure intended by the engineers and hence the structure may experience and exhibit undesired consequences. The primary interest of this research was to model the behavior of concrete under environmental excitations, such as the variation of temperature and relative humidity, during the early age after concrete placement. Experimental test results were obtained and mathematical models were developed for this research.

Modeling the effect of curing process in response to the relative humidity variation was one of the main objectives of this research. A mathematical model for back-calculating the diffusion coefficient of cured concrete from experimental test was proposed. This back-calculated diffusion coefficient of concrete was indicative of the effectiveness of curing application provided during construction. Corner deflection model for predicting lift-off displacement and climatic stress model for predicting crack formations were formulated in order to predict the distress behavior of concrete for a given design and construction scenario. Probabilistic models for lift-off displacement and cracking were formulated to predict the probabilities of such distresses. Material properties, such as strength, elastic modulus, creep, drying shrinkage, were obtained from experimental program and were used as input in these distress prediction models.

In order to assess the effectiveness of different curing compounds, two indices, such as curing index and overall curing index, were proposed. These indices were able to distinguish the difference in performance among different curing compounds. For validating the proposed corner lift-off displacement model and climatic stress model, numerical simulations were performed and the obtained results were compared with the field observations. The probabilistic models for predicting lift-off displacement and cracking behavior were validated by comparing the numerical simulation results with the field observations at Houston Intercontinental, TX. The predictions from these models were found to be in close agreement with the experimental observations. Furthermore, in order to assess the impact of a given design and construction, analytical study was performed with these models. In the sensitivity analysis, parameters of interest were the geometry of the structure, the effect of curing application, and the influence of time as well as the season of construction on the distress potentials. Numerical simulations indicated that the curing application was able to lower the early age distress potentials. The thicker slabs/overlays versus the thinner ones exhibited differences in performance in terms of distress potentials. The analytical study also revealed that it was possible to vary the distress potentials by varying the time as well as the season of construction. Finally, a constructability index was proposed in order to assist in decision making with regard to different designs and construction scenarios with a view to minimize the distress potentials in concrete structure. The results indicated that the constructability index was able to capture and demonstrate the effect of different parameters mentioned above on the constructability of rigid pavement/overlay projects.

DEDICATION

To

My Teachers

and

My Family Members

ACKNOWLEDGEMENTS

The completion of my doctoral program was not possible without the involvement of numerous individuals who supported, guided, and encouraged me to the completion of my studies for my Ph.D. Even though it is difficult to include everyone, because there were so many individuals who directly and indirectly helped me during these years, these acknowledgements attempt to express my gratitude and appreciation to those, who in some way, helped me complete this dissertation.

First, I would like to express gratitude to my committee chair, Dr. Dan Zollinger for all he has done for me, both as a supervisor and as a friend. I appreciate the role he played as a mentor by providing suggestions as well as guiding my research in the right direction. I thank him for his inspiration, encouragement, and continued support throughout the Ph.D. program. He also inspired me to higher levels of achievement and his role in my studies at Texas A&M University cannot be put into words.

I am grateful to my other committee members Dr. Robert Lytton, Dr. Dallas Little, and Dr. Thomas Wehrly for taking the time to be involved in my committee and I would like to thank them for providing valuable inputs and comments on my work. I am extremely grateful to Dr. Robert Lytton and I must express my sincere appreciation to him who always kept doors open for me and spent a significant amount of time and effort to improve my understanding of some fundamental modeling concepts utilized in this study.

I would like to thank Dr. Zachary Grasley for his time, suggestions and help for my research work. I would also like to extend my gratitude to Faisal Ahmed, Mohammad Akhteruzzaman, Mr. Laurence Oeth, Charles Gurganus, Ghassan Akrouch, Shailesh Chandra, Jose Rafael Menendez, Rocio Monge Zvietcovich, Dr. Calvin Woods, Mr. Timothy Chinn, Grover Allen, Steven Swindell, Mohsen Mahdavi, Marcus Rasulo, Sunny Goklani, Casey M. Cox, Chas Clift, Jacob Hoeffner, Harsh Jay Patel, Rebecca Cummins, Eric Ahart, and Sakib Ahmed for their help, support and inspiration during my Ph.D. program. Thanks to my friends and colleagues for the unforgettable precious moments and pleasant memories at Texas A&M University. Your company will be greatly missed.

Thank you to the Zachary Department of Civil Engineering, Texas A&M University for providing the financial support, facilities, and resources required during my doctoral program.

I would like to thank my students whose presence allowed me to proceed forward every single day during my graduate studies. The interactions during the classes, the brief conversations in the hallways, and the kind, polite, and friendly gestures from each of you will never be forgotten. The sweet memories and experiences that I have gathered while working with you as a graduate assistant teacher will always be remembered.

Thanks to my sisters and brothers-in-law for their constant care and support. Special thanks goes to my sisters, Ruwaida Bari, Rummana Bari, and Rozana Bari, who were always there for me whenever I needed them. I am deeply indebted to you for everything.

Last, but definitely not the least, I would like to express my deepest gratitude to my Dad, Professor Dr. M. Fazlul Bari and especially to my Mom, Professor Dr. Nilufar Sultana for their continuous support and love. Without your love, guidance, and never-ending support, this accomplishment would not have been possible.

TABLE OF CONTENTS

Page

ABSTRACT ii

DEDICATION iv

ACKNOWLEDGEMENTS v

TABLE OF CONTENTS viii

LIST OF FIGURES x

LIST OF TABLES xiv

1. INTRODUCTION 1

1.1 Background 1
1.2 Curing and Its Importance 2
1.3 Problem Statement 3
1.4 Importance and Motivation 6
1.5 Research Scope and Objectives 6
1.6 Organization of the Dissertation 8

2. LITERATURE REVIEW 10

2.1 Modeling Coefficient of Diffusion 10
2.2 Heat Transfer and Temperature Prediction of Concrete 15
2.2.1 Heat Generation Due to Hydration Reaction 15
2.2.2 Heat Conduction in Concrete 19
2.2.3 Heat Exchange at the Boundary of Concrete 20
2.2.4 Finite Difference Temperature Model 27
2.3 Moisture Transfer and Relative Humidity Prediction of Concrete 29
2.4 Temperature and Moisture Gradients in Concrete 33
2.5 Time Dependent Deformation of Concrete: Creep 36
2.5.1 Mechanism of Creep 36
2.5.2 Predictive Models for Creep 39
2.5.3 Rheological Model for Creep 43
2.5.4 Solidification Theory for Creep 45
2.6 Shrinkage in Concrete 47
2.6.1 Mechanism of Shrinkage 47
2.6.2 Predictive Models for Drying Shrinkage 49

2.7 Selection of Creep and Shrinkage Model 56
2.8 System Identification Method: A Solution Methodology 57

3. MODELING AND NUMERICAL IMPLEMENTATION 62

3.1 Early Age Diffusion of Concrete 62
3.1.1 Laboratory Testing Regime 62
3.1.2 Early Age Diffusion Coefficient of Cured Concrete 67
3.2 Modeling Lift-off Displacement Due to Curling and Warping 69
3.3 Modeling Climatic Stress in Concrete 75
3.3.1 Model for Thermal Strain 79
3.3.2 Hygrothermal Model for Drying Shrinkage 79
3.3.3 Model for Delayed Response (Creep) of Concrete 81
3.3.4 Scheme for Numerical Analysis 84
3.4 Probabilistic Model for Structural Failure 87

4. NUMERICAL SIMULATION RESULTS AND VALIDATION 91

4.1 Back-calculated Diffusion Coefficient of Concrete 92
4.1.1 Curing Index 97
4.2 Validation of the Lift-off Displacement Model 101
4.3 Validation of the Climatic Stress Model 110
4.4 Validation of the Probabilistic Models for Failure 115
4.4.1 Probability of Cracking 120
4.4.2 Probability of Lift-off or Debonding 124
4.5 Sensitivity Analysis 132
4.5.1 The Effect of Time of Construction or Placement 135
4.5.2 The Effect of Thickness 137
4.5.3 The Effect of Season of Construction 140
4.5.4 The Effect of Curing Compound 142
4.6 Constructability Index 145

5. CONCLUSION AND RECOMMENDATION 148

5.1 Summary and Conclusion 148
5.2 Recommendations for Further Study 154

REFERENCES 157

LIST OF FIGURES

		Page
Figure 2.1	Soil Suction Profile Due to Evaporation	12
Figure 2.2	Generalized Kelvin Model	44
Figure 2.3	Solidifying Material Subjected to Applied Stress at Time = t	46
Figure 2.4	Model Concept Diagram Showing Internal and External Material Models	52
Figure 2.5	GKM Diagram for the Material Component	55
Figure 2.6	Methods for System Identification Process	59
Figure 3.1	Curing Monitoring Device	64
Figure 3.2	Side View and Top View of the Mold with the Sealed and Filtered Chambers with Housing System	65
Figure 3.3	Test Setup in the Laboratory with the Mold and the Curing Plate	65
Figure 3.4	Entire Curing Monitoring System	66
Figure 3.5	Relative Humidity Information Collected using the Curing Monitoring System	66
Figure 3.6	Corner Lift-off Displacement Due to Curling and Warping	71
Figure 3.7	Components of Material Model for Aging Concrete	76
Figure 3.8	Model Concept Diagram Showing Internal and External Material Models	78
Figure 3.9	GKM Diagram for the Material Component	78
Figure 3.10	Stress and Strength as the Normally Distributed Variables	90
Figure 4.1	Research Implementation Framework	92

Page

Figure 4.2 Relative Humidity Data for Base Case 94

Figure 4.3 Back-calculated Diffusion Coefficient of Concrete for the Base Case 94

Figure 4.4 Relative Humidity Data for Concrete Cured with Curing Compound A 95

Figure 4.5 Back-calculated Diffusion Coefficient of Concrete with Curing Compound A 95

Figure 4.6 Relative Humidity Data for Concrete Cured with Curing Compound B 96

Figure 4.7 Back-calculated Diffusion Coefficient of Concrete with Curing Compound B 96

Figure 4.8 Calculated and the Two Extreme Diffusion Coefficients for the Base Case 99

Figure 4.9 Curing Indices for Different Curing Compounds 99

Figure 4.10 Overall Curing Indices for Different Specimens..... 100

Figure 4.11 Temperature Measurements across the Slab Thickness..... 103

Figure 4.12 Equivalent and Effective Equivalent Temperature Gradient 103

Figure 4.13 Drying Shrinkage Data and Calibrated Shrinkage Model..... 106

Figure 4.14 Evolution of Modulus of Elasticity 107

Figure 4.15 Observed Corner Lift-off Displacement and Model Predictions at Day 2 108

Figure 4.16 Observed Corner Lift-off Displacement and Model Predictions at Day 4 109

Figure 4.17 Predicted Displacement Profiles at Day 2..... 109

Figure 4.18 Predicted Displacement Profiles at Day 4..... 110

Page

Figure 4.19 Temperature Differential in Concrete Slab 112

Figure 4.20 Prediction of Time of Crack Initiation versus Experimental Observation 114

Figure 4.21 Ambient Temperature History Starting from 10 am, 28 February 2011 118

Figure 4.22 Ambient RH History Starting from 10 am, 28 February 2011..... 118

Figure 4.23 Temperature Difference between the Top and the Bottom of the Overlay Starting from 10 am, 28 February 2011 119

Figure 4.24 Humidity Difference between the Top and the Bottom of the Overlay Starting from 10 am, 28 February 2011 119

Figure 4.25 Typical Stress and Strength Evolution 121

Figure 4.26 Predicted and Observed Probability of Cracking at Different 28-Day Modulus of Rupture 123

Figure 4.27 Split Tensile Test for Measuring Split Tensile Strength 126

Figure 4.28 Split Tensile Test for Measuring Tensile Bond Strength 126

Figure 4.29 Predicted and Observed Probability of Lift-off for Various Split Tensile Bond Strength 131

Figure 4.30 Ambient Temperature History Starting from 24 February 2011..... 133

Figure 4.31 Ambient Relative Humidity History Starting from 24 February 2011 133

Figure 4.32 Ambient Temperature History Starting from 02 July 2011 134

Figure 4.33 Ambient Relative Humidity History Starting from 02 July 2011 134

Figure 4.34 The Effect of Time of Placement on Lift-off Potential..... 136

Figure 4.35 The Effect of Time of Placement on Cracking Potential 136

Page

Figure 4.36 The Effect of Slab Thickness and Time of Placement on Lift-off Potential 139

Figure 4.37 The Effect of Slab Thickness and Time of Placement on Cracking Potential 139

Figure 4.38 The Effect of Season of Construction on Lift-off Potential 141

Figure 4.39 The Effect of Season of Construction on Cracking Potential 141

Figure 4.40 Lift-off Potentials with Curing Compound during Spring 143

Figure 4.41 Cracking Potentials with Curing Compound during Spring 143

Figure 4.42 Lift-off Potentials with Curing Compound during Summer 144

Figure 4.43 Cracking Potentials with Curing Compound during Summer 144

Figure 4.44 Constructability Index for Project Constructed in Spring 146

Figure 4.45 Constructability Index for Project Constructed in Summer 147

LIST OF TABLES

		Page
Table 4.1	Concrete Properties and Pertinent Data	101
Table 4.2	Ambient Temperature, Relative Humidity, and Wind Speed	117
Table 4.3	Crack Survey Information for the Overlay Construction Project	123
Table 4.4	Compressive, Split Tensile, and Split Tensile Bond Strength Information.....	127
Table 4.5	Compressive, Split Tensile, and Split Tensile Bond Strength Information for the Overlay Construction Project	131
Table 4.6	Environmental Information for February and July	132

1. INTRODUCTION

1.1 Background

Concrete is one of the most widely used construction materials for constructing highways, roadways, intersections, airstrips, parking lots and more. It is suitable for any region and climatic conditions ranging from scorching summer to freezing winter. It provides durable and sustainable pavement surfaces with the best ride quality and offers an extended service life with the lowest life-cycle cost of all alternatives. Considering its performance and related cost, concrete has become a popular construction material for building new pavements as well as for rehabilitating and resurfacing old pavements (PCA 2013).

Environmental conditions during construction are important considerations as those influence the temperature and the relative humidity distributions within concrete affecting the strength and stress development as well as the structural deformation characteristics of slab. Rapid change in temperature relative to the strength gain of concrete can lead to thermal cracking. A dry environment during construction can accelerate the evaporation of water from concrete resulting in drying shrinkage which is defined as the strain induced by loss of water (Mindess et al. 2003). Drying shrinkage can lead to the development of tensile stress and subsequent cracking due to the restraint of shrinkage (Grasley et al. 2006). Rapid surface drying can increase the potential for other distress types such as delamination, a mode of failure which causes separation within the concrete or an overlay from the underlying layer (Czubak 2011).

Early age distresses, such as crack formation and lift-off displacement, observed in concrete pavement and overlay impact the long-term performance. Pavements with cracks and lift-off displacement are more vulnerable to external exposures and are more prone to degradation due to wheel load application. With repetitive application of environmental and wheel loads, cracks can extend and connect with other cracks resulting in a deteriorated structure. Tensile, shear, and frictional stresses can develop across the cracked portion of the slab with load applications and can exhibit distresses like spalling. The problem is mainly to do with the loss of structural integrity and ride quality due to spalled joints. Also, early age damage can shorten the fatigue life which is a function of the conditions at the time of construction. If proper measures are taken, the distress potential during the early age can significantly be minimized leading to an extended service life of pavement structure. Curing, an element of the construction process, can help to minimize a portion of the strain and stress development as well as can assist in gaining the desired strength during the early phase of construction. The importance of curing and its effect during the construction phase are discussed in the following section.

1.2 Curing and Its Importance

Providing proper curing is a requirement for concrete to develop optimum properties (Mindess et al. 2003). Curing helps to control the moisture loss from hydrating concrete controlling indirectly the amount of drying shrinkage. Curing also aids in maintaining satisfactory moisture content and temperature for a period of time after placing and

finishing the concrete; this satisfactory ambience within the pavement supports the development of the desired properties of concrete (PCA 2013). Insufficient curing can weaken the surface concrete enough to disrupt the proper strength gain and can make it vulnerable to early cracking damage and spalling under applied loading cycles.

When concrete is exposed to a dry environment, capillary pore water evaporates near the surface. Excessive evaporation can increase the permeability of the surface by five to ten fold (Powers 1947) and can result in undesirable cracking, delamination, debonding, and loss of strength (Ye et al. 2009; Walker and Bloem 1957). Curing minimizes the evaporation from the surface of concrete, assists in continued hydration and strength gain, and helps in minimizing the stress development at an early age. Curing is a way to minimize porosity and volume change in the surface of concrete. For maintaining the impermeability of the pavement surface, curing is considered to be an integral component of the construction process (Powers 1947; PCA 2013; Mindess and Young 1981, 2003; Neville 1996; Rasheeduzzafar and Al-Saadoun 1989; Taus et al. 2008).

1.3 Problem Statement

The early age distress potentials, if great enough, can be detrimental to the long-term performance of a concrete pavement. It is not possible to completely eliminate the early age damage due to such effects as inherent variability involved in the construction process as well as the interaction of various factors affected by the nature of the design. For example, one can achieve higher concrete strength by lowering the water-cement

(w/c) ratio but is expected to have higher shrinkage strain and greater potential for early age cracking. On the contrary, this potential can be lowered by increasing the w/c ratio but such measures may result in lower strength as a result. The objective during construction should be to minimize the distress potentials as much as possible through implementing proper curing management.

Proper curing management is an essential and feasible measure which can minimize the early age distress potential during construction. Curing helps to keep the environmental stresses below the tensile strength of concrete and assists in minimizing the volume instability of concrete after placement. It is, therefore, important to model the effect of curing and incorporate it in the design analysis for analyzing the outcome of the proposed design scenario.

The process of curing can be modeled as a diffusion process and the quality of curing application can be manifested in the diffusion coefficient of concrete which is a parameter in the diffusion equation. The lower the value of this parameter is the better the quality of curing application is. Such a model can further help to distinguish and rank the effectiveness of the different curing compounds available for construction.

After placing concrete, heat transfer and moisture diffusion take place in concrete depending on the ambient environmental conditions. The moisture diffusion and heat transfer process instigate the development of moisture and temperature gradients within the pavement. These gradients induce temperature and shrinkage strains that are responsible for different distresses. Since curing acts as an insulating barrier inhibiting the evaporation from concrete, it affects the moisture diffusion taking place at concrete

surface and has an influence on the drying shrinkage. Hence, it is necessary to model the influence of curing application on the moisture diffusion process taking place during construction.

As thermal dilation and drying shrinkage take place, tensile stress develops within the pavement depending on the restraint condition. In response to this tensile stress, the structure also undergo time dependent deformation called tensile creep. Tensile creep is, however, beneficial for the concrete structure as it relieves portion of the induced tensile stress due to shrinkage (D'Ambrosia 2011). Depending on the magnitude of the net tensile stress, the pavement can exhibit cracking depending on the restraint condition and/ or can debond or delaminate from the underlying layer depending on the bonding condition.

This research focuses on developing a framework to incorporate the curing process in the design analysis, to compare the effectiveness of different curing compounds, to model the effect of curing application on the moisture diffusion process, to model the cracking and lift-off displacement behavior of the slab due to induced strain composed of thermal strain, shrinkage strain, and creep strain, and finally to predict the probability of distress potentials, such as cracking and lift-off displacement or debonding, for a given design and construction scenario. The framework proposed and developed in this research can assist in decision-making process through assessing the proposed design and construction scenario and can contribute to improving the performance as well as extending the service life of concrete pavements and overlays.

1.4 Importance and Motivation

Concrete pavement is usually cured by spraying curing compound on the surface after placement. The curing compound acts as a barrier coating limiting the evaporation of the mix water from the exposed concrete (Al-Gahtani 2010). There are different curing compounds available on the market for use during pavement construction. For better pavement construction management, it is necessary to distinguish and rank these curing compounds based on their performance and effectiveness which will dictate their use and application. A mathematical model capable of distinguishing the degree of effectiveness of various curing compounds and modeling the corresponding influence on the moisture diffusion process would be an essential tool to a design and construction manager. Furthermore, modeling the linkage between the induced stress due to environmental excitations and the potential for lift-off displacement and cracking would be necessary for evaluating a given design and construction scenario. The need for such a methodology for assisting the design engineers and construction managers during the design and construction phase was the motivation for this research.

1.5 Research Scope and Objectives

This research, at first, focused on modeling the time dependent diffusion coefficient of concrete which is reflective of the quality of curing application provided during construction. To predict the development of temperature and moisture gradients in concrete after placement, finite difference temperature and moisture models were formulated. The modeled diffusion coefficient of cured concrete was incorporated in the

finite difference moisture model to reflect the effect of curing on the moisture diffusion process taking place during the construction phase. The development of thermal strain, drying shrinkage, and creep strain in response to these gradients were taken into consideration, and the corresponding lift-off displacement and cracking behavior of concrete were modeled. The parameters of these models were calibrated with the experimental test results and the model predictions were validated with the experimental observations. The potential for lift-off displacement and cracking were also formulated and these probabilistic models were further validated with the information obtained from an overlay construction project at Houston Intercontinental, TX.

The main objectives of this research are summarized below:

(i) to formulate a mathematical model for back-calculating the diffusion coefficient concrete which is reflective of the effect of curing application and to incorporate the time dependent diffusion coefficient of cured concrete in a finite difference model for predicting moisture distribution within the pavement;

(ii) to develop an index in order to differentiate the performance of different curing compounds;

(iii) to formulate a model for predicting the slab corner lift-off displacement due to the nonlinear temperature and moisture gradients within the pavement;

(iv) to formulate a model for predicting the cracking behavior of concrete under restrained condition due to the nonlinear temperature and moisture gradients within the pavement;

(v) to propose probabilistic models for predicting the potentials for lift-off displacement as well as cracking of the pavement for a given design and construction scenario; and

(vi) to propose an index for assessing the constructability of a pavement or overlay construction project for a given design and construction scenario.

The goal of this research was to develop and combine the above mentioned components into a decision making framework and to demonstrate how such information can be used in decision-making for assessing a given design and construction scenario.

1.6 Organization of the Dissertation

This dissertation has been divided into five sections. Section 1 includes an introduction to the research, curing and its importance, problem statement, importance and motivation of the research, research scope and objectives, and organization of the dissertation. Section 2 provides a literature review of the important concepts and elements required for this research. It includes a review for modeling coefficient of diffusion, heat transfer and temperature prediction of concrete, moisture transfer and relative humidity prediction of concrete, temperature and moisture gradients in concrete, time dependent deformation of concrete or creep, shrinkage of concrete, and system identification method. In Section 3, formulations of the different models have been described and discussed, such as modeling diffusion coefficient of concrete, modeling corner lift-off displacement due to curling and warping, modeling climatic stress in

concrete, and modeling probability of pavement or overlay failure. Section 4 contains the numerical simulation results obtained from the models discussed in Section 3. The simulation results and the experimental results were compared to validate the proposed models. With the validated models, sensitivity analysis was further conducted to provide insight regarding the constructability of concrete pavement and overlay projects. Finally, an index known as "constructability index" was proposed to assist in decision making for comparing different design and construction scenarios. Section 5 contains a brief summary as well as the conclusions of this research. A direction of future research was also suggested in this section.

2. LITERATURE REVIEW

In Section 1, several objectives associated with this research were identified. To address those objectives, several interrelated concepts were discussed to ensure the effective and efficient achievement of those objectives. The main focus of the literature review was to examine and discuss: (i) modeling approaches for diffusion coefficient, (ii) heat and moisture prediction schemes in concrete, (iii) modeling approach of internal temperature and moisture gradients in concrete pavement, (iv) time dependent deformation or creep in concrete, (v) drying shrinkage in concrete, and (vi) a numerical approach called system identification method for solving diffusion coefficient of concrete.

2.1 Modeling Coefficient of Diffusion

Mitchel (1979) derived a closed form solution for moisture diffusion of a soil body subjected to evaporation at the surface. The solution of the moisture diffusion equation described the suction distribution throughout the soil body as a function of time and space. He solved the diffusion equation using the Laplace transform method for known boundary conditions. This soil evaporation situation was similar to that of concrete pavement subjected to external drying and the solution was applicable for concrete subjected to evaporation at surface.

A brief description of the formulation and solution to the moisture diffusion problem solved by Mitchell is given below. This formulation is based on the assumption that a soil body is initially at a suction U_e and is subjected to atmospheric suction of U_a

at the surface. If the diffusion coefficient of the soil is assumed to be α, then the diffusion equation defining the movement of moisture through the unsaturated soil can be stated according to Equation 2.1 which is subjected to the boundary conditions given in Equations 2.2 through 2.4.

$$\frac{\partial u}{\partial t} = \alpha \frac{\partial^2 u}{\partial x^2} \tag{2.1}$$

boundary conditions:

$$u(y,0) = U_e \tag{2.2}$$

$$u(y,t) \rightarrow U_e \; as \; y \rightarrow \infty \tag{2.3}$$

$$\frac{\partial u(0,\mathrm{t})}{\partial y} = h\{u(0,\mathrm{t}) - U_a\} \tag{2.4}$$

where,

$y = depth \, along \, the \, sample \; from \, soil \, surface$

$h = evaporation \, constant$

$u(\mathrm{y},\mathrm{t}) = soil \, suction \, at \, depth \; y \; and \; time \; t$

He used a Laplace transformation to develop the closed form solution shown in Equation 2.5. The diffusion coefficient of soil calculated by Mitchel (1979) for a soil body subjected to evaporation is shown in Figure 2.1. This solution is applicable for concrete pavement subjected to evaporation and hence this solution was used in this

research to back-calculate the time dependent diffusion coefficient of cured concrete samples. The back-calculated diffusion coefficient of concrete was reflective of the effectiveness of curing provided during construction.

$$u(\mathrm{y},\mathrm{t}) = U_e + (U_a - U_e)\,erfc\left(\frac{y}{2\sqrt{\alpha t}}\right) - (U_a - U_e)\exp\left(hy + h^2\alpha t\right)erfc\left(\frac{y}{2\sqrt{\alpha t}} + \mathrm{h}\sqrt{\alpha t}\right) \tag{2.5}$$

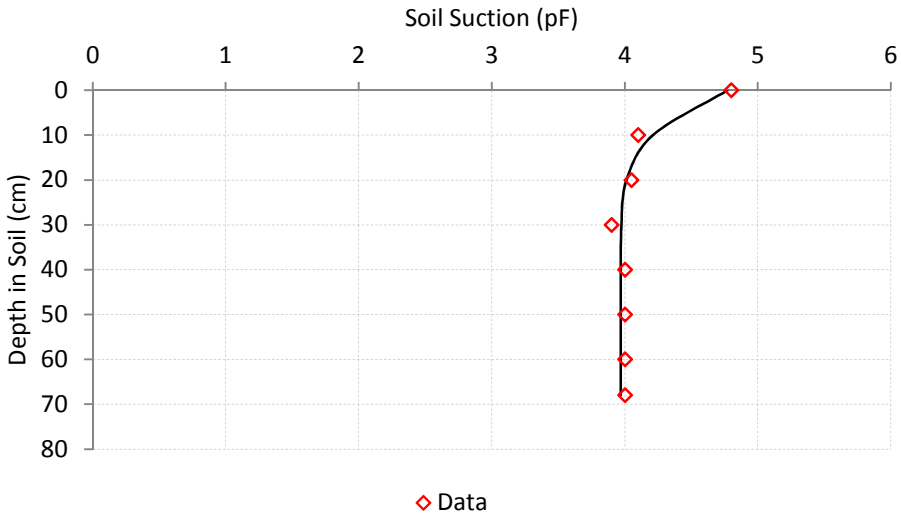

Figure 2.1: Soil Suction Profile Due to Evaporation

Goldstein (1932) provided a closed form solution to heat conduction problem in slab. The solution he provided can also be used for back-calculating the diffusion coefficient of cured concrete subjected to evaporation provided the variables for temperature and thermal conductivity were changed to moisture and moisture diffusivity, respectively. The solution to the heat conduction problem provided by Goldstein is discussed below.

Assuming a slab of thickness of 2ℓ is initially at a constant temperature and the slab is placed in a medium at a lower temperature. Without loss in generality, the heat conduction problem can be simplified by taking the initial slab temperature as unity and the medium temperature as zero (Berger 1931). If the temperature is denoted as θ, α as the thermal conductivity, h as the relative emissivity, t as the time, and z as the distance perpendicular to the face of the slab measured from the middle of the slab, then the differential equation describing the heat conduction in the slab can be expressed as shown in Equation 2.6 which is subjected to the boundary conditions expressed in Equations 2.7 through 2.9.

$$\frac{\partial \theta}{\partial t} = \alpha \frac{\partial^2 \theta}{\partial z^2} \tag{2.6}$$

boundary conditions:

$$\theta = 1 \ when \ t = 0 \tag{2.7}$$

$$\frac{\partial \theta}{\partial z} + h\theta = 0 \ when \ z = \ell \tag{2.8}$$

$$\frac{\partial \theta}{\partial z} + h\theta = 0 \ when \ z = -\ell \tag{2.9}$$

The closed form solution to Equation 2.6 obtained by Goldstein is shown in Equation 2.10.

$$\begin{aligned} \theta = 1 - &\left\{1 - erf\,\frac{\ell - z}{2\sqrt{\alpha t}} - \exp\left(h^2\alpha t + h\overline{\ell - z}\right)\left[1 - erf\left(\frac{\ell - z}{2\sqrt{\alpha t}} + h\sqrt{\alpha t}\right)\right]\right\} \\ &- \left\{1 - erf\,\frac{\ell + z}{2\sqrt{\alpha t}} - \exp\left(h^2\alpha t + h\overline{\ell + z}\right)\left[1 - erf\left(\frac{\ell + z}{2\sqrt{\alpha t}} + h\sqrt{\alpha t}\right)\right]\right\} \end{aligned} \tag{2.10}$$

By changing the temperature and thermal conductivity to moisture and moisture diffusivity, this solution can be modified to back-calculate the diffusion coefficient of cured concrete subjected to evaporation at the surface. As this solution is applicable for a slab exposed to radiation at both faces, the closed form solution can be modified for the case where evaporation is taking place only at one face of the pavement by obtaining the solution for the upper half of the slab, i.e. z ranging from the center to the face of the slab. Therefore, either Equation 2.5 or 2.10 can be used to back-calculate the diffusion coefficient of cured concrete. Because of its simple and easier expression, Equation 2.5 was used in the back-calculation procedure for this research.

2.2 Heat Transfer and Temperature Prediction of Concrete

The prediction of temperature in concrete requires taking into account the heat generation and heat transfer that takes place during the hydration reaction of concrete. The heat generation and heat transfer involve a number of interrelated mechanisms and these interrelated steps need to be modeled for accurate prediction of temperature of the concrete during the hydration reactions and the corresponding predictions can be obtained iteratively (Riding et al. 2007). Modeling the heat transfer and heat generation in concrete can be divided into three components: (i) heat generation due to hydration reaction, (ii) heat conduction within the body of concrete, and (iii) heat exchange with the environment occurring at the boundary of the concrete structure.

2.2.1 Heat Generation Due to Hydration Reaction

Within the body of available literature by authors, such as Schinder (2004) and van Breugel (1998), there is a description of available methods to model the heat generation by cement hydration. The most commonly used method combines the equivalent age maturity method and an exponential degree of hydration curve to characterize the rate of heat generation by hydration. Freieslenben Hansen and Pedersen (1977) developed the equivalent age maturity concept for concrete hydration as shown in Equation 2.11 which is also referred to as Arrhenious equation as it depends on the Arrhenius rate concept. This equation converts the real time concrete curing age to an equivalent age of concrete that is cured at any temperature (Schindler et al. 2002, Emborg 1989).

$$t_e(T_r) = \sum_0^t \exp\left(\frac{E}{R}\left(\frac{1}{273+T_r} - \frac{1}{273+T_c}\right)\right) \cdot \Delta t \tag{2.11}$$

where,

$T_r = reference\,temperature\,(°C)$

$T_c = average\,concrete\,temperature\,during\,time\,interval\,\Delta t\,(°C)$

$t_e(T_r) = equivalent\,age\,at\,the\,reference\,curing\,temperature\,(hours\,or\,days)$

$E = activation\,energy\,(J/mol)$

$R = universal\,gas\,constant\,(8.3144\,J/mol/°C)$

Freieslenben Hansen and Pedersen (1985) further described the relationship between degree of hydration and equivalent age with an exponential function. The model for degree of hydration as a function of equivalent age t_e is shown in Equation 2.12.

$$\alpha(t_e) = \alpha_u \cdot \exp\left(-\left[\frac{\tau}{t_e}\right]^{\beta}\right) \tag{2.12a}$$

$$\alpha_u = \frac{1.031 \cdot w/cm}{0.194 + w/cm} + 0.50\,p_{FA} + 0.30\,p_{SLAG} \le 1.0 \tag{2.12b}$$

$$\tau = 66.78 \cdot p_{C_3A}{}^{-0.154} \cdot p_{C_3S}{}^{-0.401} \cdot Blaine^{-0.804} \cdot p_{SO_3}{}^{-0.758} \cdot \exp\left(2.187 \cdot p_{SLAG} + 9.5 \cdot p_{FA} \cdot p_{FA-CaO}\right) \tag{2.12c}$$

$$\beta = 181.4 \cdot p_{C_3A}{}^{0.146} \cdot p_{C_3S}{}^{0.227} \cdot Blaine^{-0.535} \cdot p_{SO_3}{}^{0.558} \cdot \exp\left(-0.647 \cdot p_{SO_3}\right) \tag{2.12d}$$

where,

$t_e = equivalent\ age\ at\ reference\ temperature$ (hrs)

$\alpha(t_e) = degree\ of\ hydration\ at\ equivalent\ age, t_e$

$\alpha_u = ultimate\ degree\ of\ hydration$

$\tau = hydration\ time\ parameter$ (hrs)

$\beta = hydration\ shape\ parameter$

$w/cm = water - cementitious\ material\ ratio$

$p_{C_3A} = weight\ ratio\ of\ tricalcium\ aluminate\ to\ total\ cement\ content$

$p_{C_3S} = weight\ ratio\ of\ tricalcium\ silicate\ to\ total\ cement\ content$

$p_{SO_3} = sulfate\ weight\ ratio\ to\ total\ cement\ content$

$Blaine = Blain\ value, specific\ surface\ area\ of\ cement$ (m^2/kg)

Once the degree of hydration and equivalent age are obtained, the rate of heat generation at time *t* during hydration reaction can be defined as shown in Equation 2.13.

$$Q_h(t) = H_u \cdot C_c \cdot \left(\frac{\tau}{t_e}\right)^{\beta} \cdot \left(\frac{\beta}{t_e}\right) \cdot \alpha(t) \cdot \frac{E}{R}\left(\frac{1}{273+T_r} - \frac{1}{273+T_c}\right) \qquad (2.13)$$

where,

$Q_h(t_e) = rate\ of\ heat\ liberation\ at\ equivalent\ age, t_e\ (J/h/m^3)$

$H_u = total\ heat\ of\ hydration\ of\ cementitious\ materials$

$at\ 100\ percent\ hydration\ (J/kg)$

$C_c = cementitious\ materials\ content\ (kg/m^3)$

$T_r = reference\ PCC\ temperature\ (°C)$

$T_c = nodal\ PCC\ temperature\ (°C)$

The ultimate heat development H_u in Equation 2.13 can be estimated from the cement chemistry (Bouge 1947) and the composition of the mineral admixtures (Kishi and Maekawa 1995). The ultimate heat development is defined according to Equation 2.14.

$$H_u = H_{cem} \cdot p_{cem} + 461 \cdot p_{SLAG} + h_{FA} \cdot p_{FA} \tag{2.14}$$

where,

$H_{cem} = ultimate\ heat\ of\ hydration\ of\ the\ cement\ (J/g)$

$p_{cem} = cement\ mass\ ratio\ to\ total\ cementitious\ content$

$p_{SLAG} = slag\ mass\ ratio\ to\ total\ cementitious\ content$

$p_{FA} = fly\ ash\ mass\ ratio\ to\ total\ cementitious\ content, and$

$h_{FA} = heat\ of\ hydration\ of\ fly\ ash\ (J/kg)$

The maximum heat of hydration of cement H_{cem} in Equation 2.14 can be estimated by multiplying the percentage mass of each constituent with the respective heat of hydration as shown in Equation 2.15.

$$H_{cem} = \sum h_i \cdot p_i \tag{2.15}$$

where,

$H_{cem} = ultimate\ heat\ of\ hydration\ of\ the\ cement\ (J/g)$

$h_i = heat\ of\ hydration\ of\ individual\ i^{th}\ component\ (J/g)$, and

$p_i = mass\ ratio\ of\ i^{th}\ component\ to\ total\ cement\ content$

Equation 2.15 can further be elaborated as follows:

$$H_{cem} = 500 \cdot p_{C_3S} + 260 \cdot p_{C_2S} + 866 \cdot p_{C_3A} + 420 \cdot p_{C_4AF} + 624 \cdot p_{SO_3} + 1186 \cdot p_{FreeCaO} + 850 \cdot p_{MgO} \quad (2.16)$$

A detailed description of the heat generation model can be found elsewhere (Schindler et al. 2002; Ruiz et al. 2005; Schinder 2004).

2.2.2 Heat Conduction in Concrete

Thermal conduction is defined as the transfer of heat within a material from points of higher temperature to points of lower temperature. Thermal conduction in concrete is dependent of its moisture content, density, specific heat, and thermal conductivity. On the other hand, thermal conductivity is a material property that describes its ability to transfer heat between points in contact and is defined as the ratio of the rate of heat flow to the temperature gradient. It is an important property as it determines the rate of heat penetration into the material (Scaulon and McDonald 1994; Mindess and Young 1981; Janna 2000; Ruiz et al. 2005; Schindler et al. 2002; Riding et al. 2007). Both the thermal conductivity and specific heat of concrete are function of mixture proportions, composition, aggregate type, temperature, and degree of hydration of concrete (van Breugel 1998; Ruiz et al. 2005).

The average thermal conductivity of maturing concrete is higher than the hardened concrete and the experimental results indicated that the average thermal

conductivity of maturing concrete was 33 percent higher than the hardened concrete (Khan et al. 1995). Similar observation was reported by others, which showed a 21 percent reduction in conductivity from maturing state to hardened state (De Schutter and Taerwe 1995). In High PERformance PAVing (HIPEPAV®) II software program, a linear decline in thermal conductivity of concrete was assumed with the logarithm of time and the adopted relationship between the initial and the final thermal conductivity of concrete is shown in Equation 2.17 (Ruiz et al. 2005).

$$k_i = k_\infty \left(1.33 - 0.33 \cdot \alpha\right) \tag{2.17}$$

where,

$k_i = current\ thermal\ conductivity\ of\ the\ concrete\ (W / \mathrm{m} / ^\circ\mathrm{C})$

$k_\infty = thermal\ conductivity\ of\ mature\ concrete\ (W / \mathrm{m} / ^\circ\mathrm{C})$

$\alpha = degree\ of\ hydration$

2.2.3 Heat Exchange at the Boundary of Concrete

2.2.3.1 Convection

Convection is the mechanism of heat transfer between a surface such as concrete and the surrounding environment and this mechanism of heat transfer is affected by wind and evaporation. Convection can be forced or free depending on the wind speed next to the concrete surface. The rate of heat flow from the surface depends on the temperature difference, wind speed, and texture of the surface (Ruiz et al. 2005). Convective heat

transfer from concrete slab is governed by Newton's law of cooling as shown in Equation 2.18 (Incropera and Dewitt 2002).

$$q_c = h_c \left(T_S - T_\infty \right) \tag{2.18}$$

where,

$q_c = convection\, heat\ flux\, (W / \mathrm{m}^2)$

$h_c = convection\, coefficient\, (W / \mathrm{m}^2 / °C)$

$T_S = surface\, temperature\, (°C)$

$T_\infty = \ fluid\, temperature\, (°C)$

The fluid temperature T_∞ in Equation 2.18 can be approximated as the ambient temperature, T_a in degree Celsius (Riding et al. 2007). The expression for convection coefficient due to forced and free convection is shown in Equation 2.19 as follows (ASHRAE 1993).

$$h_c = 3.727 \cdot \mathrm{C} \cdot \left[0.9 \cdot \left(T_S + T_a \right) + 32 \right]^{-0.181} \cdot \left| T_S - T_a \right|^{0.266} \cdot \sqrt{1 + 2.857 \cdot w} \tag{2.19}$$

where,

$h_c = convection\ coefficient\ (W / m^2 / °C)$

$C = constant\ depending\ on\ the\ shape\ and\ heat\ flow\ condition$

$= 1.79\ for\ horizontal\ plates\ warmer\ than\ air$

$= 0.89\ for\ horizontal\ plates\ cooler\ than\ air$

$T_S = surface\ temperature\ (°C)$

$T_a = air\ temperature\ (°C)$

$w = wind\ speed\ (m/s)$

2.2.3.2 Solar Radiation

Solar radiation at the entrance of the earth atmosphere is called extraterrestrial radiation. Solar absorption is the absorbed flux by a pavement surface due to incoming sunrays and it causes the surface to be heated more than the interior. As a result temperature gradient develops across the slab thickness (Hsieh et al. 1989). Several factors influencing solar radiation absorption are the time of the day or year, latitude, and cloud cover, etc. (Thepchatri et al. 1977; Chapman 1982; Branco et al. 1992). Surface horizontal solar radiation depends on the extraterrestrial horizontal solar radiation which in turn depends on the day of a year, local latitude, declination, and hour angle (Radosavljević and Đorđević 2001).

The computation of solar radiation requires the determination of hour angle that involves several steps (Honsberg and Bowden 2013). The equation for Local Standard Time Meridian (LSTM), a reference meridian used for a particular time zone, can be expressed as follow:

$$LSTM = 15° \times \Delta T_{GMT} \tag{2.20}$$

where ΔT_{GMT} is the difference between the Local Time *LT* and Greenwich Mean Time *GMT* in hour. The Equation of Time *EoT* in minutes, an empirical equation that corrects for the eccentricity of the orbit and the axial tilt of earth, can be computed as follows:

$$EoT = 9.87 \cdot \sin\left(2 \cdot \frac{360}{365} \cdot (d - 81)\right) - 7.53 \cdot \cos\left(2 \cdot \frac{360}{365} \cdot (d - 81)\right) - 1.5 \cdot \sin\left(2 \cdot \frac{360}{365} \cdot (d - 81)\right) \tag{2.21}$$

where *d* is the number of days since the start of the year. After obtaining *LSTM* and *EoT*, Local Solar Time *LST* can be computed as per Equation 2.22.

$$LST = LT + \frac{\left(4 \cdot (Longitude - LSTM) + EoT\right)}{60} \tag{2.22}$$

Then the parameter of interest is the Hour Angle *HRA* that converts the *LST* into the number of degrees the sun moves across the sky and *HRA* can be computed according to Equation 2.23.

$$HRA = 15° \times (LST - 12) \tag{2.23}$$

Once the value of *HRA* is obtained, the energy of extraterrestrial radiation on horizontal surface for a particular day in a year can be calculated as follows (Radosavljević and Đorđević 2001):

$$I_{oH} = I_{SC}\left[1 + 0.033 \cdot \cos\left(\frac{360 \cdot n}{365}\right)\right] \cdot \left(\sin L \cdot \sin \delta + \cos L \cdot \cos \delta \cdot \cos\left(HRA\right)\right) \quad (2.24)$$

where,

$I_{oH} = extraterrestrial\ radiation\ on\ horizontal\ surface\ (W / \mathrm{m}^2)$

$I_{SC} = solar\ constant = 1352 \pm 21 (W / \mathrm{m}^2)$

$n = a\ day\ in\ a\ year \left(1 \le n \le 365\right)$

$L = local\ latitude$

$\delta = declination\ in\ degrees = 23.45 \times \left(\frac{360}{365}\left(284 + n\right)\right)$

Finally, the surface horizontal solar radiation can be further updated by considering cloud cover *C* as shown in Equation 2.25:

$$q_s = \left(0.91 - 0.7 \times C\right) \times I_{oH} \quad (2.25)$$

where q_s is the surface horizontal solar radiation in (W/m^2).

2.2.3.3 Atmospheric Radiation

Objects or matters that are at a temperature greater than zero degrees Kalvin emit radiation. The gases that are at a higher temperature in the atmosphere also emits radiation though electromagnetic waves causing heat transfer. The heat transfer from the gas particles follow the Stefan-Boltzmann law as shown in Equation 2.26 (Riding et al. 2007, Ruiz et al. 2005).

$$q_a = \sigma \varepsilon_a \left(T_a\right)^4 \tag{2.26}$$

where,

$q_a = heat\ flux\ from the\ air\ (W / \mathrm{m}^2)$

$\varepsilon_a = emissivity\ of\ the\ air$

$T_a = air\ temperature\ (K)$

The emissivity ε_a in Equation 2.26 is a function of atmospheric water vapor pressure, temperature, and cloud cover fraction and can be modeled according to Equation 2.27 (Wojcik 2004; Brutsaert 1975).

$$\varepsilon_a = C + 1.24(1-C) \times \left(\frac{e_a}{T_a}\right)^{\frac{1}{7}} \tag{2.27}$$

where,

$\varepsilon_a = emissivity\ of\ the\ air$

$C = cloud$ cover fraction

$e_a = atmospheric\ water\ vapor\ pressure\ (millibars)$

$T_a = air\ temperature\ (K)$

Atmospheric water vapor pressure can be computed from the saturated water vapor pressure and relative humidity of the air. The expression for saturated water vapor pressure, as shown in Equation 2.28, is applicable for temperatures ranging from 0 to 200 ºC (32 to 392 ºF) (ASHRAE 1993).

$$P_{ws} = \exp\left[\frac{C_1}{T_a} + C_2 + C_3 T_a + C_4 T_a^2 + C_5 T_a^3 + C_6 \ln(T_a)\right] \qquad (2.28)$$

where,

$P_{ws} = saturated\ water\ vapor\ pressure$

$C_1 = -5.8002206 \times 10^3$

$C_2 = -5.516256$

$C_3 = -4.8640239 \times 10^{-2}$

$C_4 = 4.1764768 \times 10^{-5}$

$C_5 = -1.4452093 \times 10^{-8}$

$C_6 = 6.5459673$

The partial water vapor pressure can then be calculated using Equation 2.29 shown below (ASHRAE 1993).

$$e_a = R_h \times P_{ws} \times \left(\frac{10 millibar}{kPa} \right) \tag{2.29}$$

where,

$$R_h = air\ relative\ humidity\ (\%)$$

2.2.3.4 Radiation from Concrete Surface

Concrete surface also emits radiation similar to atmospheric gas particles as a part of the heat transfer process. The radiation emitted by concrete surface also follows the Stefan-Boltzmann law as shown in Equation 2.30.

$$q_c = \varepsilon_c \sigma \left(T_c \right)^4 \tag{2.30}$$

where,

$$q_c = heat\ lost\ from\ concrete\ (W / \mathrm{m}^2)$$

$$\varepsilon_c = emissivity\ of\ concrete\ surface$$

$$T_c = temperature\ of\ concrete\ surface\ (K)$$

2.2.4 Finite Difference Temperature Model

The basic equation of heat transfer model for hydrating concrete in two dimensions is governed by the following Fourier law.

$$\frac{d}{dx}\left(k \cdot \frac{dT}{dx}\right) + \frac{d}{dy}\left(k \cdot \frac{dT}{dy}\right) + Q_H = \rho \cdot c_p \cdot \frac{dT}{dt} \tag{2.31}$$

where,

$T = Temperature\,(^\circ\mathrm{C})$

$k = thermal\ conductivity\,(\mathrm{W/\,m/\,^\circ C})$

$Q_H = rate\ of\ heat\ generation\,(\mathrm{W/\,m^3})$

$\rho = \mathrm{density}\,(\mathrm{kg/\,m^3})$

$\mathrm{c_p} = specific\ heat\ capacity\,(J\ /\ kg\ /\ ^\circ\mathrm{C})$

$x, y = directions\ of\ heat\ flow$

$t = time$

If only one dimension is considered, Equation 2.31 can further be rewritten as shown in Equation 2.32 (Jonasson et al. 1995; Byfors 1980).

$$\frac{d}{dx}\left(k \cdot \frac{dT}{dx}\right) + Q_H = \rho \cdot c_p \cdot \frac{dT}{dt} \tag{2.32}$$

To solve the transient heat transfer problem, finite-difference method (FDM) was utilized in this research to predict the early age temperature distribution in concrete. The temperature distribution in concrete is governed by the heat generation in concrete (i.e. due to hydration reaction), heat conduction within the body, and heat exchange (i.e. convection, solar absorption, and irradiation) happening at the boundary surface due to the ambient environment. Boundary conditions representing the heat exchange occurring

at the surface were considered to solve the heat transfer problem in hand. There are several methods to solve FDM problems. Crank-Nicolson scheme, an implicit method, even though harder to implement but is unconditionally stable to solve FDM problems (Ames 1992; Burden and Faires 1997; Isaacson and Keller 1994; Recktenwald 2004; Riedel 2013). Therefore, the Crack-Nicolson algorithm was implemented to solve the heat transfer problem in concrete for this research.

2.3 Moisture Transfer and Relative Humidity Prediction of Concrete

Similar to the heat transfer process happening in hydrating concrete, concrete also undergoes moisture transfer while interacting with ambient environment. The ambient relative humidity is the driving force for such transfer. In comparison to the heat transfer process in concrete, the moisture transfer or diffusion in concrete is more complicated due to the complex pore structure (Yuan and Wan 2002). The moisture transfer in concrete can be modeled by applying the diffusion theory with appropriate boundary conditions. If we consider one-dimensional flow, the nonlinear diffusion equation for moisture transfer problem can be expressed as follows.

$$\frac{d\left(RH\right)}{dt} = \frac{d}{dz}\left(\alpha \cdot \frac{d\left(RH\right)}{dz}\right) + \frac{d\left(RH_s\right)}{dt} \tag{2.33}$$

where,

$RH = relative\ humidity\ of\ concrete$

$d\left(RH_s\right) = change\ in\ RH\ due\ to\ hydration$

$\alpha = diffusion\ coefficient\ of\ concrete\ (\mathrm{m}^2/s)$

$z = direction\ of\ moisture\ flow$

$t = time\ (\mathrm{s})$

For mixtures have higher water-cement ratio, the change in relative humidity due to hydration reaction becomes negligible and hence Equation 2.33 can be rewritten as shown in Equation 2.34.

$$\frac{d\left(RH\right)}{dt} = \frac{d}{dz}\left(\alpha \cdot \frac{d\left(RH\right)}{dz}\right) \tag{2.34}$$

Once concrete is placed at the construction site, the moisture transfer occurs at the concrete surface governed by the ambient relative humidity condition. The equation describing the boundary condition at the surface of concrete can be expressed as follows:

$$D_{a,w} \cdot \left.\frac{d\left(RH\right)}{dz}\right|_{z=0} = k \times \left(RH_s - RH_{amb}\right) \tag{2.35}$$

where,

$$RH_s = relative\ humidity\ of\ concrete\ surface$$

$$RH_a = ambient\ relative\ humidity$$

$$D_{a,w} = diffusion\ coefficient\ of\ water\ vapor\ in\ air\ (m^2/s)$$

$$k = convection\ mass\ transfer\ coefficient\ (m/s)$$

The diffusion coefficient of water vapor in air $D_{a,w}$ in Equation 2.35 can be estimated using Equation 2.36 provided by Bolz and Tuve (1976):

$$D_{a,w} = -2.775\times10^{-6} + 4.479\times10^{-6}T + 1.656\times10^{-10}T^2 \qquad (2.36)$$

where T is the film temperature in Kelvin. The film temperature can be obtained by averaging the temperature of the air stream and the temperature of the concrete surface (ASHRAE 2005).

The determination of convective mass transfer coefficient k in Equation 2.35 involves several steps. At first the air properties, such as density and kinematic viscosity needs to be determined for the corresponding air film temperature. Then for a given wind speed, kinematic viscosity of air, diffusion coefficient of water vapor in air, the corresponding Renolds number R_e and Schmidt number S_c needs to be obtained. Sherwood number S_h is also needed and can be determined using the computed R_e and S_c. The expressions for R_e, S_c, and S_h are shown in Equation 2.37.

$$
\begin{aligned}
&Renolds\ number: R_e = \frac{U_\infty L}{\nu} \\
&Schmidt\ number: S_c = \frac{\nu}{D_{a,w}} \\
&Sherwood\ number: S_h = 0.664 R_e^{1/2} S_c^{1/3} \left(for\ laminar\ flow \right) \\
&\qquad\qquad\qquad S_h = 0.037 R_e^{4/5} S_c^{1/3} \left(for\ turbulent\ flow \right)
\end{aligned}
\tag{2.37}
$$

where,

$U_\infty = velocity\ of\ air\ stream \left(\mathrm{m}/s \right)$

$L = characteristics\ length \left(m \right)$

$\nu = kinematic\ viscocity\ (\mathrm{m}^2/s)$

$D_{a,w} = diffusion\ coefficient\ of\ water\ vapor\ in\ air\ (\mathrm{m}^2/s)$

$k = convective\ mass\ transfer\ coefficient \left(m/s \right)$

Once the Sherwood number is computed, the corresponding convective mass transfer coefficient can be determined according to Equation 2.38 (ASHRAE 2005; Zhi et al. 2010; Nellis and Klein 2009; Nguyen 2013).

$$
k = \frac{S_h D_{a,w}}{L} \tag{2.38}
$$

The FDM was used again in this research to solve the transient moisture transfer problem in concrete. The diffusion equation given in Equation 2.34 coupled with the

moisture transfer boundary condition at the concrete surface were formulated and solved by employing Crank-Nicolson algorithm to obtain the relative humidity distribution in concrete with time.

2.4 Temperature and Moisture Gradients in Concrete

Once the temperature and moisture distribution in concrete slab is obtained through finite difference method, the next step is to compute the curling and warping strain due to such distributions. The temperature and moisture distributions across concrete slab can lead to differential shrinkage and development of tensile stresses depending on the restraint condition. Previously researchers have used the linear temperature and moisture gradient concept to estimate the corresponding tensile stresses (Westergaard 1927; Bradbury 1938) even though the actual gradients were found to be highly nonlinear (Thomlinson 1940; Mirambell 1990; Dempsey 1969; Janssen 1986; Armaghani et al. 1988; Choubane and Tia 1992; Korenev and Chernigovskaya 1962). The assumption of linear temperature and moisture gradient across pavement thickness can result in underestimation in the resultant strain and stress development.

Mohamed and Hansen (1996) took into account the nonlinear temperature gradient in pavement and proposed an approach to convert the nonlinear gradient to an equivalent linear gradient between the top and the bottom of the slab. They proposed a third degree polynomial as shown in Equation 2.39 to represent the shape of the temperature profile across the slab thickness.

$$\Delta T = A + B \cdot z + C \cdot z^2 + D \cdot z^3 \tag{2.39}$$

where ΔT is the temperature difference between any point in the pavement and the bottom, and z is the coordinate measured from the mid slab depth. The equivalent linear temperature difference between the top and the bottom of the slab can then be obtained as

$$\Delta T_{eq} = -12\left(\frac{B \cdot h}{12} + \frac{D \cdot h^3}{80}\right) \tag{2.40}$$

where h is the slab thickness. Once the temperature gradient is computed, the corresponding thermal strain due to such temperature difference can be computed as follows:

$$\varepsilon_T = \alpha \cdot \Delta T_{eq} \tag{2.41}$$

where,

ε_T = *thermal strain*

α = *coefficient of thermal expansion*

ΔT_{eq} = *equiavent linear temperature difference*

The nonlinear moisture gradient across the slab thickness can induce drying shrinkage in concrete pavement. In a similar fashion adapting the equivalent linearization concept

proposed by Mohamed and Hansen (1996), the nonlinear moisture distribution across slab thickness can be converted into equivalent linear moisture difference coefficient (Jeong and Zollinger 2005). Using the equivalent humidity difference coefficient, the drying shrinkage strain induced in concrete can be computed as shown in Equation 2.42.

$$\varepsilon_{sh} = \varepsilon_{ult} \cdot \Delta\left[1-\left(\frac{RH}{100}\right)^3\right]_{eq} \tag{2.42}$$

where,

$$\varepsilon_{sh} = shrinkage\ strain$$

$$\varepsilon_{ult} = ultimate\ shrinkage\ strain$$

$$\Delta\left[1-\left(\frac{RH}{100}\right)^3\right]_{eq} = equiavent\ humidity\ difference$$

The drying shrinkage strain ε_{sh} computed from the equivalent humidity difference coefficient and the ultimate shrinkage ε_{ult} of concrete was based on the concrete shrinkage model developed by Baźant and Panuala (1978a).

2.5 Time Dependent Deformation of Concrete: Creep

2.5.1 Mechanism of Creep

Creep is the delayed mechanical response of concrete due to viscoelastic deformation of the paste under applied or sustained stress (Lee 2007; D'Ambrosia 2011). Creep is mainly a property of the paste component and it is restrained by the aggregate present in concrete (Mindess et al. 2003). Stresses can generate due to internal forces that can be attributed to changes in pore pressure and temperature as well as due to external forces, for example, applied structural load. Creep is considered to be a problem as it can result in loss in prestressing force in prestressed concrete structure. Tall structures and long span bridges can undergo large deflection as a result of creep due to the sustained weight of the structure. However, creep is also considered as beneficial under restrained conditions from a durability standpoint as it helps to relax the tensile stress induced in structures and can help minimize the potential for cracking. Many researchers have studied creep in concrete and tried to explain the mechanism of creep. However, none of these can explain adequately the mechanism of creep (Neville et al. 1983). Few mechanisms regarding occurrence of creep are summarized below. Interested readers are referred to Altoubat (2000), Tamtsia and Beaudoin (2000), Grasley (2006), Lee (2007), and D'Ambrosia (2011) for summaries on mechanism of creep.

- Seepage theory states that creep might be caused due to induced stress in the physically bound water under external load causing seepage of physically bound water from micropores to capillary pores (Powers 1967);
- Interlayer theory states that creep could be attributed to structural changes in Calcium-Silicate-Hydrate (C-S-H) layers, i.e. deformation and restructuring the assembly C-S-H particles, and consequent formation of new interlayer spaces (Feldman 1972);
- Viscous shear theory is based on the hypothesis that the sliding of C-S-H globules or layers induced by localized nanoscale shear stresses might result in creep deformation (Jennings 2004; Reutz 1968);
- Plastic flow theory states that the slippage along planes in crystal lattice may contribute to creep (Neville et al. 1983);
- The stress-induced dissolution theory is based on the notion that phases, such as CH may dissolve under high stress and reform again in a stress free state, contributing to creep deformation (Mindess et al. 2002).
- Sellevold and Richards (1972) proposed the short-term creep mechanism, verified by Scherer (2000), stating that redistribution of capillary water under load results in creep deformation; and
- Creep may result from permanent deformation due to microcracking, recrystallization, and formation of new physical bonds in the hydration products (Altoubat 2000; D'Ambrosia 2011).

Concrete, when exposed to drying, exhibits additional creep which is called drying creep. This phenomenon is called the Pickett effect which was first observed by Pickett (1942). Several empirical relationships regarding drying creep were formulated which were dependent on basic creep and free shrinkage (L'Hermite 1959; Gamble and Parrot 1978). Bazant and Panula (1978b) proposed an empirical relationship for drying creep as a function of drying shrinkage and mixture properties. Apparently, drying creep is more of a complex interaction between free shrinkage and basic creep (Altoubat 2000).

Several mechanisms were proposed by researchers to explain the phenomenon of drying creep, however none of them are universally accepted (Neville 1981). Basic and drying creep were separated experimentally by superposition analysis under the assumption that creep is linearly proportional to applied stress (Kovler 1994; Altoubat 2000). Several proposed theories regarding the mechanism of drying creep are stated below:

- The superposition of stresses due to drying shrinkage and external load leads to additional strain due to the nonlinearity in the stress strain relationship (Pickett 1942);
- The stress-induced shrinkage mechanism suggest that when drying is combined with external loading, shrinkage is influenced by applied loading, i.e. shrinkage increases under compressive load while decreases under tensile loads (Bazant and Xi 1994; Bazant and Chern 1985; Wittmann and Roelfstra 1980; Wittmann 1993).

- Microcracks might be another possible source of drying creep. Under high drying gradient microcracks form. The microcracks might contribute to an increase in the rate of creep (Pickett 1942; Bazant and Xi 1994); and
- Bazant et al. (1997) proposed the microprestress-solidification theory suggesting that creep in the bridging nanostructure is the source of drying creep. Drying creep is manifested with the increase in creep rate in the bridging nanostructures due to the decrease in internal relative humidity.

It is generally believed that combination of these suggested sources are responsible for both the compressive and tensile drying creep (Bazant and L'Hermite 1988, Altoubat 2000, Grasley 2006).

2.5.2 Predictive Models for Creep

ACI committee 209 (1992) recommended a prediction equation for creep compliance function based on the work of Branson et al. (1977). The ultimate creep coefficient in the creep compliance function was modified by correction factors based on curing, relative humidity, load duration, slump, aggregate, and air content. The model for compliance function is shown in Equation 2.43.

$$J\left(t,t^{'}\right)=\frac{1}{E\left(t^{'}\right)}\left(1+\frac{\left(t-t^{'}\right)^{\psi}}{d+\left(t-t^{'}\right)^{\psi}}\cdot v_{u}\right) \tag{2.43}$$

where,

$$J\left(t,t^{'}\right) = compliance\ function\ at\ time\ t\ \ for\ a\ loading\ at\ t^{'}$$

$$E\left(t^{'}\right) = Young\ 's\ modulus\ of\ \ elasticity\ at\ the\ loading\ time\ t^{'}$$

$$d,\psi = constants$$

D'Ambrosia (2011) reexamined the validity of the ACI creep equation for the prediction of tensile creep at early ages due to restrained drying and autogeneous shrinkage. He found that the ultimate creep coefficient parameter used in the model needed to be modified beyond the recommended range to fit the experimental data at early ages. To improve the predictive capability of the model, he modified the ACI equation by incorporating the following creep correction factor.

$$K_{EA}{}^{c} = 1 + \frac{r}{t^{'}}\left(\frac{1}{t-s}\right) \tag{2.44}$$

where t is the time, t' is the loading time, and s is the setting time, in days. Parameter r depends on the early age strength gain and was obtained by fitting experimental data. He showed that the value of the correction factor becomes unity as the loading age exceeds seven days and thereby the equation reduces to its original form.

Bazant and Baweja (1995) developed the B3 model for predicting the creep compliance of concrete. The creep compliance function and expressions for the

parameters are shown in Equation 2.45. Detailed description and explanation regarding the B3 model can be found elsewhere (Bazant and Baweja, 1995).

$$J\left(t,t'\right) = q_1 + C_o\left(t,t'\right) + C_d\left(t,t'\right) \tag{2.45a}$$

$$C_o\left(t,t'\right) = q_2 Q\left(t,t'\right) + q_3 \ln\left[1+\left(t-t'\right)^n\right] + q_4 \ln\left(t/t'\right) \tag{2.45b}$$

$$C_d\left(t,t'\right) = q_5\left[\exp\left\{-8H\left(t\right)\right\} - \exp\left\{-8H\left(t'\right)\right\}\right]^{1/2} \tag{2.45c}$$

where,

$J\left(t,t'\right) = compliance\ function\ at\ time, t\ for\ a\ loading\ at\ time, t'$

$q_1 = instantaneous\ compliance$

$C_o\left(t,t'\right) = basic\ creep\ component$

$C_d\left(t,t'\right) = drying\ creep\ component$

$Q\left(t,t'\right) = binomial\ integral$

$q_2, q_3, q_4, n = empirical\ material\ parameters$

$q_5 = constant\ related\ to\ ultimate\ creep$

$H\left(t\right) = average\ relative\ humidity\ of\ across\ section\ as\ a\ function\ of\ time$

If the applied stress on the concrete specimen is σ at time t', the creep strain can be computed as $J(t, t')\sigma$. The total strain in B3 model is calculated according to Equation 2.46.

$$\varepsilon(t) = J(t,t')\sigma + \varepsilon_{sh}(t) + \alpha\Delta T(t) \tag{2.46}$$

where $\varepsilon_{sh}(t)$ is the shrinkage strain and $\alpha\Delta T$ is the thermal strain.

Østergaard et al. (2001) modified the B3 model in order to describe the early age tensile creep behavior of concrete. They showed that the original model was not able to give the accurate prediction of tensile creep for loading ages less than one day. He proposed an additional factor to account for the observed discrepancies. He modified the parameter q_2 according to

$$q_2 = q_2\left(\frac{t'}{t' - q_6}\right) \tag{2.47}$$

where q_6 is approximately the set time of concrete (D'Ambrosia and Lange 2005; D'Ambrosia et al. 2004; Grasley et al. 2006). D'Ambrosia (2011) used the B3 model with the modification of Østergaard et al. (2001) to compare its predictive capability of the tensile creep with the experimental data and he concluded that no additional terms were required in the model to account for the early age drying creep.

2.5.3 Rheological Model for Creep

In the literature there are several creep models based on a rheologic chain. Lee (2007) provided a summary of some available rheologic models for creep. Most of the models found in the literature used Generalized Kelvin Model (GKM) to represent more complex behavior.

Zienkiewicz et al. (1968) used a GKM model (see Figure 2.2) to describe the concrete creep assuming that the applied stress was constant during a short time interval *Δt*. The expression for creep was given as follows.

$$\Delta\varepsilon_c = \sum_{i=1}^{n} \Delta\varepsilon_c^{\,i} = \sum_{i=1}^{n} \left(\frac{\sigma}{\eta_i} - \frac{E_i}{\eta_i} \varepsilon_c^{\,i} \right) \tag{2.48}$$

where,

$i = number\ of\ \ Kelvin\ chains$

$\Delta\varepsilon_c^{\,i} = creep\ increament\ of\ i^{th}\ Kelvin\ chain$

$E_i = spring\ constant\ of\ i^{th}\ Kelvin\ chain$

$\eta_i = dash - pot\ constant\ of\ i^{th}\ Kelvin\ chain$

$\sigma = inital\ stress\ value\ at\ the\ start\ of\ \ the\ interval$

$\varepsilon_c^{\,i} = inital\ creep\ strain\ value\ at\ the\ start\ of\ \ the\ interval$

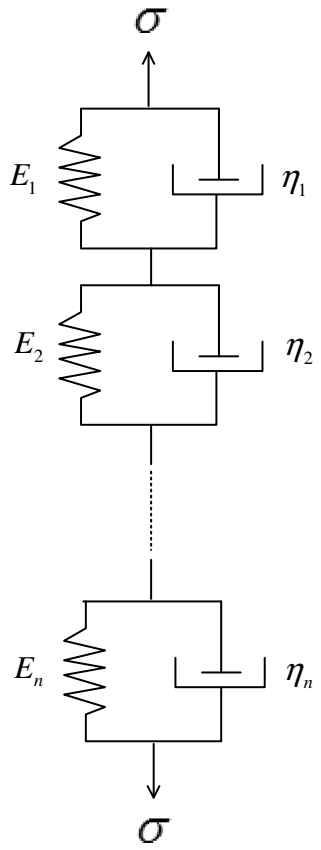

Figure 2.2: Generalized Kelvin Model

Bazant and Prasannan (1989a) used a Kelvin chain to describe the solidified matter with non-aging elastic moduli and viscosities. They derived an exact solution of GKM under the assumption that the stress varied linearly in a short time interval Δt as shown in Equation 2.49.

$$\Delta\gamma = \Delta\sigma \sum_{i=1}^{n} \frac{1}{E_i}\left(1 - \frac{\tau_i}{\Delta t}\left(1 - e^{-\frac{\Delta t}{\tau_i}}\right)\right) + \sum_{i=1}^{n}\left(\frac{\sigma}{E_i} - \gamma_i\right)\left(1 - e^{-\frac{\Delta t}{\tau_i}}\right) \qquad (2.49)$$

where,

$i = number\ of\ \ Kelvin\ chains$

$\Delta\gamma_c = creep\ increament\ at\ time\ interval\ \Delta t$

$\Delta\sigma = stress\ increament\ at\ time\ interval\ \Delta t$

$E_i = spring\ stiffness\ of\ i^{th}\ Kelvin\ chain$

$\tau_i = retardation\ time\ of\ i^{th}\ Kelvin\ chain$

$\sigma = inital\ stress\ value\ at\ the\ start\ of\ \ the\ interval$

$\gamma_i = inital\ component\ of\ i^{th}\ Kelvin\ chain\ at\ the\ start\ of\ interval\ \Delta t$

2.5.4 Solidification Theory for Creep

Solidification theory was proposed by Bazant (1977) to account for the effect of aging on creep. The underlying concept of the solidification theory is that the hydration products are non-aging viscoelastic material on a micro scale basis and the aging effect is manifested on a macro scale by the gradual solidification and volume growth of hydration product that accounts for the aging effect on creep. The thermodynamic justification of the solidification theory was published in (Bazant 1979) and summaries of this theory can be found in these references (Altoubat 2000; Grasley 2006; Lee 2007; D'Ambrosia 2011). The conceptual diagram of the solidification theory provided by Carol and Bazant (1993) is shown in Figure 2.3. The underlying concept of the theory is that the hydration products solidify in a stress free state and the newly solidified layer formed at age *t* participates in carrying the stress induced by load applied after time *t*. Bazant and Prasannan (1989b) derived an incremental form of solution for analyzing creep under varying stress as shown in Equation 2.50. The solidification theory, being

based on strong theoretical background and having a simple final form of solution, seems to be promising for describing concrete creep with material aging and has been used by researchers to explain the creep phenomenon of concrete (Lee 2007).

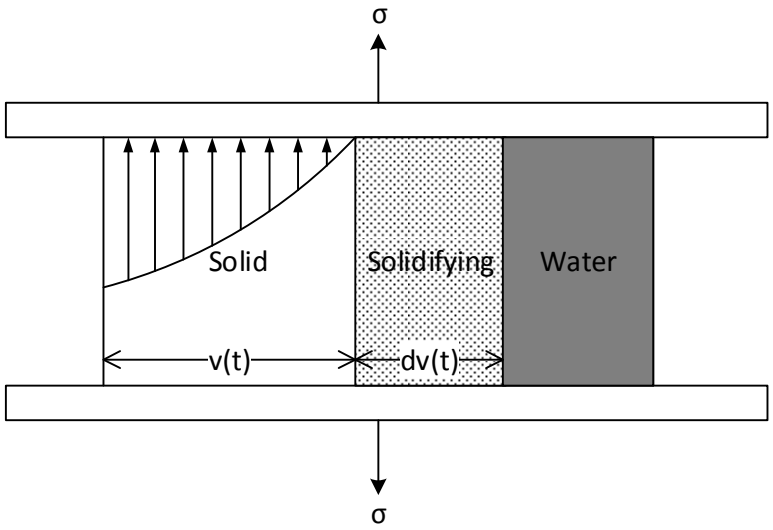

Figure 2.3: Solidifying Material Subjected to Applied Stress at Time = t (after D'Ambrosia 2011)

$$\Delta\gamma_c = \frac{\Delta\sigma}{v_e\left(t_o + \Delta t/2\right)}\sum_{i=1}^{n}\frac{1}{E_i}\left(1-\frac{\tau_i}{\Delta t}\left(1-\mathrm{e}^{-\frac{\Delta t}{\tau_i}}\right)\right)+\frac{1}{v_e\left(t_o+\Delta t/2\right)}\sum_{i=1}^{n}\left(\frac{\sigma}{E_i}-\gamma_i\right)\left(1-\mathrm{e}^{-\frac{\Delta t}{\tau_i}}\right) \tag{2.50}$$

where,

$$t_o = initial\ time\ at\ the\ beginning\ of\ interval\ \Delta t$$

$$v_e\left(t_o + \Delta t/2\right) = effective\ load - bearing\ volume\ at\ time\left(t_o + \Delta t/2\right)$$

The other variables are defined earlier in Equation 2.49.

2.6 Shrinkage in Concrete

2.6.1 Mechanism of Shrinkage

The driving mechanism of shrinkage is the reduction in internal humidity in concrete due to self-desiccation and external drying. The shrinkage due to external drying is called drying shrinkage and the same due to internal drying or self-desiccation is called autogenous shrinkage. External drying is a diffusion controlled process. The diffusion depends on the pore microstructure of the hardened cement paste. As the pore micro structure changes during hydration reaction with time, the trend in early age drying shrinkage may differ substantially from the long-term drying shrinkage trend (D'Ambrosia, 2011).

2.6.1.1 Drying Shrinkage

When concrete is placed in a dry environment i.e. the ambient humidity is lower than the internal humidity, moisture diffuses towards the surface. External drying results in removal of pore water causing volume reduction which is known as drying shrinkage.

There are three mechanisms for external drying: (i) capillary surface tension, (ii) disjoining pressure, and (iii) surface free energy (Mindess and Young 1981). Capillary surface tension develops in the pore fluid due to the reduction in pore fluid pressure. With the development of tension force, a balancing compressive stress develops in the solid microstructure that induces shrinkage (Bissonette et al. 2001). Disjoining pressure develops due to the adsorbed water on the C-S-H surface. The removal of moisture on the C-S-H reduces the disjoining pressure and this reduction in the disjoining pressure contributes to shrinkage (Powers 1968; Ferrais and Wittmann 1987; Lee 2007). The surface energy (tension) of C-S-H depends on the adsorbed water layers which is responsive to the partial vapor pressure. With the reduction in the partial vapor pressure, the thickness of the adsorbed layer also decreases. The reduction in the layer thickness creates a net compression on the solid inducing microscale shrinkage (Powers 1968; Mindess and Young 1981; Grasley et al. 2006). Therefore in short with the reduction in internal relative humidity, drying stress develops and deforms the microstructure, and hence shrinkage is manifested on a bulk scale (Lee 2007).

2.6.1.2 Autogenous Shrinkage

The difference between autogenous shrinkage and external drying shrinkage is that in autogenous shrinkage the relative humidity is lowered internally by chemical reaction due to cement hydration. The hydration reaction consumes water that causes volume reduction leading to the formation of empty pores. As the hydration reaction continues, the water is consumed from larger pores followed by successively smaller pores. Once

the pores smaller than 50 nm begin to empty, autogenous shrinkage is induced by a similar mechanism that induces external drying shrinkage. The use of low water-cement ratio and some mineral admixtures in the mix accentuates the autogenous shrinkage problem furthermore (Barcelo 2003; Grasley 2006).

2.6.2 Predictive Models for Drying Shrinkage

ACI committee 209 (1992) recommended the prediction equation for drying shrinkage as given in Equation 2.51.

$$\varepsilon_s\left(t,t_o\right)=\frac{\left(t-t_o\right)^{\alpha}}{f_c+\left(t-t_o\right)^{\alpha}}\varepsilon_u^s \tag{2.51}$$

where,

$t_o = time\ at\ which\ drying\ begins$

$\varepsilon_u^s = ultimate\ shrinakge$

$f_c\ and\ \alpha = constants$

ACI provided recommendation for the numerical values of each constant based on standard test condition and provided equations to account for deviations from the standard test conditions as well. They also provide an estimation of the ultimate shrinkage based on initial moisture curing durations, ambient relative humidity, volume-surface ratio of the specimen, slump of concrete, fine aggregate proportion, cement content, and air content (D'Ambrosia 2011; Lee 2007). D'Ambrosia (2011) showed that

the ACI shrinkage model was not able to predict the early age shrinkage accurately compared to the experimental observations. He modified the current ACI model by incorporating the following shrinkage correction factor as shown in Equation 2.52.

$$K_{EA}{}^{s} = \left[1 + \frac{z}{t_o}\left(\frac{1}{t-s}\right)\right] \tag{2.52}$$

where t is time, t_o is the length of curing, s is the setting time in days. Parameter z was obtained by fitting experimental data and it depends on the diffusion rate. He showed that the shrinkage correction factor approaches unity as the curing time exceeds seven days, thus the model reduces to its original form.

Similar to the creep compliance function for concrete, Bazant and Baweja (1995) incorporated an empirical expression for drying shrinkage in the B3 model mentioned before. The expression for drying shrinkage in the B3 model is shown in Equation 2.53.

$$\varepsilon_{SH}\left(t, t_s\right) = \tanh\left(\frac{\left(t-t_s\right)}{\tau_{SH}}\right)^{\frac{1}{2}} k_h \varepsilon_{SH\infty} \tag{2.53}$$

where,

$t_s = duration\ of\ initial\ wet\ curing$

$\varepsilon_{SH\infty} = ultimate\ shrinakge$

$k_h\ and\ \tau_{SH} = parameters\ depending\ on\ ambient\ relative\ humidity$ $and\ specimen\ geometry$

These empirical models have been developed based on the deformation for a specific geometry and these models consider the bulk strain over cross sectional average. It does not give the differential shrinkage across the location domain of the specimen. However, for certain circumstances, such as in moisture curling, the average shrinkage strain cannot capture the deformation and the differential shrinkage strain is required to explain such deformation (Lee 2007).

D'Ambrosia (2011) proposed a modeling technique to predict concrete shrinkage as a response to internal stress in an aging viscoelastic porous medium. He used the relationship between relative humidity and capillary pressure to predict the shrinkage stress induced in concrete. The model prediction indicated good agreement with the shrinkage data for both sealed and drying conditions. The material model that he used was divided into two sets: an internal set representing the solid skeleton and an external set representing the porous body as shown in Figure 2.4. The material models accounted for both the aging viscoelastic behavior and the responses due to changes in temperature and internal relative humidity. Combination of the two model sets allowed for the coupled creep and shrinkage analysis for aging viscoelastic material.

The internal model responded to changes in pressure due to any fluctuation in internal relative humidity as well as to any changes in external applied stress. The external set, however, responded to the changes in external applied load only. The aging material properties were incorporated using the solidification theory. D'Ambrosia (2011) reported that after calibrating the internal and external creep function of the material

model, the prediction of the model was in good agreement with the drying shrinkage data obtained through experimentation.

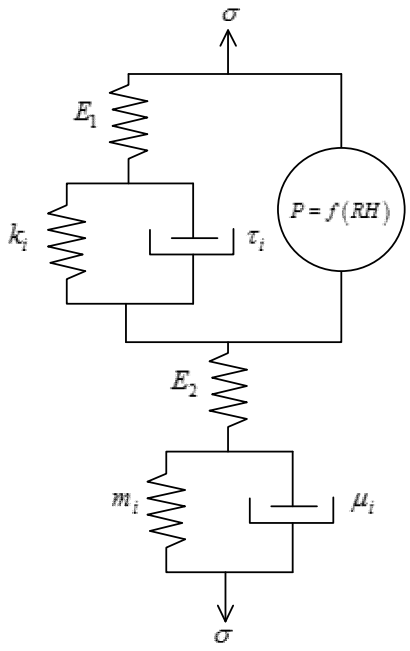

Figure 2.4. Model Concept Diagram Showing Internal and External Material Models (after D'Ambrosia 2011)

During the validation phase of this model, capillary pressure was computed from the internal relative humidity of concrete using the Kelvin-Laplace equation as shown below.

$$p = \ln(RH)\frac{RT}{v} \tag{2.54}$$

where,

$p = pore\ pressure$

$RH = relative\ humidity$

$R = universal\ gas\ constant$

$T = temperature\ in\ Kelvin$

$v = molar\ volume\ of\ water$

The drying shrinkage was modeled using a hygrothermal strain model shown in Equation 2.55 (Bentz et al. 1998) as a function of capillary pore pressure.

$$\varepsilon = \frac{pS}{3}\left[\frac{1}{K} - \frac{1}{K_S}\right] \tag{2.55}$$

where,

$p = pore\ pressure$

$S = saturation\ factor$

$K = bulk\ modulus\ of\ porous\ body$

$K_s = bulk\ modulus\ of\ solid\ skeleton$

For the internal and external component shown in Figure 2.4, the total deformation in one dimension was written as follows.

$$\varepsilon_{total} = \varepsilon_{el_1} + \varepsilon_{cr_1} + \varepsilon_{el_2} + \varepsilon_{cr_2} \tag{2.56}$$

where,

$\varepsilon_{total} = total\ deformation$

$\varepsilon_{el_1} = instantaneous\ elastic\ deformantion\left(internal\right)$

$\varepsilon_{cr_1} = time-dependent\ viscoelastic\ deformantion\left(internal\right)$

$\varepsilon_{el_2} = instantaneous\ elastic\ deformantion\left(external\right)$

$\varepsilon_{cr_2} = time-dependent\ viscoelastic\ deformantion\left(external\right)$

For a small time step, $\Delta t = t_{i+1}$-t_i, total stain was modeled and solved in an incremental form as shown below.

$$\Delta\varepsilon_{total} = \Delta\varepsilon_{el_1} + \Delta\varepsilon_{cr_1} + \Delta\varepsilon_{el_2} + \Delta\varepsilon_{cr_2} \tag{2.57}$$

For the Generalized Kelvin Model shown in Figure 2.5 representing the internal and external material components, the incremental stress at each time step was computed according to the expression shown in Equation 2.58.

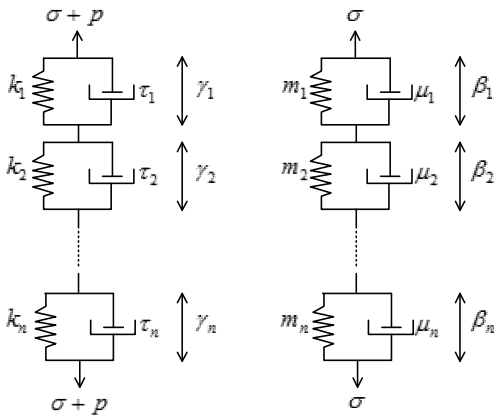

Figure 2.5: GKM Diagram for the Material Component (D'Ambrosia 2011)

$$\Delta\sigma = J^{-1}\Delta\varepsilon_{total} - R \tag{2.58}$$

where,

$$J = compliance\ function\ at\ each\ step$$

$$= \frac{1}{E_1} + \frac{1}{E_2} + \frac{F(\sigma_o + p_o)}{v(t_o)} \sum_{i=1}^{n} \frac{1}{k_i} \left\{ 1 - \frac{\tau_i}{\Delta t} \left(1 - e^{-\Delta t / \tau_i} \right) \right\}$$

$$+ \frac{F(\sigma_o)}{v(t_o)} \sum_{i=1}^{n} \frac{1}{m_i} \left\{ 1 - \frac{\mu_i}{\Delta t} \left(1 - e^{-\Delta t / \mu_i} \right) \right\}$$

$$R = \frac{\Delta p}{E_1} + \frac{F(\sigma_o + p_o)}{v(t_o)} \sum_{i=1}^{n} \left(\begin{array}{l} \frac{\Delta p}{k_i} \left\{ 1 - \frac{\tau_i}{\Delta t} \left(1 - e^{-\Delta t / \tau_i} \right) \right\} \\ + \left(\frac{\sigma + p}{k_i} - \gamma_i \right) \left(1 - e^{-\Delta t / \tau_i} \right) \end{array} \right)$$

$$+ \frac{F(\sigma_o)}{v(t_o)} \sum_{i=1}^{n} \left(\frac{\sigma}{m_i} - \beta_i \right) \left(1 - e^{-\Delta t / \mu_i} \right)$$

E_1 *and* E_2 = *internal and external elastic moduli at each step*

F = *creep magnification factor*

$v(t_o)$ = *effective load bearing volume*

k_i *and* m_i = *internal and external Kelvin chains*

τ_i *and* μ_i = *internal and external retardation time*

The model was validated using several experimental geometries and the predictions of the drying shrinkage and stress distribution indicated good agreement with the experimental observations (D'Ambrosia 2011).

2.7 Selection of Creep and Shrinkage Model

In the previous sections, several existing empirical creep and shrinkage model, such ACI model and B3 model, were summarized. D'Ambrosia (2005, 2011) showed that the ACI model and the B3 creep and shrinkage model in its existing form were not able to predict the early age creep and shrinkage of concrete. He proposed modifications to these existing models to improve the predictability of the creep and shrinkage behavior of concrete. Also, these empirical models, such as the shrinkage model, were developed based on the deformation with a specific geometry and these model provide bulk strain over the cross sectional average rather than the differential shrinkage (Lee 2007). Lee (2007) mentioned that such predictions can be applicable for certain structural analysis whose global behavior is not governed by differential shrinkage. However, for certain cases, such as moisture curling, differential shrinkage across the thickness of the slab is

required to explain the curling behavior of the structure. Hence, because of these limitations, these empirical models were not selected in this research.

The solidification theory, discussed previously, seems to be promising for describing the concrete creep with material aging because of its strong theoretical background and simple final form of solution (Lee 2007). Due to these benefits many researchers, such as Baweja et al. (1998), Altoubat (2000), Grasley (2006), Lee (2007), and D'Ambrosia (2011), have adapted the theory for analyzing concrete creep. D'Ambrosia (2011) used the solidification theory and proposed a material model (see section 2.6.2) to predict the early age autogenous shrinkage and drying shrinkage of concrete. Such model facilitated the coupled creep and shrinkage analysis for concrete and the model predictions were found to be in good agreement with the experimental observation. Hence, the material model proposed by D'Ambrosia (2011) based on the solidication theory were used in this research.

2.8 System Identification Method: A Solution Methodology

System identification (SID) method is an iterative approach which is used to identify the characteristics of a system using the input and output data from the system. The purpose of this method is to identify a mathematical model that can describe the behavior of a real physical process or a system. The mathematical representation or model is considered to be identical to the system when the error between the output of the model and the system satisfies the error criterion. The model parameters should be updated using some parameter adjustment algorithm till the desired level of agreement is

achieved (Natke 1982). Using SID with an efficient parameter adjustment algorithm, mathematical models with several unknowns can be calibrated accurately and convergence can be obtained rapidly (Wang and Lytton 1993). Many researchers, for example Wang and Lytton (1993), Lytton et al. (2010), and Lee (2010), have successfully implemented SID method in their research efforts to identify appropriate mathematical models to represent the behavior of the system of interest.

Successful implementation of SID requires accurately measured output data of the unknown system, a suitable model representing the behavior of the system, and an efficient parameter adjustment algorithm (Wang and Lytton 1993). Three general strategies are available for minimizing the error in the system identification method: (i) forward approach, (ii) inverse approach, and (iii) generalized approach. These three strategies are depicted in Figure 2.6. Forward approach involves minimizing the output error between the model and the system using the same input. The inverse approach deals with minimizing the input error using the same output. Generalized approach is a combination of forward and inverse approaches provided that the model is invertible (Natke 1982).

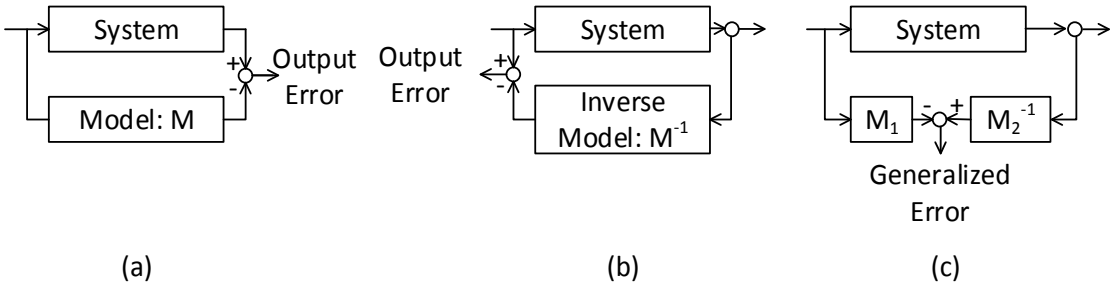

Figure 2.6: Methods for System Identification Process. (a) Forward Model, (b) Inverse Model, and (c) Generalized Model (Natke 1982)

A parameter adjustment and adaptation algorithm was developed by Wang and Lytton (1993) based on the Taylor series expansion. A brief description and formulation of the parameter adjustment algorithm is given below (Wang and Lytton 1993). Assuming a mathematical model defined by n parameters as shown in Equation 2.59, is appropriate for describing the behavior of a system:

$$f = f\left(p_1, p_2, ..., p_n; x, t\right) \tag{2.59}$$

where x and t are independent spatial and temporal variable. The parameter adjustment algorithm can be expressed as follows.

$$\left[F_{ki}\right]\left\{\beta_i\right\} = \left\{r_k\right\} \tag{2.60}$$

where,

$$[F_{ki}] = sensitivity\ matrix = \sum_{k=1}^{m}\sum_{i=1}^{n}\frac{\partial f_k}{\partial p_i}\frac{p_i}{f_k}\left(m \times n\ matrix\right)$$

$$m = number\ of\ output\ data$$

$$n = number\ of\ model\ parameters$$

$$f_k = mathematical\ model$$

$$p_i = model\ parameters$$

$$\{\beta_i\} = change\ vector\ (\text{relative change of parameters})$$

$$= [\beta_1, \beta_2, ..., \beta_n]^T$$

$$\{r_k\} = residual\ vector\ (\text{relative change of parameters})$$

$$= [r_1, \mathrm{r}_2, ..., \mathrm{r}_m]^T$$

The residual vector is determined from the outputs of the model and the real system. The minimization of the error in the residual vector is analogous to the reduction of error used in least squared error analysis; however, because of the presence of random error, the values in the residual vector should not be forced to zero (Zollinger et al. 2008). The elements of the sensitivity matrix $[F_{ki}]$ reveal the sensitivity of the output f_k to the model parameters p_k. The vector β is an unknown vector and reflects the relative changes in the parameters of interest. Depending on the condition of the sensitivity matrix, whether well behaved or ill conditioned, generalized inverse procedure or singular value decomposition technique can be used to obtain stable solutions (Stubbs 1987; Torpunuri 1990; Press et al. 2007). Equation 2.60 can be rewritten as follows:

$$\{\beta_i\} = \left[F_{ki}^{\,T} \, F_{ki} \right]^{-1} \left[F_{ki} \right]^{T} \{r_k\} \tag{2.61}$$

After obtaining the values of β after the first iteration, the new set of parameters are updated in the next iteration as:

$$p_i^{j+1} = p_i^{j} \left(1 + \beta_i\right) \tag{2.62}$$

where j is the iteration count. Solutions of the parameters are obtained by minimizing the change vector $\{\beta\}$ iteratively; therefore, the iteration process is repeated until the desired convergence is reached (Wang and Lytton 1993). In this research, SID method was used as a solution methodology to back-calculate the time dependent diffusion coefficient of cured concrete using the relative humidity measurements of the concrete and the ambient environment.

3. MODELING AND NUMERICAL IMPLEMENTATION

In this section, modeling efforts to meet the objectives of this research described in Section 1 are addressed. The first objective of this research was to incorporate the effect of curing into the pavement design analysis. Therefore, a mathematical model for back-calculating the diffusion coefficient of cured concrete, which is reflective of the curing quality, was discussed. In the subsequent sections, the formulation of a corner displacement model as well as the development of climatic stress model in a slab subjected to temperature and relative humidity variations are shown. Finally, representing the variability associated with the strength and stress, the formulation of probabilistic models for predicting lift-off displacement and cracking for a given design scenario is described.

3.1 Early Age Diffusion of Concrete

3.1.1 Laboratory Testing Regime

The early age diffusion coefficient α for concrete changes with time as the hydration reaction progresses. In order to back-calculate the moisture diffusion coefficient of cured concrete during early ages, internal relative humidity (RH) of concrete and ambient relative humidity information were required. The internal and ambient relative humidity information of a cured concrete sample were obtained by following the laboratory testing regime proposed by Ye (2007). The back-calculated diffusion coefficient of a

cured concrete sample is reflective of the quality of curing provided during construction. Furthermore, as subsequently shown it is also possible to rank the performance of different curing compounds based on the back-calculated diffusion coefficients of cured concrete samples.

In order to conduct experiment as per a laboratory testing regime proposed by Ye (2007), a curing monitoring system and a high accuracy weighing scale were used. Figure 3.1 shows the curing monitoring device used in this research. The weighing scale was used to obtain the moisture loss data and the curing monitoring system was used to collect three different temperature and relative humidity's: (i) of the ambient environment, (ii) of the concrete surface, and (iii) inside of the concrete sample. The relative humidity measurements at the surface and inside the concrete were termed as filtered relative humidity and sealed relative humidity, respectively. Concrete mixture was prepared and placed in a cylindrical mold of 12 inch in diameter and 4 inch in height. After placing concrete in the mold, the curing monitoring system was placed over the mold.

The curing monitoring system consisted of two chambers: (i) sealed chamber and (ii) filtered chamber. The sealed chamber collected the temperature and relative humidity information inside the concrete sample whereas the filtered chamber collected the temperature and relative humidity information of the surface of the concrete sample. Figure 3.2 shows the schematics of the different components of the test setup. Figure 3.3 presents an example of concrete placement in the mold as well as the two chambers of the curing monitoring device used in the experiment.

After placing the sealed and filtered chambers over the mold, the curing monitoring device was mounted over the chambers using a housing system. Figure 3.4 shows the entire setup of the curing monitoring system for obtaining the temperature and relative humidity information from a cured concrete sample. Figure 3.5 presents an example of internal and ambient relative humidity information collected for a cured concrete sample using the laboratory testing regime discussed above.

Figure 3.1: Curing Monitoring Device (Sun 2013)

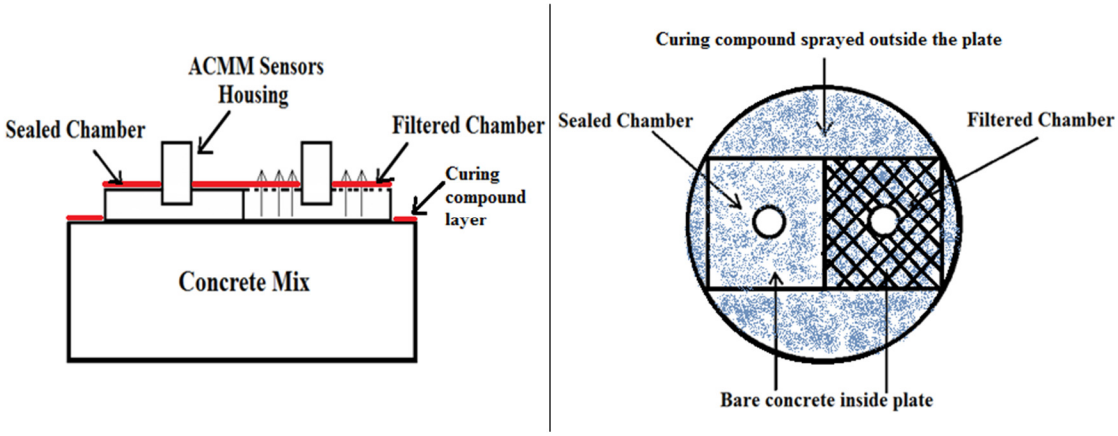

Figure 3.2: Side View and Top View of the Mold with the Sealed and Filtered Chambers with Housing System (Zollinger 2013)

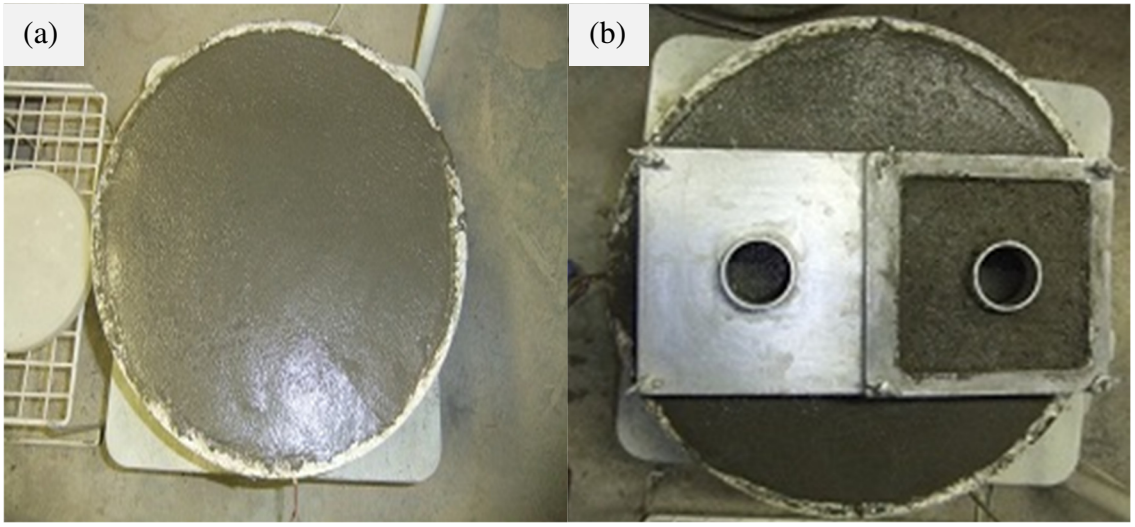

Figure 3.3: Test Setup in the Laboratory with the Mold and the Curing Plate. (a) Concrete Placed in the Mold and (b) Curing Plate Placed over the Mold (Sun 2013)

Figure 3.4: Entire Curing Monitoring System (Sun 2013)

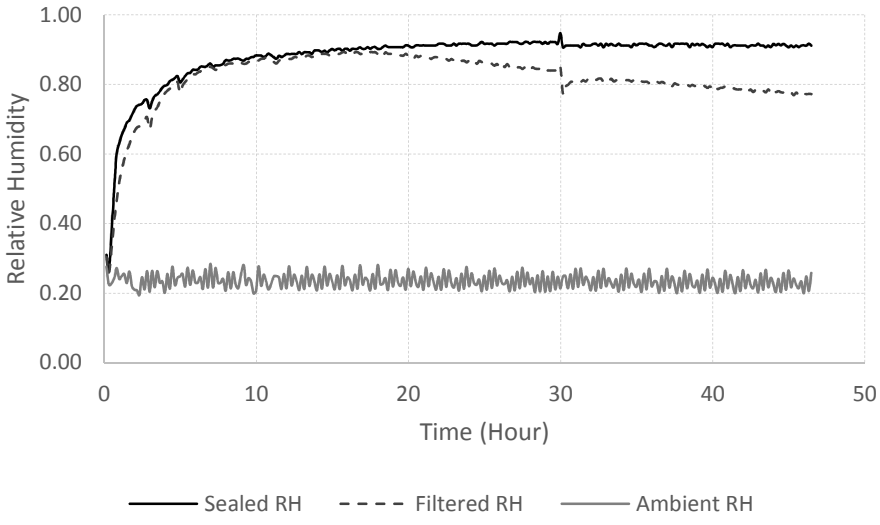

Figure 3.5: Relative Humidity Information Collected using the Curing Monitoring System

3.1.2 Early Age Diffusion Coefficient of Cured Concrete

In this section, a procedure for back-calculating the diffusion coefficient of cured concrete with the collected relative humidity information is discussed. The moisture diffusion equation derived by Mitchell (1979) in Equation 2.5 along with the system identification method as a solution methodology were utilized for back-calculating the diffusion coefficient of cured concrete sample. As mentioned before, this back-calculated diffusion coefficient of cured concrete is reflective of the effectiveness of curing provided during the construction phase.

Mitchell derived the moisture diffusion equation for soil with constant diffusion coefficient α and constant evaporation constant h. However, in this case as the concrete is undergoing hydration reaction, these variables are changing with time. Hence, the equation derived by Mitchell was modified by making the diffusion coefficient α and the evaporation constant h as a time dependent variable. Hence, for the case of concrete, Equation 2.5 can be rewritten as follows:

$$RH(\mathrm{z},\mathrm{t}) = RH_c(t) + \{RH_a(t) - RH_c(t)\} \cdot erfc\left(\frac{z}{2\sqrt{\alpha(t)\cdot t}}\right)$$
$$-\{RH_a(t) - RH_c(t)\} \cdot \exp\left[h(t)\cdot z + \{h(t)\}^2 \cdot \alpha(t)\cdot t\right] \cdot erfc\left(\frac{z}{2\sqrt{\alpha(t)\cdot t}} + h(t)\cdot\sqrt{\alpha(t)\cdot t}\right) \quad (3.1)$$

where,

$$RH\left(z,t\right) = relative\ humidity\ of\ concrete\ at\ depth\ z\ at\ time\ t$$

$$RH_a\left(t\right) = ambient\ relative\ humidity\ at\ time\ t$$

$$RH_c\left(t\right) = sealed\ or\ concrete\ relative\ humidity\ at\ time\ t$$

The other variables in Equation 3.1 were described in Equations 2.1 through 2.5. The expression given in Equation 3.1 is the mathematical model that gives the relative humidity of concrete at any depth and time for a given value of diffusion coefficient, evaporation constant as well as the ambient and concrete (sealed) humidity. The unknown parameters *α(t)* and *h(t)* can be solved using the partial derivatives of Equation 3.1 and SID method as follows:

$$\begin{matrix} [F] & & [\beta] & = & [r] \end{matrix}$$

$$\left[\frac{\partial RH\left(z,t\right)}{\partial \alpha\left(t\right)} \cdot \frac{\alpha\left(t\right)}{\overline{RH\left(z,t\right)}} \quad \frac{\partial RH\left(z,t\right)}{\partial h\left(t\right)} \cdot \frac{h\left(t\right)}{\overline{RH\left(z,t\right)}}\right] \begin{bmatrix} \dfrac{\alpha\left(t\right)_{i+1} - \alpha\left(t\right)_i}{\alpha\left(t\right)_i} \\ \dfrac{h\left(t\right)_{i+1} - h\left(t\right)_i}{h\left(t\right)_i} \end{bmatrix} = \left[\frac{RH\left(z,t\right)_m - \overline{RH\left(z,t\right)}}{\overline{RH\left(z,t\right)}}\right] \tag{3.2}$$

where,

$$\overline{RH\left(z,t\right)} = calculated\ relative\ humidity\ from\ Equation\ 3.1$$

$$RH\left(z,t\right)_m = measured\ relative\ humidity$$

The matrix in Equation 3.2 can be rewritten and solved as follows:

$$[\beta] = \left[F^T F \right]^{-1} [F]^T [r] \tag{3.3}$$

and the new set of updated parameters required for the next iteration can be obtained as shown below:

$$\alpha(t)_{i+1} = \alpha(t)_i \cdot (1+\beta) \tag{3.4}$$

$$h(t)_{i+1} = h(t)_i \cdot (1+\beta) \tag{3.5}$$

where *i* is the iteration count. For a given time *t* the iterations were continued till the elements in the change vector *[β]* were less than 0.05 and the parameter *α(t)* and *h(t)* were considered as the final result for that given time *t*. The procedure was repeated for the remaining time steps to obtain the history of diffusion coefficient *α* for the given cured concrete specimen. The numerical example of the back calculation procedure is provided in Section 4.

3.2 Modeling Lift-off Displacement Due to Curling and Warping

Concrete pavement deforms into a concave configuration when the pavement is subjected to a resultant negative gradient of temperature and moisture through the thickness. The deformation of the slab due to a temperature gradient is called curling and likewise that for moisture gradient is called warping. The tendency of slab deformation due to such gradients can induce tensile stress at the interface of the slab and the

underlying layer. If the negative temperature and moisture gradients are high enough, the interfacial tensile stress will be higher and the slab edge or corner may separate from the underlying structure as in an overlay. Therefore, it is essential to model the slab curling and warping behavior in order to assess the potential for interfacial separation. Westergaard (1926) derived a closed form solution for assessing the interfacial displacement and tensile stress due to the temperature gradients where he characterized the curling or thermal bending stresses in concrete pavements as a result of restrained vertical movements by the dead weight of the slab. His solution was derived based on the assumption that the temperature through the thickness of the slab was linear even though such linear gradient is nonexistent in concrete pavement. His solution has been widely used by other researchers, e.g. Yoder and Witczak (1975) and Okamoto et al. (1991) for estimating the thermal stress in a curled pavement (Tang and Zollinger 1993).

Later, a variation of the methodology was described by Tang and Zollinger (1993) and then by Wang and Zollinger (2000) to determine the slab separation displacement along the slab-underlying structure interface due to curling and warping. The methodology described herein represents an improvement in terms of how boundary conditions were taken into account. Medium-thick plate theory provided the basis for arriving at the different boundary conditions required for modeling the slab corner lift-off displacement. Figure 3.6 presents a concrete slab which is resting on a subgrade and is subjected to curling and warping. The coordinate system of the slab is also shown in the figure. The solution of the displacement w due to curling and warping was assumed to be of the general form shown in Equation 3.6.

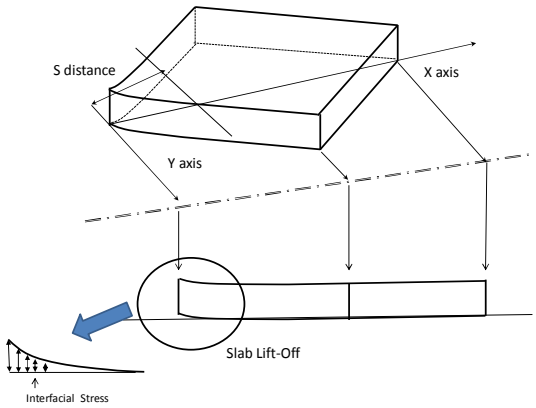

Figure 3.6: Corner Lift-off Displacement Due to Curling and Warping

$$w = \left(A_1 \cos x + A_2 \sin x\right)\left(B_1 \cos y \cosh y + B_2 \sin y \sinh y\right) e^{-x} \tag{3.6}$$

where,

$w = slab\,corner\,displacement$

$A_1, A_2, B_1, B_2 = coefficients$

$X = distance\,along\,the\,X\,axis$

$Y = distance\,along\,the\,Y\,axis$

$x = dimensionless\,distance = X/\ell$

$y = dimensionless\,distance = Y/\ell$

$\ell = radius\,of\,relative\,stiffness = \sqrt[4]{\dfrac{E(t)\cdot h^3}{12\left(1-\nu^2\right)k}}$

$h = slab\,thickness$

$k = modulus\,of\,subgrade\,reaction$

$E = elastic\,modulus\,of\,concrete$

This form of equation was chosen based on its capability to represent the effect of the boundary conditions on the lift-off displacement.

Now letting the bending moment and the shear force in the *X* direction be denoted as M_x and V_x, respectfully per unit width of the cross section and using the medium-plate theory, the moment at the slab corner, i.e. at (0, 0), can be expressed as:

$$M_x = D\left\{\frac{\partial^2 w}{\partial x^2} + \nu\frac{\partial^2 w}{\partial y^2} + \frac{\varepsilon(1+\nu)}{h}\right\} = 0 \tag{3.7}$$

where,

$$\nu = Poisson's\ ratio$$

$$\varepsilon = total\ strain$$

$$D = flexural\ rigidity\ of\ slab = \frac{E(t)\cdot h^3}{12(1-\nu^2)}$$

The other variables in Equation 3.7 were denoted in Equation 3.6. It should be noted that the total strain ε is composed of thermal strain, drying shrinkage strain, and creep strain.

Assuming that the slab corner detaches itself from the underlying layer due to curling and warping and let the separation distance of the slab along the *X* direction be denoted as *S*, i.e. the slab is in contact with the underlying layer at a distance *S* from the corner along the *X* axis. The bending moment at the point of contact, i.e. (S, 0), in the *X* direction can be given as:

$$M_x = D\left\{\frac{\partial^2 w}{\partial x^2} + \nu\frac{\partial^2 w}{\partial y^2} + \frac{\varepsilon(1+\nu)}{h}\right\} = -\frac{1}{6}S^2 h\rho \tag{3.8}$$

where ρ is the density of concrete.

Because the slab has not separated from the underlying layer at a distance $X=S$, the deflection at that point will still be zero. Hence, the deflection at the point of contact can be written as:

$$\left(A_1 \cos s + A_2 \sin s\right) B_1 \, e^{-s} = 0 \tag{3.9}$$

where $s = S/\ell$ and other variables were denoted before.

Using the medium-thick plate theory, the equation for shear force can also be written for the given curling-warping lift-off displacement problem. The shear force along the X axis denoted as V_x at the corner of the slab, i.e. at (0, 0), is zero and can be expressed as:

$$V_x = D\left(\frac{\partial^3 w}{\partial x^3} + \nu\frac{\partial^3 w}{\partial x \partial y^2}\right) = 0 \tag{3.10}$$

Once the slab corner deflects upward from the ground, the shear force at the point of lift-off along the X axis, i.e. at $X=S$ and $Y=0$, has to be equal to the dead weight

of the portion of the slab that has separated itself from the underlying layer. The shear force along the *X* axis at the point of contact can be given as:

$$V_x = D\left(\frac{\partial^3 w}{\partial x^3} + \nu\frac{\partial^3 w}{\partial x \partial y^2}\right) = -\frac{1}{2}Sh\rho \tag{3.11}$$

Substituting the expression for deflection *w* in Equation 3.6 into Equations 3.7 through 3.11 and after simplifying these equations, the end expressions are given in order in Equations 3.12 through 3.16 as follows.

$$A_2 B_1 - \nu A_1 B_2 - \frac{\varepsilon(1+\nu)}{h}\cdot\frac{l^2}{2} = 0 \tag{3.12}$$

$$\begin{aligned}&\left(A_1 \sin s - A_2 \cos s\right) B_1 + \nu\left(A_1 \cos s + A_2 \sin s\right) B_2 \\ &\qquad = \frac{l^2 e^s}{2}\left(-\frac{S^2 h\rho}{6D} - \frac{\varepsilon(1+\nu)}{h}\right)\end{aligned} \tag{3.13}$$

$$\left(A_1 \cos s + A_2 \sin s\right) B_1\, e^{-s} = 0 \tag{3.14}$$

$$B_1\left(A_2 + A_1\right) - B_2\left(A_1 - A_2\right) = 0 \tag{3.15}$$

$$\begin{aligned}&\left\{A_1\left(\cos s - \sin s\right) + A_2\left(\sin s + \cos s\right)\right\}\left(B_1\right) \\ &+\left\{\left(A_2 - A_1\right)\cos s - \left(A_2 + A_1\right)\sin s\right\}\ \left(B_2\right) = -\frac{Sh\rho l^3 e^s}{4D}\end{aligned} \tag{3.16}$$

For a given curling and warping situation material properties, such as υ, ρ, k, $E(t)$, and slab dimensions such as, length, width, and thickness h, are known beforehand. In the above mentioned system of equations there are five unknowns A_1, A_2, B_1, B_2, and S that need to be solved. Since there are five equations as well as five unknowns, the system of equations can be solved for a given total strain ε. The corresponding vertical displacement w and the delamination or separation distance S can then be obtained for the given curling and warping problem.

3.3 Modeling Climatic Stress in Concrete

Placement of concrete at the construction site exposes concrete pavement to environmental excitations, such as temperature and moisture variations. Concrete slab experience volume change due to such excitations and this results in the development of undesired stress even before being exposed to traffic loading. Once the stress is sustained in the structure, concrete will exhibit time dependent deformation called creep. Besides these, the material properties will evolve with time as the hydration reaction continues. All these complicated aspects make it difficult to predict the structural response of concrete due to the temperature and moisture variations as well as due to the applied mechanical load (Lee 2007).

The material model used in this research was a combination of the models proposed by Lee et al. (2011) and D'Ambrosia (2011). The model has components that represents the instantaneous response to stress, delayed response to stress (i.e. creep),

volume change due to temperature and moisture variation, as well as the effect of aging on its properties. Figure 3.7 shows the material model used in this study.

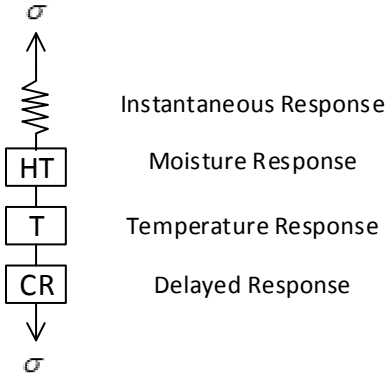

Figure 3.7: Components of Material Model for Aging Concrete (after Lee 2007)

Each component in the material model is connected in series indicating that each of the strain components are independent of each other and the total strain can be obtained by accumulating the individual strain components. It should be noted that the superposition of strains is only valid for infinitesimal strain assumptions. In this research, it was assumed that the concrete structure was uncracked and hence the strain was small enough making the infinitesimal strain assumption to be valid. Based on the series model, the total strain can be expressed as:

$$\varepsilon_{Total} = \varepsilon_{EL} + \varepsilon_{T} + \varepsilon_{HT} + \varepsilon_{CR} \tag{3.17}$$

where,

$$\varepsilon_{Total} = total\ strain$$

$$\varepsilon_{EL} = elastic\ strain$$

$$\varepsilon_{T} = thermal\ strain$$

$$\varepsilon_{HT} = hygrothermal\ strain$$

$$\varepsilon_{CR} = creep\ strain$$

In the incremental form, Equation 3.17 can be rewritten as:

$$\Delta\varepsilon_{Total} = \Delta\varepsilon_{EL} + \Delta\varepsilon_{T} + \Delta\varepsilon_{HT} + \Delta\varepsilon_{CR} \tag{3.18}$$

An internal material model representing the solid skeleton and an external material model representing the porous body proposed by D'Ambrosia (2011) were used to model the elastic strain, hygrothermal strain, and creep strain components. The conceptual diagram for the model is shown in Figure 3.8. Combination of the internal and external material models enabled to perform the coupled shrinkage and creep analysis. It should be noted that the internal model responds to the applied stress σ as well as the capillary stress p, whereas the external model responds only to the applied stress σ. The GKM models used by D'Ambrosia (2011) for representing the internal and external components are presented in Figure 3.9.

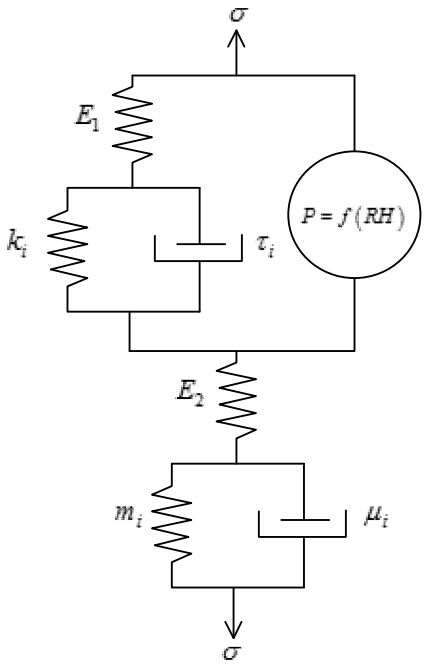

Figure 3.8: Model Concept Diagram Showing Internal and External Material Models (D'Ambrosia 2011)

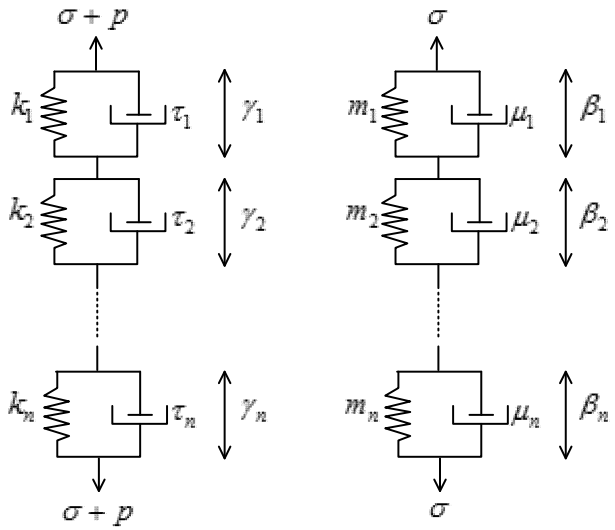

Figure 3.9: GKM Diagram for the Material Component (D'Ambrosia 2011)

3.3.1 Model for Thermal Strain

Concrete expands and contracts due to increase and decrease in temperature, respectively. Thermal strain ε_T in concrete can be calculated from the coefficient of thermal expansion α and the change in temperature ΔT. Thermal strain can be expresses as follows.

$$\varepsilon_T = \alpha \cdot \Delta T \tag{3.19}$$

For a short time interval Δt the increment in thermal strain can be written as follows.

$$\Delta\varepsilon_T = \varepsilon_T\left(t+\Delta t\right) - \varepsilon_T\left(t\right) \tag{3.20}$$

3.3.2 Hygrothermal Model for Drying Shrinkage

The model for drying shrinkage due to moisture variation has been reviewed (see Equation 2.55) in Section 2 and is restated here for convenience.

$$\varepsilon = \frac{pS}{3}\left[\frac{1}{K} - \frac{1}{K_S}\right] \tag{3.21}$$

where,

$$p = pore\ fluid\ pressure$$

$$S = saturation\ factor$$

$$K = bulk\ modulus\ of\ concrete$$

$$K_S = bulk\ modulus\ of\ solid\ skeleton$$

The pore fluid pressure can be computed using the Kelvin-Laplace equation shown in Equation 2.54. The bulk modulus can be obtained from the modulus of elasticity with a constant Poisson's ratio. The saturation factor *S* can be described using the desorption isotherm that states the relationship between the saturation and the relative humidity. An approximate relationship for *S* as a function of the relative humidity was proposed by D'Ambrosia (2011) and this expression for *S*, as shown in Equation 3.22, was used in this study.

$$S = \frac{RH}{100} \tag{3.22}$$

where,

$$RH = relative\ humidity$$

For a short time interval Δt the hygrothermal strain can be written in incremental form as follows.

$$\Delta\varepsilon_{HT} = \varepsilon_{HT}(t+\Delta t) - \varepsilon_{HT}(t) \tag{3.23}$$

3.3.3 Model for Delayed Response (Creep) of Concrete

3.3.3.1 Solidifying Model for Creep

Lee et al. (2011) employed a model for creep based on the solidifying material theory (Bazant, 1977) and the implementation of the solidifying material model was based on the work done by Bazant and Prasanna (1989a, 1989b). D'Ambrosia (2011) also used the solidification theory to derive a material model for aging concrete. The creep model employed in this research was based on the work done by D'Ambrosia (2011).

The material model, as described previously in this section, consisted of an internal set and an external set as shown in Figure 3.8. The model had two components: (i) non-aging viscoelastic response of the hydration product, and (ii) aging effect incorporated by the effective load-bearing volume growth of the hydration product. The one dimensional expression of the creep rate of the internal and external viscoelastic component can be given as:

$$\dot{\varepsilon}_{CR_{INT}} = \frac{\dot{\gamma}_{CR_{INT}}}{v(t)} \tag{3.24}$$

$$\dot{\varepsilon}_{CR_{EXT}} = \frac{\dot{\gamma}_{CR_{EXT}}}{v(t)} \tag{3.25}$$

where,

$$\dot{\gamma}_{CR_{INT}} \text{ and } \dot{\gamma}_{CR_{EXT}} = non-aging\ viscoelastic\ response$$

$$v(t) = effective\ \ load-bearing\ volume$$

The effective load bearing volume can be given as:

$$\frac{1}{v(t)} = \left(\frac{\lambda_o}{t}\right)^m + \alpha \tag{3.26}$$

where m, λ_o, and α are material constants that depend on the hydration rate. The non-aging viscoelastic response of the model was implemented using separate chains of GKMs for both the internal and the external material components as shown in Figure 3.9. Assuming that the stress in the solid material varies linearly during the short interval Δt the incremental creep response can be computed according to Equation 3.27.

$$\begin{aligned}\Delta\gamma = &\frac{1}{v(t_o)}\sum_{i=1}^{n}\left[\frac{(\Delta\sigma+\Delta p)}{k_i}\left\{1-\frac{\tau_i}{\Delta t}\left(1-e^{-\Delta t/\tau_i}\right)\right\}+\left(\frac{\sigma+p}{k_i}-\gamma_i\right)\left(1-e^{-\Delta t/\tau_i}\right)\right] \\ &+\frac{1}{v(t_o)}\sum_{i=1}^{n}\left[\frac{\Delta\sigma}{m_i}\left\{1-\frac{\mu_i}{\Delta t}\left(1-e^{-\Delta t/\mu_i}\right)\right\}+\left(\frac{\sigma}{m_i}-\beta_i\right)\left(1-e^{-\Delta t/\mu_i}\right)\right]\end{aligned} \tag{3.27}$$

where,

$\Delta\sigma = incremental\ stress$

$\Delta p = incremental\ pore\ fluid\ pressure$

$k_i\ and\ m_i = internal\ and\ external\ Kelvin\ chains$

$\tau_i\ and\ \mu_i = internal\ and\ external\ retardation\ time$

The specific creep compliance exhibit different behavior under uniaxial tension versus compression (Atrushi 2003). This directional characteristics of creep was incorporated here in a similar manner following the work of Lee et al. (2011). Depending on the stress status, either tension or compression, the parameters of the internal and external GKMs were modified as follows:

for internal set,

$$k_i = k_i^{tension} \; for\left(\sigma + p\right) > 0 \tag{3.28}$$

$$k_i = k_i^{compression} \; for\left(\sigma + p\right) < 0 \tag{3.29}$$

for external set,

$$m_i = m_i^{tension} \; for\, \sigma > 0 \tag{3.30}$$

$$m_i = m_i^{compression} \; for\, \sigma < 0 \tag{3.31}$$

3.3.4 Scheme for Numerical Analysis

After modeling each strain component, such as thermal, hygrothermal, and creep strain as a function of time, the next step was to compute the stress induced in concrete due to these imposed strains. Piece-wise static analysis was the fundamental scheme for solving this time-dependent problem. The temperature and relative humidity history was divided into n steps of small time interval Δt and with the known stress at the beginning of the time step, the resultant induced stress by the excitation history was obtained and was accumulated at the end of each time step. In this incremental formulation, it was assumed that the material properties were constant at the beginning of the time step. After the completion of the stress computation for a given time step, the material properties were updated at the end of that time step and these updated properties were used at the beginning of the next time step. The formulation described here is for the i^{th} time step. For convenience, all the known information at the beginning of the time step was denoted with a subscript 'o'. For example, the time at the beginning of time step was denoted as t_o and the stress and pore pressure were denoted as σ_o and p_o, respectively. A description of similar numerical implementation can be found in the work done by Lee (2007) and Lee et al. (2011).

The incremental total strain, as shown in Equation 3.18, is restated here for convenience.

$$\Delta\varepsilon_{Total} = \Delta\varepsilon_{EL} + \Delta\varepsilon_{T} + \Delta\varepsilon_{HT} + \Delta\varepsilon_{CR} \tag{3.32}$$

Considering the material model being composed of an internal and an external set as shown in Figure 3.8, the incremental creep strain can be given as:

$$\Delta\varepsilon_{CR} = \frac{1}{v(t_o)}\sum_{i=1}^{n}\left[\left(\frac{\Delta\sigma+\Delta p}{k_i}\right)\left\{1-\frac{\tau_i}{\Delta t}\left(1-e^{-\Delta t/\tau_i}\right)\right\}+\left(\frac{\sigma_o+p_o}{k_i}-\gamma_i\right)\left(1-e^{-\Delta t/\tau_i}\right)\right]$$
$$+\frac{1}{v(t_o)}\sum_{i=1}^{n}\left[\frac{\Delta\sigma}{m_i}\left\{1-\frac{\mu_i}{\Delta t}\left(1-e^{-\Delta t/\mu_i}\right)\right\}+\left(\frac{\sigma_o}{m_i}-\beta_i\right)\left(1-e^{-\Delta t/\mu_i}\right)\right] \tag{3.33}$$

And the elastic strain can be written as:

$$\Delta\varepsilon_{EL} = \Delta\sigma\left[\frac{1}{E_1(t_o)}+\frac{1}{E_2(t_o)}\right] \tag{3.34}$$

Substituting Equations 3.33 and 3.34 into Equation 3.32, total strain increment can be expressed as:

$$\Delta\varepsilon_{Total} = \Delta\sigma\left[\frac{1}{E_1(t_o)}+\frac{1}{E_2(t_o)}\right]+\Delta\varepsilon_T+\Delta\varepsilon_{HT}$$
$$+\frac{1}{v(t_o)}\sum_{i=1}^{n}\left[\left(\frac{\Delta\sigma+\Delta p}{k_i}\right)\left\{1-\frac{\tau_i}{\Delta t}\left(1-e^{-\Delta t/\tau_i}\right)\right\}+\left(\frac{\sigma_o+p_o}{k_i}-\gamma_i\right)\left(1-e^{-\Delta t/\tau_i}\right)\right] \tag{3.35}$$
$$+\frac{1}{v(t_o)}\sum_{i=1}^{n}\left[\frac{\Delta\sigma}{m_i}\left\{1-\frac{\mu_i}{\Delta t}\left(1-e^{-\Delta t/\mu_i}\right)\right\}+\left(\frac{\sigma_o}{m_i}-\beta_i\right)\left(1-e^{-\Delta t/\mu_i}\right)\right]$$

After rearranging Equation 3.35, the incremental stress can be given as:

$$\Delta\sigma = J^{-1}\cdot\left(\Delta\varepsilon_{Total} - \Delta\varepsilon_{T} - \Delta\varepsilon_{HT} - \Delta\overline{\varepsilon_{CR}}\right) \tag{3.36}$$

where,

$$J = compliance\ \ function\ at\ each\ time\ step$$

$$= \frac{1}{E_1(t_o)} + \frac{1}{E_2(t_o)} + \frac{1}{v(t_o)}\sum_{i=1}^{n}\frac{1}{k_i}\left\{1 - \frac{\tau_i}{\Delta t}\left(1 - e^{-\Delta t/\tau_i}\right)\right\}$$

$$+ \frac{1}{v(t_o)}\sum_{i=1}^{n}\frac{1}{m_i}\left\{1 - \frac{\mu_i}{\Delta t}\left(1 - e^{-\Delta t/\mu_i}\right)\right\}$$

$$\Delta\overline{\varepsilon_{CR}} = \frac{1}{v(t_o)}\sum_{i=1}^{n}\left[\frac{\Delta p}{k_i}\left\{1 - \frac{\tau_i}{\Delta t}\left(1 - e^{-\Delta t/\tau_i}\right)\right\} + \left(\frac{\sigma_o + p_o}{k_i} - \gamma_{io}\right)\left(1 - e^{-\Delta t/\tau_i}\right)\right]$$

$$+ \frac{1}{v(t_o)}\sum_{i=1}^{n}\left(\frac{\sigma_o}{m_i} - \beta_{io}\right)\left(1 - e^{-\Delta t/\mu_i}\right)$$

At the beginning of each time step, thermal strain, hygrothermal strain, and $\Delta\overline{\varepsilon_{CR}}$ are known quantities. Therefore if the total strain is known, the stress increment at each time step can be computed from Equation 3.36.

3.4 Probabilistic Model for Structural Failure

Structural failure of concrete is a broad aspect that requires consideration during the design phase. In this study two modes of failure, such as (i) lift-off displacement and (ii) cracking were considered to assess and evaluate the given design and construction scheme. Assessment of the reliability of a given design and construction scenario can be performed by adopting the Stress-Resistance (S-R) model which is commonly applied to structural safety evaluation (Ang and Tang 1984; Tokumaru et al. 1987; JSCE 2002; van Breugel and Lockhorst 2001; Kanda et al. 2008).

When applying the S-R model to the problem of cracking, it is assumed that cracking will be induced when the restrained stress (the crack driving force, S) exceeds the critical level of tensile strength (the resistance force, R) of concrete, i.e. $S \geq R$. In this research, the stress was denoted by σ and the strength was denoted by f with an appropriate subscript.

The probability of failure, for instance cracking, can be modeled assuming that the σ and the f are random variables and they follow a certain probability distribution. Therefore, following the work of Nakamura et al. (1999), the probability of cracking P_{cr} can be expresses as:

$$P_{cr} = \mathrm{P}\left(Z = \sigma_{cr} - f_t \geq 0\right) \tag{3.37}$$

Imamoto et al. (2004) simplified the calculation of P_{cr} as shown in Equation 3.38 by assuming that σ_{cr} and f_t are independent from each other and they follow normal distribution.

$$P_{cr} = \phi\left[\frac{\xi - 1}{\sqrt{COV\left[f_t\right]^2 + \xi^2 \cdot COV\left[\sigma_{cr}\right]^2}}\right] \tag{3.38}$$

where,

$\phi = standard\ normal\ probability\ distribution\ function$

$\sigma_{cr} = cracking\ stress$

$f_t = tensile\ strength\ of\ concrete$

$COV\left[\sigma_{cr}\right] = coefficient\ of\ variation\ of\ \sigma_{cr}$

$COV\left[f_t\right] = coefficient\ of\ variation\ of\ f_t$

$$\xi = \frac{\mu_\sigma}{\mu_f}$$

$\mu_{\sigma_{cr}} = expected\ value\ of\ \sigma_{cr}$

$\mu_{f_t} = expected\ value\ of\ f_t$

After simplification, Equation 3.38 can be rewritten as

$$P_{cr} = \phi\left[\frac{\xi - 1}{\sqrt{COV\left[f_t\right]^2 + \xi^2 \cdot COV\left[\sigma_{cr}\right]^2}}\right] \tag{3.39}$$

Using a similar analogy as described above, the probability of lift-off or debonding can also be computed. The lift-off or separation of a slab will occur when the debonding stress (force inducing lift-off, $\sigma_{lift\text{-}off}$) exceeds the tensile bond strength of concrete (the resistance force, f_{tb}). The probability of lift-off can be modeled in a similar manner like Equation 3.37 (Nakamura et al. 1999), that is

$$P_{lift-off} = \mathrm{P}\left(Z = \sigma_{lift-off} - f_{tb} \geq 0\right) \tag{3.40}$$

Equation 3.40 can be further simplified as Equation 3.39 as follows:

$$P_{lift-off} = \phi\left[\frac{\mu_{\sigma_{lift-off}} - \mu_{f_{tb}}}{\sqrt{\mu_{\sigma_{lift-off}}{}^2 \cdot COV\left[\sigma_{lift-off}\right]^2 + \mu_{f_{tb}}{}^2 \cdot COV\left[f_{tb}\right]^2}}\right] \tag{3.41}$$

where,

$\phi = standard\ normal\ probability\ distribution\ function$

$\sigma_{lift-off} = lift-off\ or\ debonding\ stress$

$f_{tb} = tensile\ bond\ strength\ of\ concrete$

$COV\left[\sigma_{lift-off}\right] = coefficient\ of\ variation\ of\ \sigma_{lift-off}$

$COV\left[f_{tb}\right] = coefficient\ of\ variation\ of\ f_{tb}$

$\mu_{\sigma_{lift-off}} = expected\ value\ of\ \sigma_{lift-off}$

$\mu_{f_{tb}} = expected\ value\ of\ f_{tb}$

Therefore, using Equations 3.39 and 3.41 the probability of cracking as well as the probability of lift-off can be assessed, respectively with time. The concept of the probability of failure has been demonstrated in Figure 3.10 according to the description given above. The intersection between the stress and the strength distribution represents the area of failure (or the probability of failure) as enclosed within the thick line in the following figure.

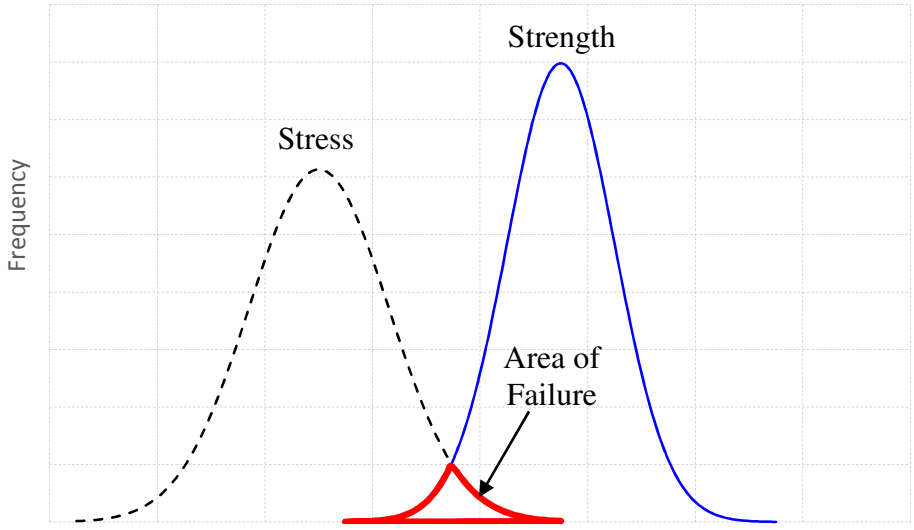

Figure 3.10: Stress and Strength as the Normally Distributed Variables (after Radlinska 2008)

4. NUMERICAL SIMULATION RESULTS AND VALIDATION

In the preceding section, several model formulations were presented and described. In this section, the validation as well as the application of those models were discussed. In the first subsection, the application of the back-calculation procedure was outlined for obtaining the diffusion coefficients of concrete samples cured with different curing compounds. With the quantified diffusion coefficients, the concept of curing index and overall curing index were proposed to facilitate the comparison and the decision making with regard to curing compound selection. The following two subsections describe the validation efforts for the corner lift-off displacement model and the climatic stress model for concrete pavement. The material properties as well as other information used in the validation procedure were obtained from the slab test performed by Jeong and Zollinger (2005). The fourth subsection dealt with the validation effort of the probabilistic model for lift-off displacement and cracking failures and the simulation results from the probabilistic models were compared with the field experiment performed by a third entity in Houston, TX. In the fifth subsection, sensitivity analysis was conducted to provide insight regarding the influence of the different important factors on the constructability of overlay and concrete pavement. In the last subsection, the results from the sensitivity analysis were combined to formulate a constructability index to illustrate how the proposed index can assist in decision making with regard to different design and construction scenarios. The different components of the research implementation framework are shown in Figure 4.1.

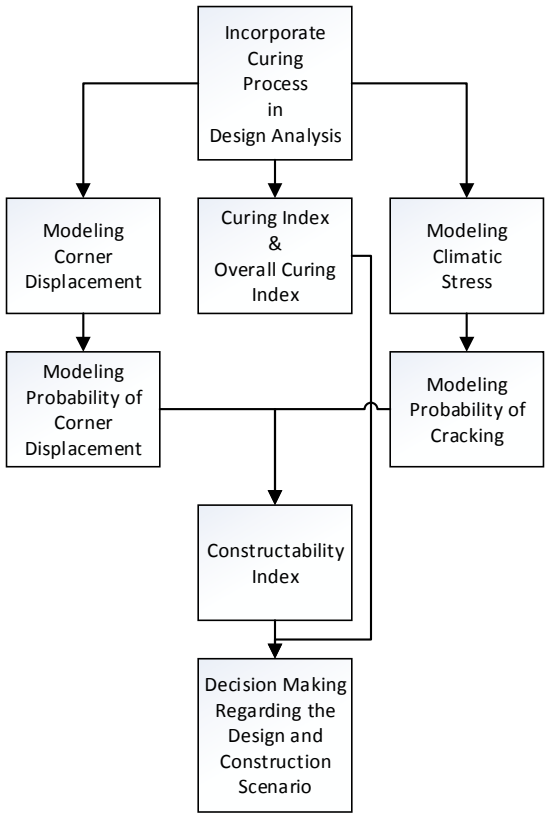

Figure 4.1: Research Implementation Framework

4.1 Back-calculated Diffusion Coefficient of Concrete

In Section 3, laboratory testing regime and mathematical model (see Equations 3.1 through 3.5) for computing the early age diffusion coefficient of concrete cured with curing compound were described. Application of a numerical procedure, i.e. system identification method, for aiding in back-calculation of diffusion coefficient was also discussed. In this section, relative humidity information collected in the laboratory were presented and the resulting back-calculated diffusion coefficients of different cured concrete samples were illustrated.

In order to demonstrate the back-calculation procedure, three different concrete samples with the same water-cement ratio were prepared. In order to facilitate the comparison of the effectiveness of different curing compound, one concrete sample was prepared without applying any curing compound on it and this sample was considered to be as the base case scenario. The other two samples were cured with two different curing compounds in the laboratory. The two different resin based compounds used in this study were denoted by symbolic terms, such as A and B. After preparing the concrete specimens as shown in Figure 3.3, each curing compound was applied on the respective specimens at a rate of one gallon per 225 square feet of concrete surface.

For each specimen, three different relative humidity measurements were obtained: (i) the sealed relative humidity (i.e. inside concrete sample), (ii) the filtered relative humidity (i.e. at concrete surface), and (iii) the ambient relative humidity at a frequent interval. System identification method was used to back-calculate the diffusion coefficients of the different concrete samples for each observation. Figures 4.2 through 4.7, respectively present the collected relative humidity data for the three different concrete samples as well as the corresponding back-calculated diffusion coefficients. It may be noted that for the concrete sample cured with curing compound B, the relative humidity data were collected up to hour 47. The corresponding back-calculated diffusion coefficient indicated that the diffusion coefficient at hour 47 reached a plateau. Hence, the stabilized diffusion coefficient was extrapolated and extended up to hour 72 based on the observed trend to keep the observation range consistent with other samples.

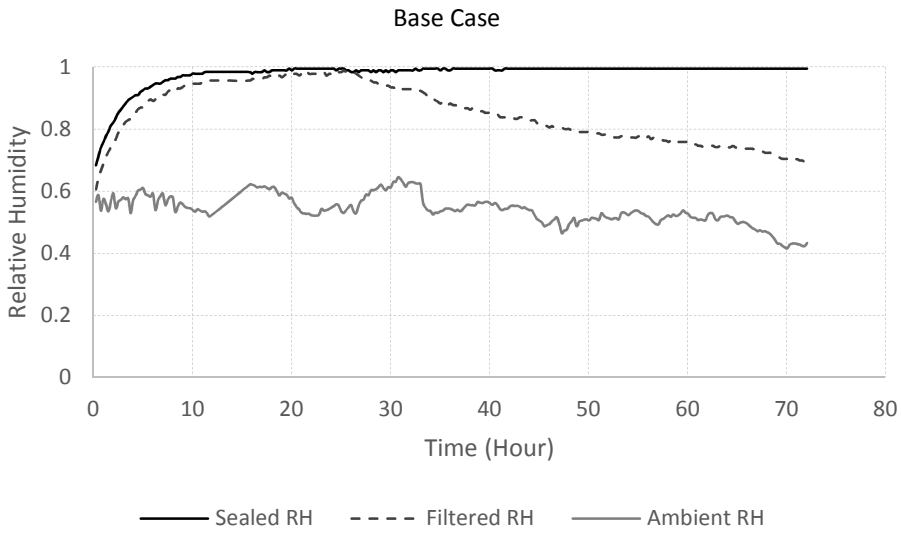

Figure 4.2: Relative Humidity Data for the Base Case

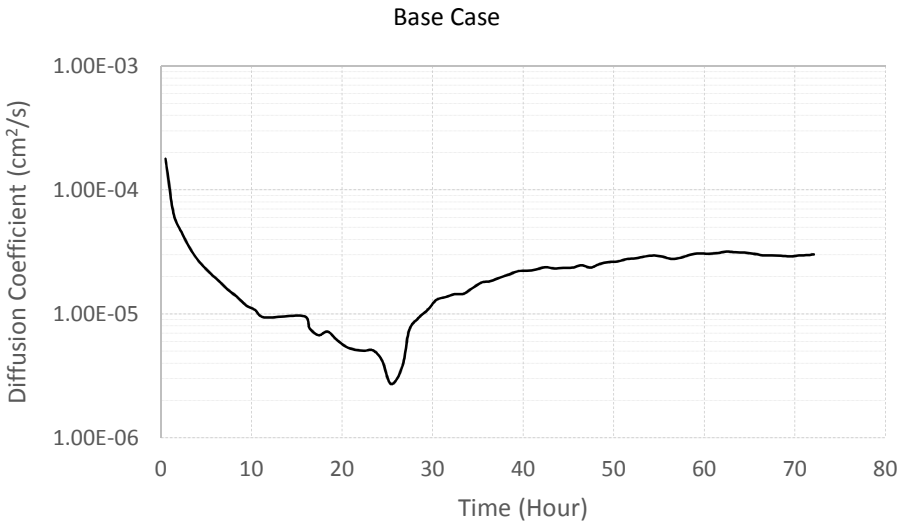

Figure 4.3: Back-calculated Diffusion Coefficient of Concrete for the Base Case

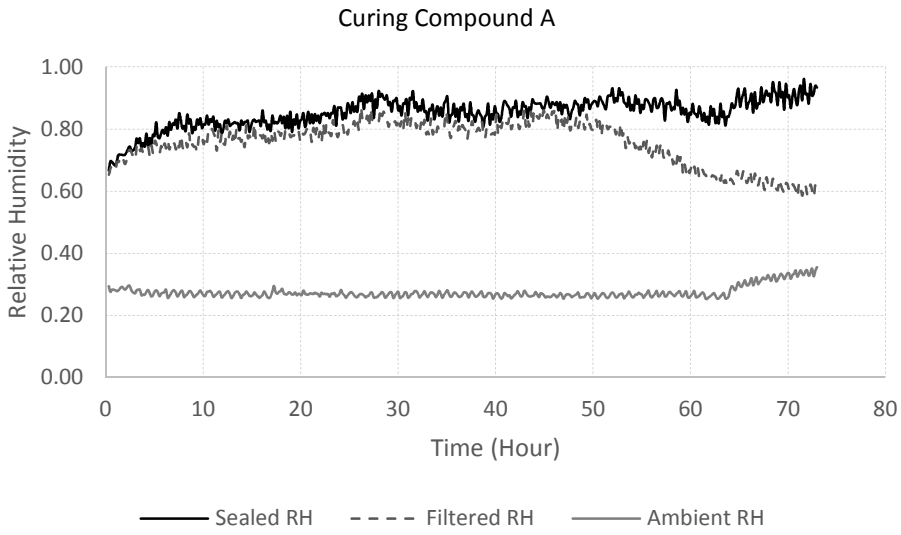

Figure 4.4: Relative Humidity Data for Concrete Cured with Curing Compound A

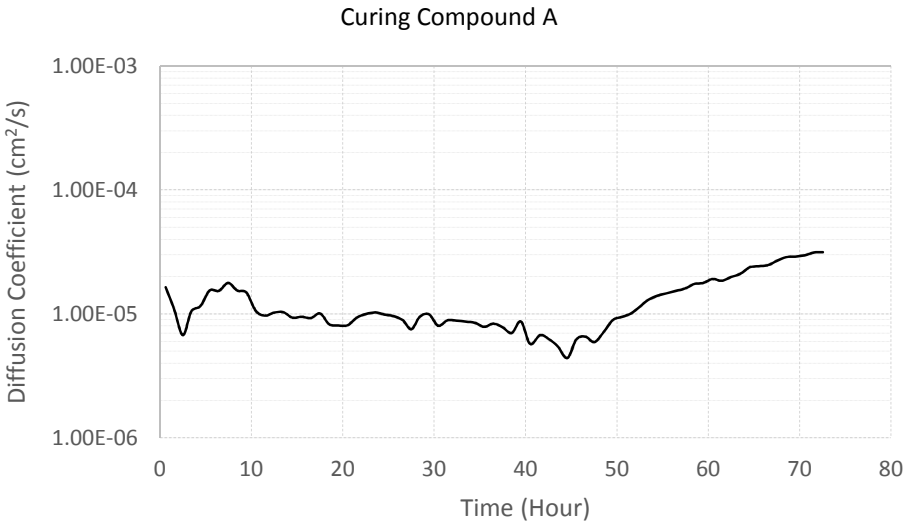

Figure 4.5: Back-calculated Diffusion Coefficient of Concrete with Curing Compound A

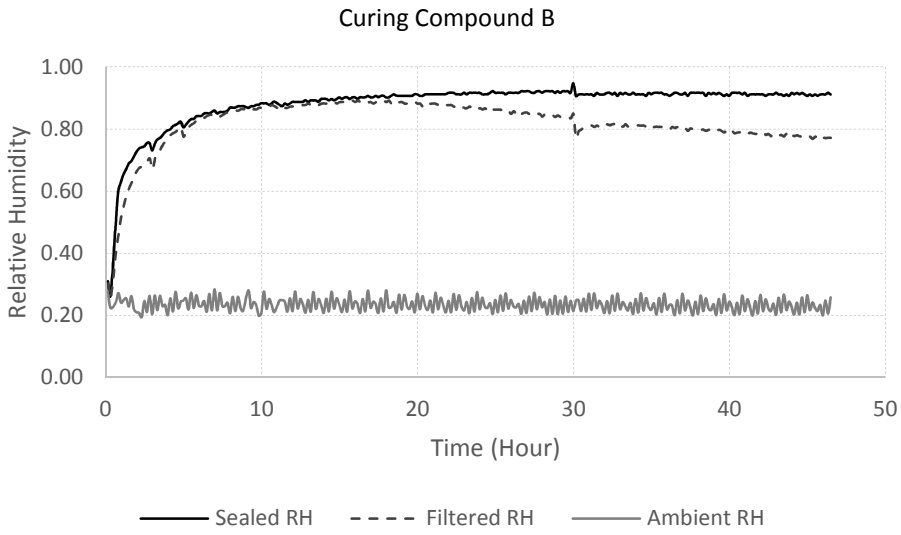

Figure 4.6: Relative Humidity Data for Concrete Cured with Curing Compound B

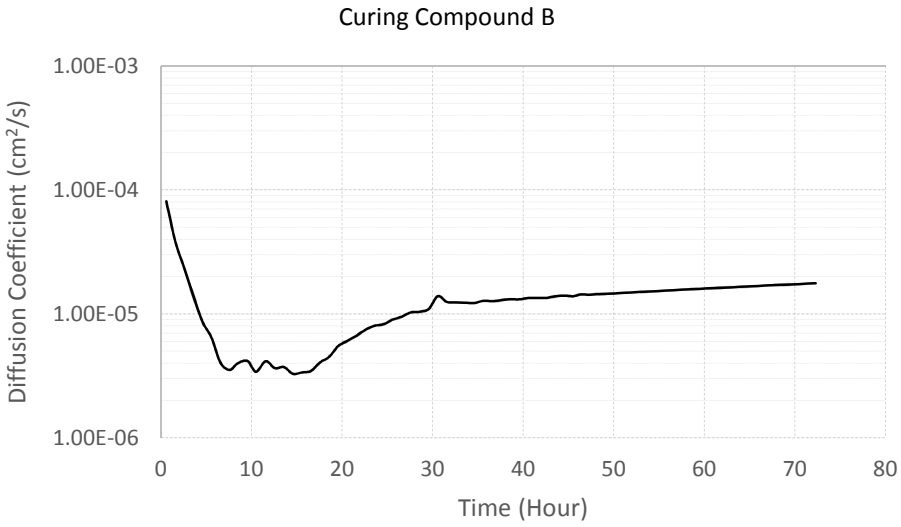

Figure 4.7: Back-calculated Diffusion Coefficient of Concrete with Curing Compound B

It can be seen from Figures 4.3, 4.5, and 4.7 that the diffusion coefficient of cured concrete starts with a higher value (i.e. about 1×10^{-4} cm^2/s) after placement. But as the curing compound (or the bleed water as in the base case) starts becoming effective with time, the diffusion coefficient exhibits a gradual decline in magnitude followed by reaching a lowest value. After some time as the curing compound (or the bleed water as in the base case) starts becoming ineffective, an increase in the value of the diffusion coefficient can be observed exhibiting higher moisture diffusion rate. These histories of diffusion coefficient depict the fact that curing compound helps to minimize the moisture diffusion rate from concrete sample to the surrounding environment. The time dependent back-calculated diffusion coefficient was used as an input in the finite difference moisture model described in Section 2.3 to perform the sensitivity analysis described in the later part of this section.

4.1.1 Curing Index

In order to compare the performance of different curing compounds, a curing index (CI), ranging from 0 to 1, was proposed in this study. The calculated diffusion coefficient obtained from the laboratory test was compared against the two possible extremes, i.e. the lowest possible (worst case) and the highest possible (best case) diffusion coefficient. Since the curing compound acts as an insulation or barrier coating, the lowest possible diffusion coefficient can theoretically be obtained when the curing-insulation prevents any moisture loss from the concrete surface resulting in the concrete surface humidity (i.e. filtered) being equal to or approaching to be equal to the inside concrete humidity

(i.e. sealed). In contrast, when curing-insulation fails to prevent any moisture loss from concrete resulting in the concrete surface humidity being equal to or approaching to be equal to the ambient humidity, the concrete is going to have the highest possible diffusion coefficient. Therefore, a time-dependent curing index was formulated as follows based on the concept stated above:

$$Curing\ Index, CI(t) = \frac{\alpha_{highest}(t) - \alpha_{calc}(t)}{\alpha_{highest}(t) - \alpha_{lowest}(t)} \tag{4.1}$$

where,

$\alpha_{calc}(t) = calculated\ diffusion\ coefficient\ obtained\ \ from\ test\ at\ time\ t$

$\alpha_{lower}(t) = lowest\ \ possible\ diffusion\ coefficient\ at\ time\ t$

$\alpha_{higher}(t) = highest\ \ possible\ diffusion\ coefficient\ at\ time\ t$

A curing compound with CI equal to one indicates that it is able to provide the perfect insulation against moisture loss from concrete whereas a CI of zero would indicate the opposite. For demonstration purpose, the highest, the calculated, and the lowest diffusion coefficient of concrete for the base case is shown in Figure 4.8. The curing indices computed for the base case as well as for the other specimens cured with curing compounds A and B are shown in Figure 4.9. This time dependent CI history can be useful for inspection and monitoring during the construction phase of rigid pavements. For example, the construction manager can monitor the CI curve with time during the

construction and if the CI drops below a certain threshold value, the manager can apply additional coating of curing compound to reach the desired level of CI value.

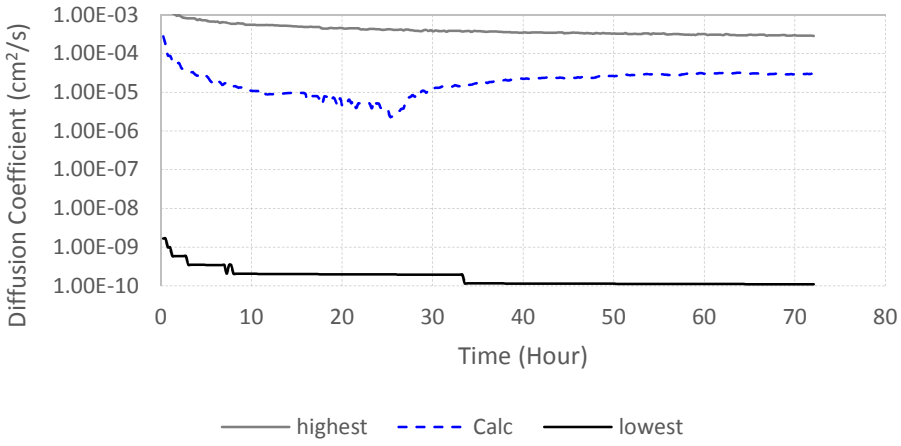

Figure 4.8: Calculated and the Two Extreme Diffusion Coefficients for the Base Case

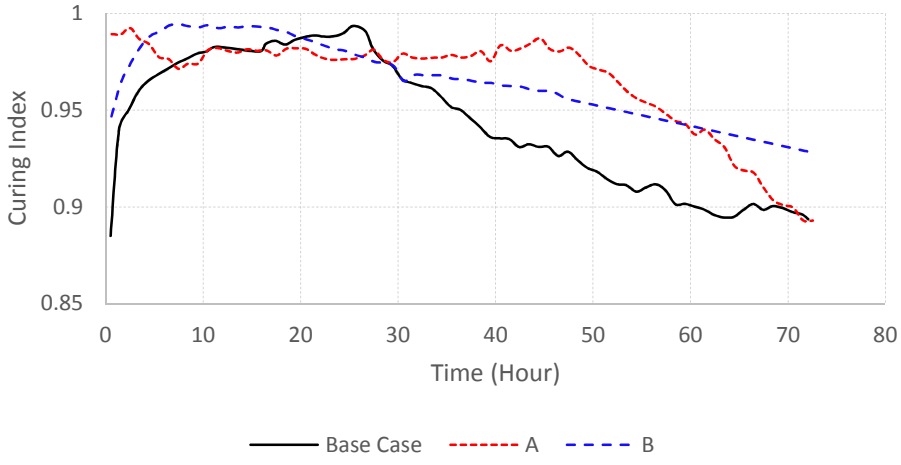

Figure 4.9: Curing Indices for Different Curing Compounds

In order to compare the overall performance of the curing compounds up to a given time span, for example 72 hours, an additional index called the "overall curing index" was proposed which is shown in Equation 4.2. The index was formulated by taking the ratio between the area under the observed curing index curve to the area under the ideal curing index curve. The ideal CI curve would have a value of one throughout the first 72 hours and therefore, the area under the ideal curing index curve would be (72×1.0=) 72 CI-hour. The overall curing indices for the given specimens were computed from the CI histories shown in Figure 4.9 and are presented in Figure 4.10.

$$Overall\,Curing\,Index, CI_{overall} = \frac{area\ under\ the\ CI\ curve}{area\ under\ the\ ideal\ CI\ curve} \tag{4.2}$$

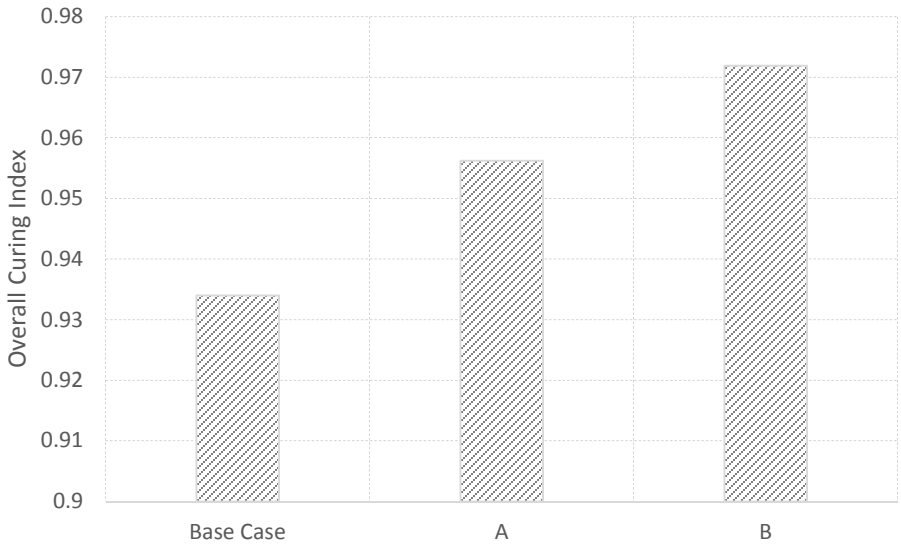

Figure 4.10: Overall Curing Indices for Different Specimens

4.2 Validation of the Lift-off Displacement Model

In this section, the lift-off displacement model proposed in Section 3 (see Equation 3.6) was validated with the experimental data collected by Jeong and Zollinger (2005). They reported information regarding several key parameters, for example the internal temperature and relative humidity, the evolution of strength and elastic modulus, the unit weight, the coefficient of thermal expansion, and the ultimate shrinkage of concrete, that were essential for performing the validation effort. The temperature gradient observed at the setting time of concrete, called the set gradient, was taken into consideration during the validation process. The concrete properties and the pertinent information required for this validation are presented in Table 4.1.

Table 4.1. Concrete Properties and Pertinent Data

Thickness (in)	Unit Weight (lb/ft^3)	Poisson's Ratio	Modulus of Subgrade Reaction, (pci)	Coefficient of Thermal Expansion (per °C)	Ultimate Shrinkage
12	144	0.15	100	11.3×10^{-6}	524×10^{-6}

The thermal strain was calculated using the simple linear thermal strain model described in Section 2. The temperature differences or gradients between the top and the bottom of the pavement were calculated from the measured temperatures at different locations across the slab thickness, reported by Jeong and Zollinger (2005). The nonlinear temperature gradient was converted to an equivalent linear temperature gradient ΔT_{eq}, as shown in Equation 2.40 in Section 2, following the method proposed by Mohamed and Hansen (1996).

The set gradient or the built-in gradient of slab, i.e. the temperature gradient observed during the final setting time of concrete, was accounted for in the analysis. According to Jeong and Zollinger (2005), the concrete was placed at 10:15 am and the final set occurred at 3:30 pm. The temperature gradient observed during the setting time of concrete is presented in Figure 4.11. The coordinate across the slab thickness was set equal to zero at the mid slab and the coordinate was considered to be positive while moving upward from the mid slab and vice versa. The equivalent temperature set gradient computed using Equation 2.40 was found to be +10.89 °C. The positive temperature gradient indicated that the temperature at the slab surface was higher than that at the bottom during setting. As the temperature difference between the top and the bottom of the slab starts dropping below +10.89 °C, the slab corner will tend to curl up and hence the built-in temperature gradient in this case was computed as -10.89 °C. Figure 4.12 shows the equivalent linear temperature gradient and the equivalent linear temperature gradient including the set gradient defined as the effective linear temperature gradient between the top and the bottom of the pavement.

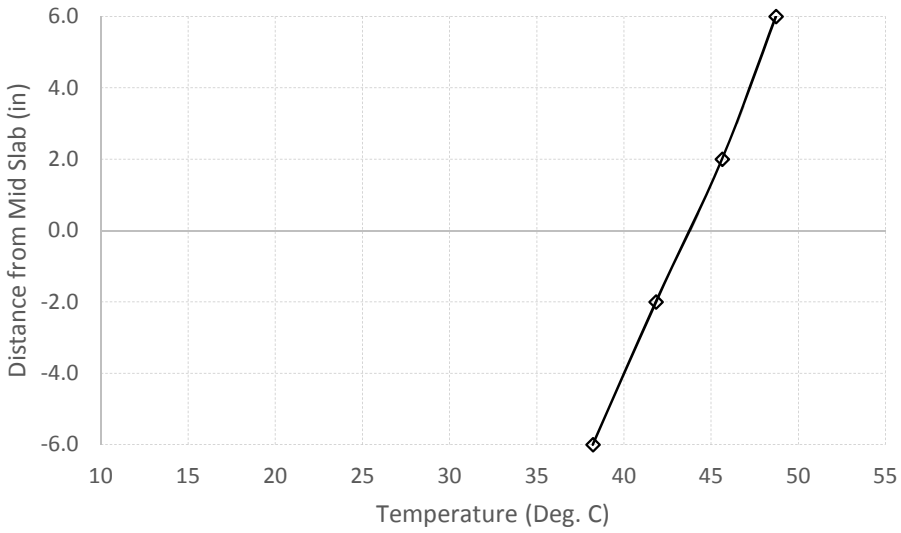

Figure 4.11: Temperature Measurements across the Slab Thickness

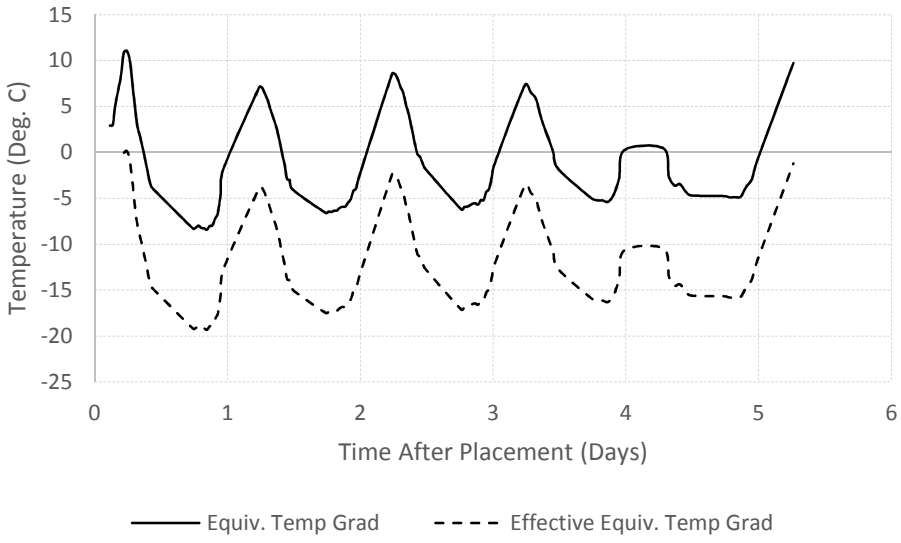

Figure 4.12: Equivalent and Effective Equivalent Temperature Gradient

The thermal strain including the built-in curling was computed using Equation 2.41 given in Section 2 and is rewritten here for convenience.

$$\varepsilon_T = \alpha \cdot \Delta T_{eq} + \alpha \cdot \Delta T_{set} \tag{4.3}$$

where,

$\varepsilon_T = thermal\ strain$

$\alpha = coefficient\ of\ thermal\ expansion$

$\Delta T_{eq} = equiavent\ linear\ temperature\ difference$

$\Delta T_{set} = equiavent\ linear\ temperature\ difference\ during\ setting$

The value of the coefficient of thermal expansion was reported in Table 4.1 and the value of ΔT_{set} used in this study was equal to -10.89 °C. The strain associated with the built-in curling was found to be as -1.23×10^{-4}.

The shrinkage strain was computed using the drying shrinkage model shown in Equation 4.4 instead of the model shown in Equation 2.42 because the former indicated a better fit with the corner displacement observations compared to that by the later.

$$\varepsilon_{sh} = \varepsilon_{ult} \cdot \Delta \left[\frac{100 - RH}{100} \right]_{eq} \tag{4.4}$$

where,

$$\varepsilon_{sh} = shrinkage\ strain$$

$$\varepsilon_{ult} = ultimate\ shrinkage\ strain$$

$$\Delta\left[\frac{100 - RH}{100}\right]_{eq} = equiavent\ shrinkage\ potential\ difference$$

$$RH = measured\ relative\ humidity\ within\ pavement$$

The computation of the equivalent linear shrinkage potential difference was performed in a similar fashion to the computation of the equivalent linear temperature difference ΔT_{eq}. The potential for drying shrinkage was obtained by computing the difference between 100% relative humidity and the measured relative humidity at different locations across the slab thickness. Once the shrinkage potential indicated by *(100-RH)/100* was obtained at each location across the slab thickness, the nonlinear shrinkage potential difference between the top and the bottom of the slab was converted to an equivalent linear shrinkage potential difference according to the method proposed by Mohamed and Hansen (1996).

The delayed response of concrete i.e. the creep strain ε_{CR} was computed following the numerical scheme described for Equations 3.32 through 3.36. For the creep function, as shown in Equation 3.33, a series of four Kelvin chains were used in each creep function (internal and external) with the retardation times τ and μ having values of 0.1, 1.0, 10, and 100 days. The coefficients k_i and m_i in Equation 3.33 were calibrated to fit the shrinkage data (Jeong and Zollinger 2005) shown in Figure 4.13.

With the given excitation history, the temperature and relative humidity were divided into n steps of small time interval Δt. In a restrained condition, the structural response of the slab due to the induced excitation was computed at each time step. Once the incremental stress $\Delta\sigma$ was computed using Equation 3.36, the incremental creep strain $\Delta\varepsilon_{CR}$ was updated according to Equation 3.33 for that given time step. The incremental creep strain was accumulated to obtain the total creep strain and the process was repeated for the entire time history of interest.

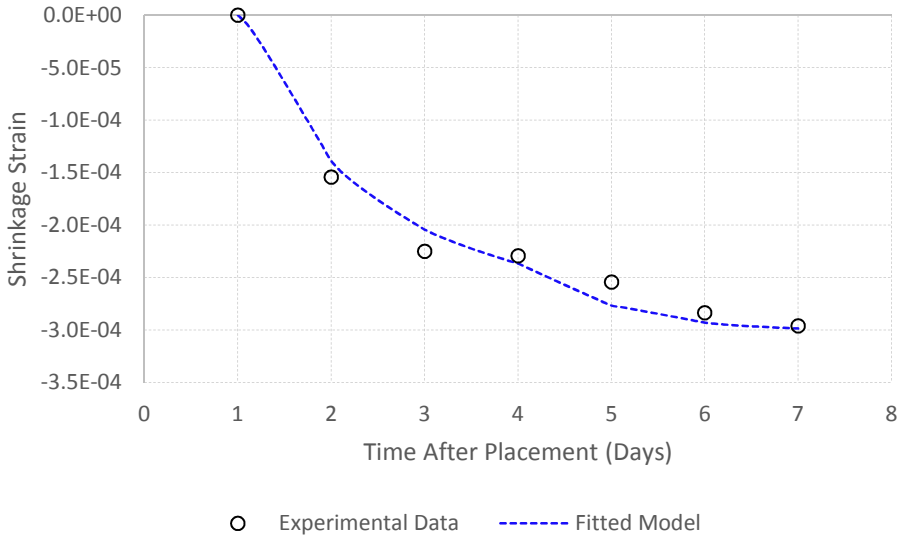

Figure 4.13: Drying Shrinkage Data and Calibrated Shrinkage Model

Finally, the time dependent total strain ε_{Total} was computed by adding the thermal strain, drying shrinkage, and creep strain together as shown below:

$$\varepsilon_{Total}(t) = \varepsilon_{T}(t) + \varepsilon_{sh}(t) + \varepsilon_{CR}(t) \tag{4.5}$$

in which all the variables have been defined before. This total strain was one of the required input for Equations 3.12 through 3.16 for solving the displacement model.

The modulus of elasticity was also another required input that goes into the displacement model. Jeong and Zollinger (2005) computed the evolution of elastic modulus based on field samples and the reported elastic modulus with time is shown in Figure 4.14.

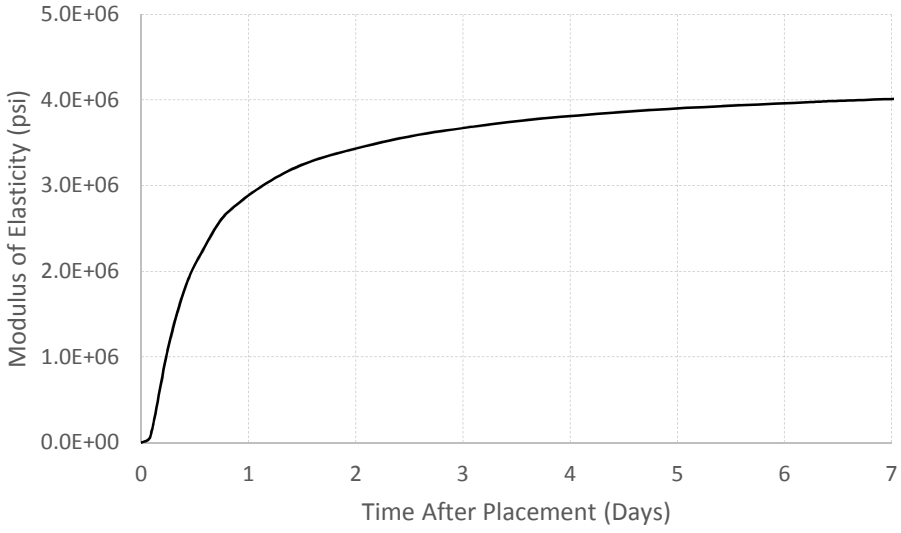

Figure 4.14: Evolution of Modulus of Elasticity (Jeong 2003, Jeong and Zollinger 2005)

The concrete properties shown in Table 4.1 and the elastic modulus *E(t)* shown in Figure 4.14 were provided to the lift-off displacement model. The thermal strain and the shrinkage strain were computed for the given temperature and relative humidity histories reported by Jeong and Zollinger (2005). The creep strain corresponding to the excitation history was computed according to the procedure described above. The lift-off displacement of the pavement observed on the second and fourth day after placement was compared with the model predictions for illustration purpose and the comparisons are shown in Figures 4.15 and 4.16, respectively. It can be observed that the model predictions were in good agreement with the field observations. The displacement of the slab along the diagonal was further computed and few examples of the displacement profiles predicted by the model at different times of the day are shown in Figures 4.17 and 4.18, respectively.

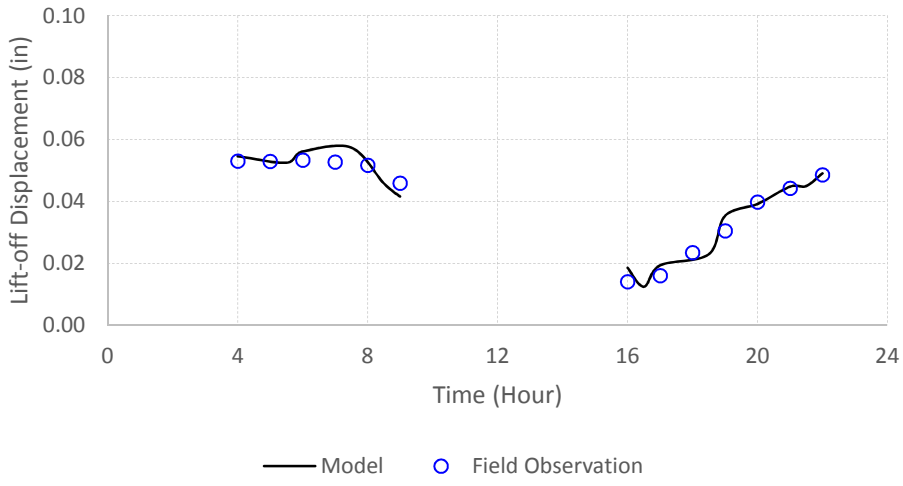

Figure 4.15: Observed Corner Lift-off Displacement and Model Predictions at Day 2

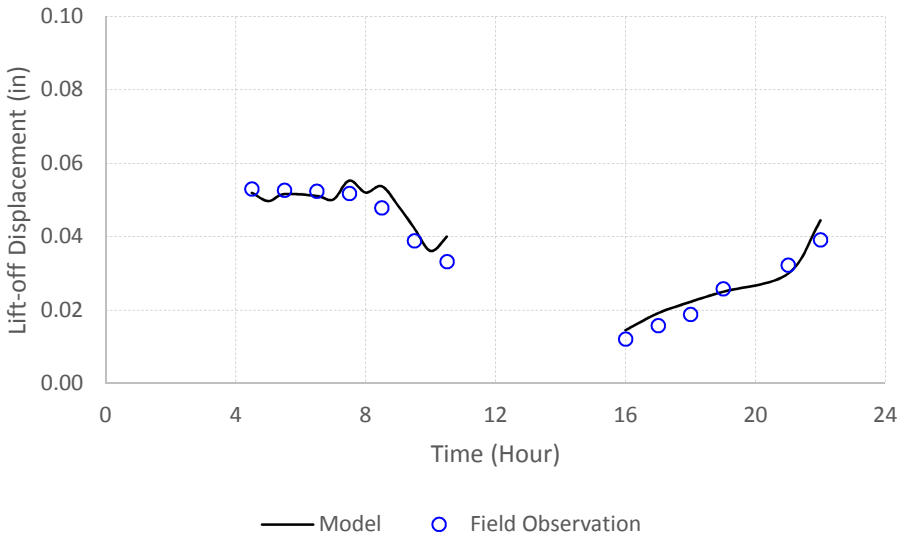

Figure 4.16: Observed Corner Lift-off Displacement and Model Predictions at Day 4

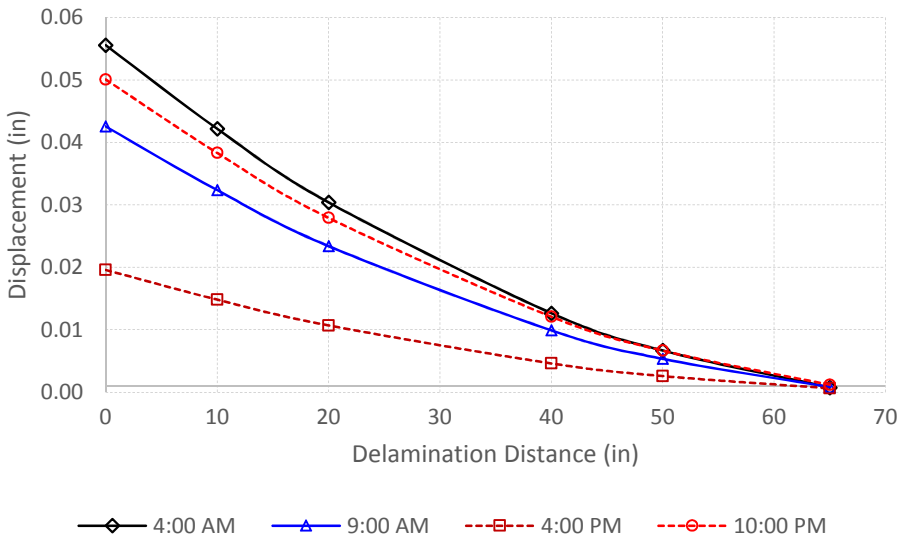

Figure 4.17: Predicted Displacement Profiles at Day 2

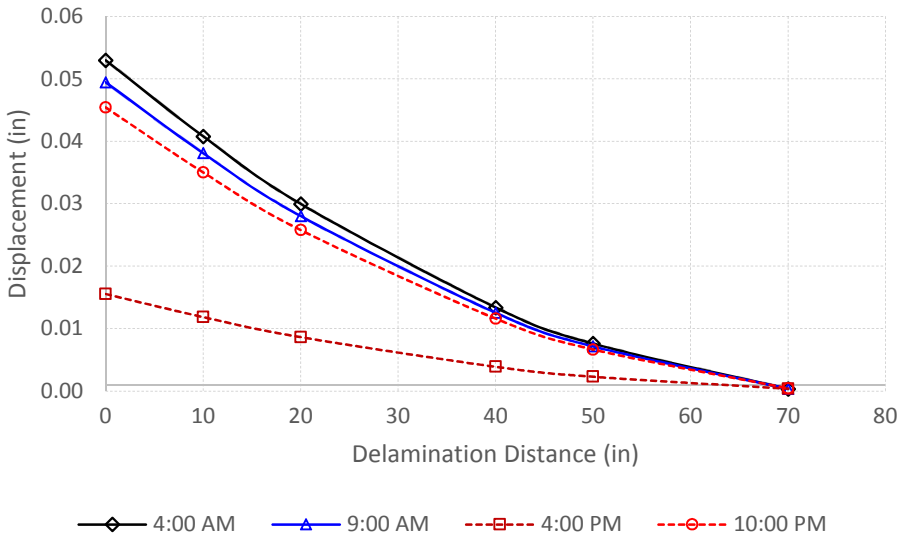

Figure 4.18: Predicted Displacement Profiles at Day 4

4.3 Validation of the Climatic Stress Model

When a slab undergoes bending in both the *x* and *y* directions, for instance as is in the case of temperature curling, the stresses in both directions can be superimposed to obtain the total stress. The stress in the *x* direction due to bending in the *x* direction can be obtained as (Huang 2004):

$$\sigma_x = \frac{E \cdot \varepsilon_x}{1-\nu^2} \tag{4.6}$$

where,

$$\sigma_x = stress\,in\,x\ direction$$

$$\varepsilon_x = strain\ in\,x\ direction$$

$$\nu = Poisson's\,ratio$$

$$E = elastic\,modulus\,of\ concrete$$

The total stress in the *x* direction due to bending in both the *x* and *y* directions can be given as:

$$\sigma_{x_{Total}} = \sigma_x + \nu \cdot \sigma_y \tag{4.7}$$

where, σ_y is the stress in the *y* direction due to bending in the *y* direction.

If Δt is the temperature differential between the top and the bottom of the slab as shown in Figure 4.19 and α be the coefficient of thermal expansion, the maximum strain in the *x* and *y* directions for a completely restrained slab can be given as:

$$\varepsilon_x = \varepsilon_y = \frac{\alpha \cdot \Delta t}{2} \tag{4.8}$$

where, ε_y is the strain in *y* direction. Therefore, the total stress in the *x* direction, shown in Equation 4.7 due bending in both the *x* and *y* directions can be written as:

$$\sigma_{x_{Total}} = \frac{E \cdot \left(\frac{\alpha \cdot \Delta t}{2} \right)}{1-\nu^2} + \nu \cdot \frac{E \cdot \left(\frac{\alpha \cdot \Delta t}{2} \right)}{1-\nu^2} \tag{4.9}$$

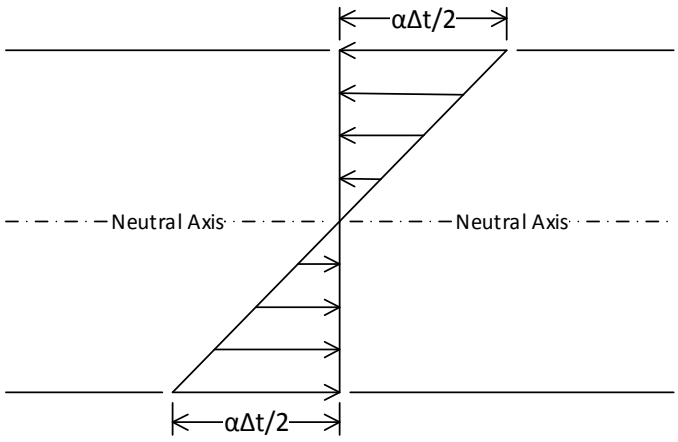

Figure 4.19: Temperature Differential in Concrete Slab (after Huang 2004)

After simplifying Equation 4.9, the total stress due to curling can be expressed as (Huang 2004):

$$\sigma_{x_{Total}} = \frac{E}{(1-\nu)} \cdot \left(\frac{\alpha \cdot \Delta t}{2} \right) \tag{4.10}$$

The concept described above was applied in this research to predict the induced curling and warping stress in the concrete pavement and the prediction of climatic stress was validated against the experimental observation reported by Jeong and Zollinger (2001).

Equation 3.36 in Chapter 3, rewritten here in Equations 4.11 for convenience, was used in the computation of stress development due to the resulting thermal, hygrothermal, and creep strain.

$$\Delta\sigma = J^{-1} \cdot \left(\Delta\varepsilon_{Total} - \Delta\varepsilon_{T} - \Delta\varepsilon_{HT} - \Delta\overline{\varepsilon_{CR}} \right) \tag{4.11}$$

If a slab is completely restrained and prevented from movement, $\Delta\varepsilon_{Total}$ in the above equation becomes zero. Hence, Equation 4.11 can be rewritten as:

$$\Delta\sigma = J^{-1} \cdot \left\{ -\left(\Delta\varepsilon_{T} + \Delta\varepsilon_{HT} + \Delta\overline{\varepsilon_{CR}} \right) \right\} \tag{4.12}$$

In order to compute the total stress in one direction due to the bending in both directions of the pavement, Equation 4.12 can be modified in the light of Equation 4.10 as follows:

$$\Delta\sigma = J^{-1} \cdot \frac{\left\{ -\left(\Delta\varepsilon_{T} + \Delta\varepsilon_{HT} + \Delta\overline{\varepsilon_{CR}} \right) \right\}}{\left(1 - \nu \right)} \tag{4.13}$$

The temperature and relative humidity profiles at the construction site reported by Jeong and Zollinger (2005) was used in the validation effort of the climatic stress model. The nonlinear temperature and pore fluid pressure gradients in the pavement were converted to equivalent linear gradients, similar to the one shown in Figure 4.19,

using the linearization concept proposed by Mohamed and Hansen (1996). The variables $\Delta\varepsilon_T$, $\Delta\varepsilon_{HT}$, and $\Delta\overline{\varepsilon_{CR}}$ in Equation 4.12 were known at the beginning of each time step. The restrained tensile stress was computed incrementally using Equation 4.13 and was accumulated in the result at the end of time step.

Model predicted environmental stress and concrete strength curves are plotted in Figure 4.20. The two curves intersect between hour 9 and hour 10 after placement and this indicates the time interval when cracks are likely to occur. The experiment observations of Jeong and Zollinger (2005) indicated that cracks were formed between hour 11 and hour 12 after concrete placement and the time interval of crack occurrence at the experimental site is illustrated by the shaded area in the graph.

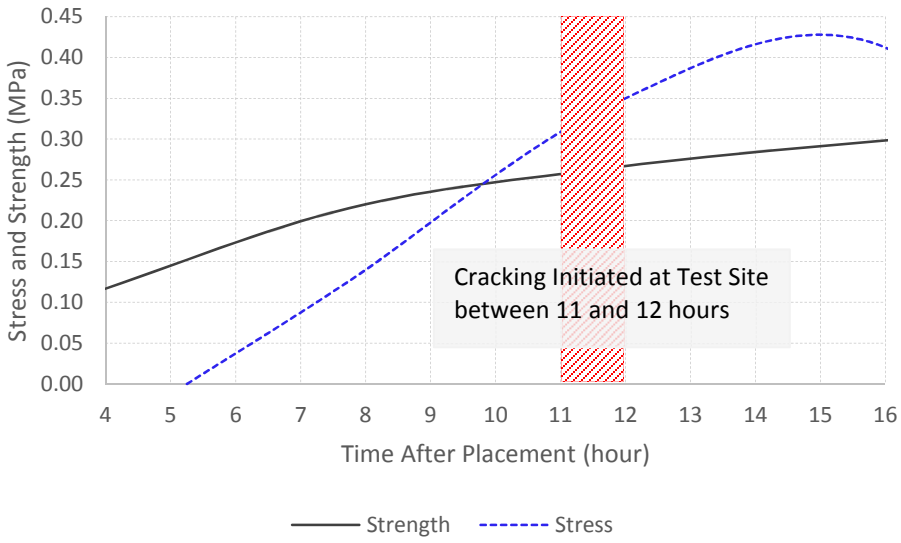

Figure 4.20: Prediction of Time of Crack Initiation versus Experimental Observation

From Figure 4.20 it can be concluded that the prediction of the climatic stress model seems to be in reasonable agreement with the experimental observation.

4.4 Validation of the Probabilistic Models for Failure

In this research, two modes of failure were considered, such as lift-off displacement or debonding and crack formation. The formulation of the probability of crack formation and the probability of lift-off have been mentioned before in Equations 3.39 and 3.41, respectively. The probabilistic models were validated using the available information for an overlay construction project in Houston Intercontinental, TX. The date and time of construction were known and the corresponding weather history, such as ambient temperature, ambient relative humidity, and wind speed, were obtained from the website (The Weather Underground, LLC 2014).

The overlay, with a design water-cement ratio of 0.42, was of 8 inch in thickness and was constructed over an existing concrete pavement of 18 inch starting on 23 February 2011. The available weather information contained the minimum and maximum ambient temperature and relative humidity as well as average wind speed. The weather history was used to model the development of temperature and relative humidity gradients within the concrete overlay starting from the time of placement up to the next 72 hours. Since the temperature and relative humidity follow a sinusoidal pattern, a sine function was used to model the daily temperature and relative humidity variations during the construction period. The minimum and maximum temperatures and relative

humidities for each day up to the first 72 hours were used to fit the sine function to represent the ambient temperature and relative humidity variations.

The prevalent weather information during the construction period used in this validation effort are shown in Table 4.2. The minimum and maximum temperatures were assumed to occur around 7 am and 16 pm, respectively and the maximum and minimum relative humidities were assumed to commence during the same hours, i.e. 7 am and 16 pm, respectively. The placement of concrete started at 10 am and hence the sinusoidal curves were fitted through the minimum and maximum temperatures and relative humidities starting from 10 am for that particular day up to the next 72 hours. The ambient temperature and relative humidity modeled with sine functions, for example starting on 28 February 2011 up to next 72 hours, are shown in Figures 4.21 and 4.22, respectively. It should be noted that the time of concrete placement 10 am was denoted as hour 1 and the subsequent hours were denoted sequentially in the above mentioned figures.

Finite difference numerical scheme, as described in Section 2, was used to model the temperature and relative humidity distribution within the concrete overlay for a given ambient temperature and relative humidity histories. For the finite difference models, appropriate temperature and humidity boundary conditions, such as convection, solar radiation, atmospheric radiation, concrete radiation, and moisture convection, described in Equations 2.18, 2.25, 2.26, 2.30, and 2.35 were incorporated to predict the temperature and humidity gradients developed within the overlay. The finite difference models were solved for the weather histories shown in Figures 4.21 and 4.22, and the

simulated temperature and humidity differences between the top and the bottom of the overlay are presented in Figures 4.23 and 4.24, respectively for illustration purpose. The obtained temperature and humidity gradients were converted to equivalent linear temperature difference, equivalent linear shrinkage potential difference, and equivalent linear pressure gradient to further model the strain and stress development in the concrete overlay.

Table 4.2. Ambient Temperature, Relative Humidity, and Wind Speed

Date of Construction	Temperature (°C)		Relative Humidity (%)		Wind Speed (mph)
	Min	Max	Min	Max	Average
23 Feb. 2011	18.9	27.2	51	97	9.2
24 Feb. 2011	20.0	26.1	60	94	10
25 Feb. 2011	11.7	25.0	32	100	5
26 Feb. 2011	10.5	22.8	72	93	5
27 Feb. 2011	19.4	28.3	55	93	12
28 Feb. 2011	12.8	25.6	19	83	11
01 Mar. 2011	7.8	23.9	19	80	6
02 Mar. 2011	7.8	23.9	21	71	4
03 Mar. 2011	7.8	22.8	55	100	4
04 Mar. 2011	17.2	25	52	100	7
05 Mar. 2011	8.9	18.9	51	100	8
06 Mar. 2011	4.4	20.6	22	79	9

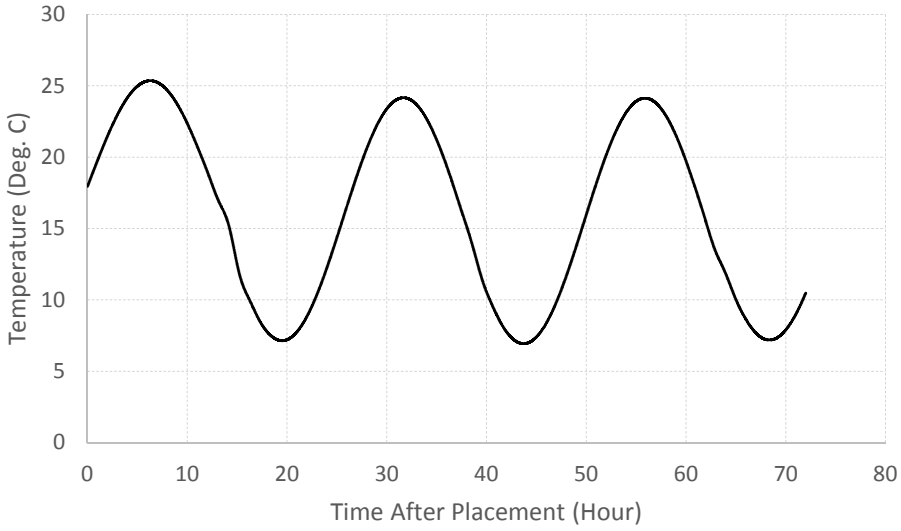

Figure 4.21: Ambient Temperature History Starting from 10 am, 28 February 2011

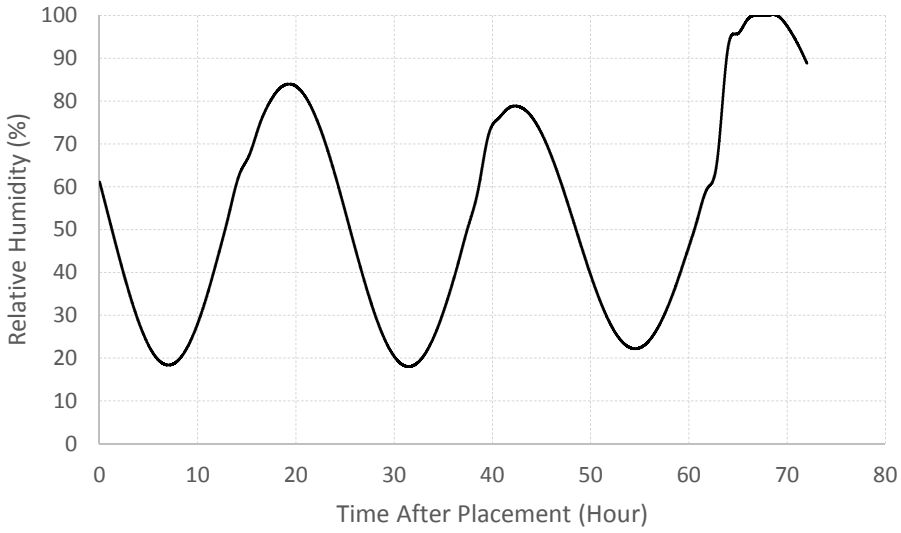

Figure 4.22: Ambient RH History Starting from 10 am, 28 February 2011

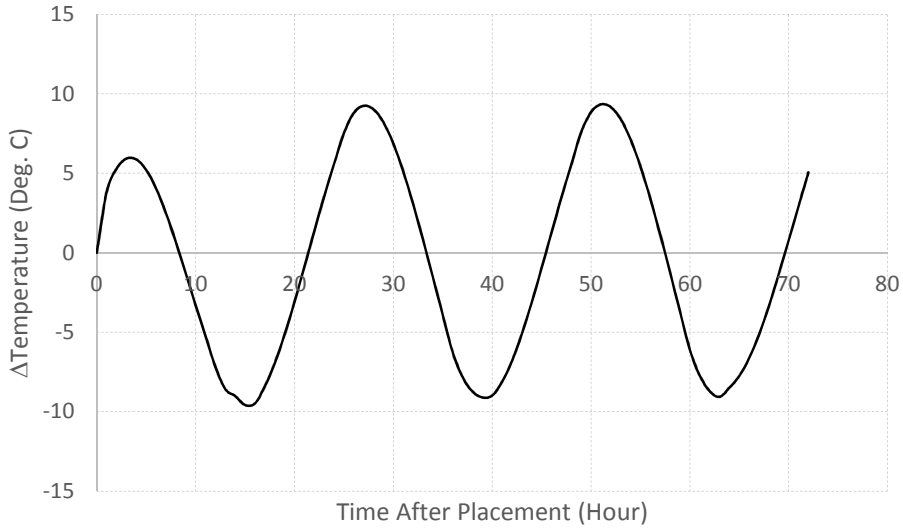

Figure 4.23: Temperature Difference between the Top and the Bottom of the Overlay Starting from 10 am, 28 February 2011

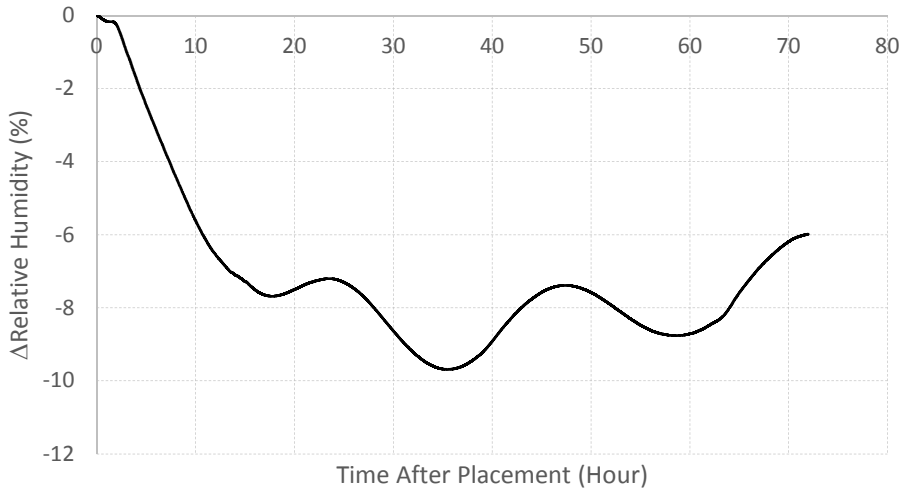

Figure 4.24: Humidity Difference between the Top and the Bottom of the Overlay Starting from 10 am, 28 February 2011

4.4.1 Probability of Cracking

Given the history of stress σ and the strength development f, the probability of crack formation during the early age of concrete can be described using Equation 3.39 which is rewritten here for convenience.

$$P_{cr} = \phi\left[\frac{\mu_\sigma - \mu_f}{\sqrt{\mu_f{}^2 \cdot COV[f]^2 + \mu_\sigma{}^2 \cdot COV[\sigma]^2}}\right] \tag{4.14}$$

where,

$P_{cr} = probability\ of\ cracking$

$\phi = standard\ normal\ probability\ distribution\ function$

$\mu_\sigma = expected\ value\ of\ \sigma$

$\mu_f = expected\ value\ of\ f$

$COV[\sigma] = coefficient\ of\ variation\ of\ \sigma$

$COV[f] = coefficient\ of\ variation\ of\ f$

The incremental stress $\Delta\sigma$ development for the overlay project in Houston was modeled according the numerical scheme described for Equation 4.13. The evolution of strength, in this case modulus of rupture, was modeled using Equation 4.15 which is similar to the form of equation describing the evolution of compressive strength provided by ACI Committee 209 (ACI Committee 209 1992). Using the stress and the strength evolution model described above, a typical stress versus strength curve is shown in Figure 4.25.

$$f_r(t) = \left(\frac{t}{a + b \cdot t} \right) \cdot f_{r_{28}} \tag{4.15}$$

where,

$f_r = modulus\ of\ rupture\ at\ age\ t$

$f_{r_{28}} = modulus\ of\ rupture\ at\ age\ of\ 28\ days$

$t = age\ of\ concrete\ in\ days$

$a, b = fitting\ parameters$

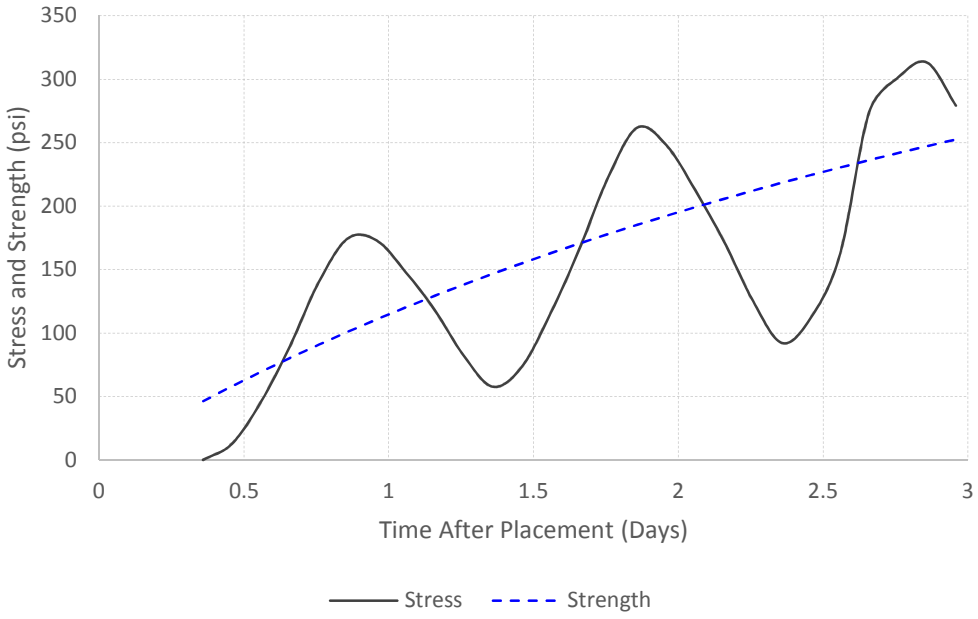

Figure 4.25: Typical Stress and Strength Evolution

For the overlay construction project, the modulus of rupture at 28 days was considered to be 700 psi based on the knowledge of the agency specification for concrete strength. The coefficient of variations of stress and strength, as shown in Equation 4.14, was assumed to be 0.25 and 0.15, respectively. Since there was not enough information available to be confident on the modulus of rupture of 700 psi, the probability estimations were performed based on a strength envelop having a lower limit of 600 psi and an upper limit of 800 psi extending one standard deviation of 100 psi (≈ 700×0.15) around the mean strength (≈ 700 psi).

Field observations, i.e. crack survey information, were available for the overlay panels paved on each day. Table 4.3 presents the number of panels paved on each day and the number of panels that experienced cracking subsequently. As for example, on February 23, 48 panels were paved and 17 panels out of those 48 panels cracked eventually. Therefore, the percentage of panels that were cracked was estimated to be as 35.4.

Figure 4.26 shows the predicted as well as the observed probability or percent cracking for each day of paving operation. The predicted probability envelop was computed for a 28 day strength envelop ranging from 600 psi to 800 psi with a mean strength of 700 psi. Another additional narrower 28 day strength envelop was added ranging from 650 psi to 750 psi to compute a further narrower cracking-probability envelop. The observed percentages of slab cracking were superimposed with the probability envelops to compare the accuracy of the prediction. It can be seen that three field observations on February 23, February 24 and March 02 of 2011 were within the

narrower envelop. The observations on February 25 and March 01 of 2011 fell within the wider envelop.

Table 4.3. Crack Survey Information for the Overlay Construction Project

Date of Construction	No. of Panels Paved	No. of Cracked Panels	Percent of Slab Cracked
02/23/2011	48	17	35.4
02/24/2011	12	2	16.7
02/25/2011	78	7	9.0
03/01/2011	76	28	36.8
03/02/2011	77	36	46.8
03/03/2011	3	2	66.7

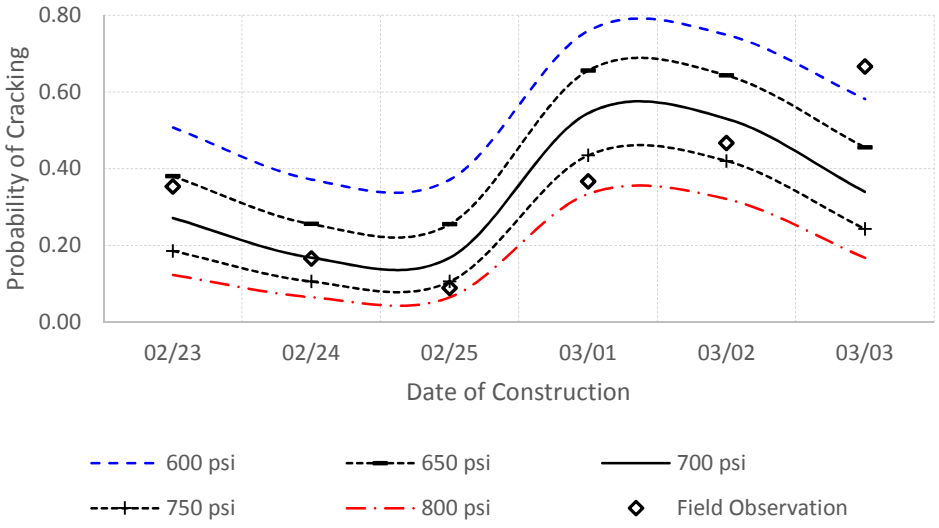

Figure 4.26: Predicted and Observed Probability of Cracking at Different 28-Day Modulus of Rupture

It should be noted that the observed percent cracking for the construction on February 25 of 2011 was in close proximity to the narrower envelop represented by the strength of 750 psi and the corresponding observed cracking probability versus predicted cracking probability were 9% versus 10.6%, respectively. The only observation that was outside the predicted probability envelop was associated with the panels paved on March 03 of 2011. However, this observation might be considered as an anomaly or outlier as three panels might not constitute a sufficient sample size to make a conclusive evidence of the accuracy of the prediction. Hence, it can be concluded that with reasonable assumptions on strength variations, the probability of cracking model predictions were in sufficient agreement with the field observations.

4.4.2 Probability of Lift-off or Debonding

The probability of lift-off can be estimated using Equation 3.41, which is rewritten in Equation 4.16, provided the stress and strength history are known. The tensile stress at the interface between the overlay and the old pavement due to corner lift-off displacement can be computed by multiplying the corresponding lift-off displacement and the modulus of subgrade reaction *k* as shown in Equation 4.17 (Shin 2000). The strength, in this case termed as split tensile bond strength (Shin 2000), was estimated in this study by relating the split tensile strength of concrete with the split tensile bond strength of concrete.

The split tensile strength of a cylindrical concrete specimen can be obtained as per ASTM C496 by applying load laterally along the diameter till the specimen splits at

the middle. The schematic diagram depicting the split tensile test of concrete is shown in Figure 4.27. The split tensile bond strength between the old concrete substrate and the new overlay concrete can be obtained by a testing procedure developed by Shin (2000). In his method, Shin casted a concrete cylinder, cured and dried it for 60 days to make it of similar condition of an old substrate. The cylinder was then saw-cut in half longitudinally as shown in Figure 4.28 and was placed in a mold. The remaining space in the mold was then filled with the new overlay concrete. The split tensile bond strength was obtained by following the similar procedure as per ASTM C 496.

$$P_{lift-off} = \phi\left[\frac{\mu_{\sigma_{lift-off}} - \mu_{f_{tb}}}{\sqrt{\mu_{\sigma_{lift-off}}{}^2 \cdot COV\left[\sigma_{lift-off}\right]^2 + \mu_{f_{tb}}{}^2 \cdot COV\left[f_{tb}\right]^2}}\right] \tag{4.16}$$

where,

$\phi = standard\ normal\ probability\ distribution\ function$

$\sigma_{lift-off} = lift-off\ or\ debonding\ stress$

$f_{tb} = split\ tensile\ bond\ strength\ of\ concrete$

$COV\left[\sigma_{lift-off}\right] = coefficient\ of\ variation\ of\ \sigma_{lift-off}$

$COV\left[f_{tb}\right] = coefficient\ of\ variation\ of\ f_{tb}$

$\mu_{\sigma_{lift-off}} = expected\ value\ of\ \sigma_{lift-off}$

$\mu_{f_{tb}} = expected\ value\ of\ f_{tb}$

$$\sigma_{lift-off} = k \cdot \Delta \tag{4.17}$$

where,

$$\sigma_{lift-off} = lift-off\ or\ debonding\ stress$$

$$k = modulus\ of\ subgrade\ reaction$$

$$\Delta = corner\ lift-off\ displacement\ of\ slab$$

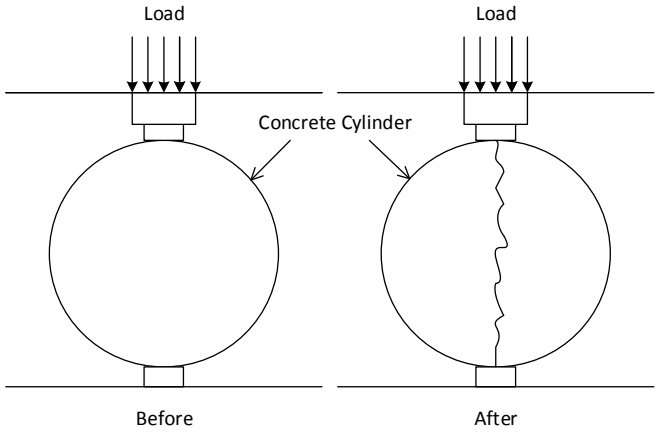

Figure 4.27: Split Tensile Test for Measuring Split Tensile Strength

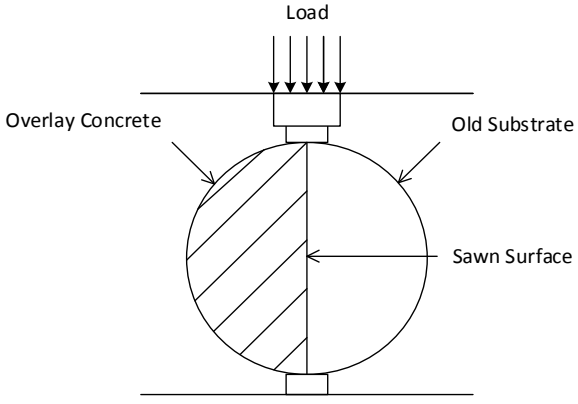

Figure 4.28: Split Tensile Test for Measuring Tensile Bond Strength (after Shin, 2000)

In his study, Shin reported the compressive strength and the 7-day split tensile bond strength for the four different specimens as shown in Table 4.4. The 7-day split tensile bond strength was used to back-calculate the 28-day split tensile bond strength using the strength evolution model having the similar form as Equation 4.15. The split tensile strength for those specimens were estimated from the reported compressive strength using Equation 4.18 proposed by Arioglu et al. (2006).

Table 4.4. Compressive, Split Tensile, and Split Tensile Bond Strength Information

Sample	Water-Cement Ratio	Compressive Strength (psi)	Split Tensile Bond Strength (psi)		Split Tensile Strength (psi)	Bond Strength Factor
		28-day	7-day	28-day	28-day	
(1)	(2)	(3)	(4)	(5)	(6)	(7)=(6)/(5)
HPC	0.30	8187	109	155	712	4.60
FRC II	0.40	7460	215	306	672	2.20
FRC	0.51	4387	194	276	481	1.74
OPC	0.65	4217	253	260	469	1.30

$$\frac{f_{tsp}}{f_c} = 0.387 \cdot f_c^{-0.37} \tag{4.18}$$

where,

$$f_{tsp} = split\ tensile\ strength\ (MPa)$$

$$f_c = compressive\ strength\ (MPa)$$

With Shin's reported split tensile bond strength and the estimated split tensile strength from Equation 4.18, a parameter termed as "bond-strength- factor" was defined as follows:

$$f_{tb} = \frac{f_{tsp}}{bond - strength - factor} \tag{4.19}$$

where f_{tb} is the split tensile bond strength. The bond-strength-factor was used later to estimate the split tensile bond strength for the overlay construction project in Houston, TX. The estimated bond strength factor for the four specimens of Shin's study are shown in Table 4.4. It can be seen from Table 4.4 that the bond strength factor varied from about one to five for the different specimens having varied water-cement ratio.

For the overlay construction project in Houston, the strength of concrete was estimated using Bolomey's equation (Bolomey 1935; Brandt 1995; Brandt 1998; Rajamane and Ambily, 2012; de Larrard 1999) as shown in Equation 4.20:

$$f_c = A\left(\frac{1}{w/c} - 0.5\right) \tag{4.20}$$

where A is an empirical constant related to cement and aggregate, w/c is the water-cement ratio, and f_c is the compressive strength in MPa. The split tensile strength was then estimated using Equation 4.18 with the estimated compressive strength. Finally, the 28-day split tensile bond strength f_{tb} was computed using the bond-strength-factor and the split tensile strength f_{tsp} according to Equation 4.19. The evolution of split tensile bond strength was then computed from the 28-day split tensile bond strength using a similar form of strength evolution model as shown in Equation 4.15. Finally, using the computed stress and strength, the probability of lift-off or debonding was then computed using Equation 4.16. The coefficient of variations for the stress and the strength in Equation 4.16 were assumed to be 0.25 and 0.15, respectively.

Therefore, for a water-cement ratio of 0.42, the estimated 28-day compressive strength f_c and 28-day split tensile strength f_{tsp} were found to be 5,245 psi and 540 psi, respectively. From Table 4.4, it can be seen that the bond-strength-factor was 2.20 for a water-cement ratio of 0.40. For the given problem in hand with a water-cement ratio of 0.42, the bond-strength-factor can be approximated as 2.20. Henceforth, the lift-off - probability was computed with the split tensile bond strength f_{tb} estimated from the bond-strength-factor of 2.20. However, as there was not enough information available to be confident in the estimation of split tensile bond strength, a strength envelop was used in the computation of the probability of lift-off. The strength envelop was estimated with

the bond-strength-factors varying between 2 and 3. The resulting 28-day split tensile bond strengths estimated from the bond-strength-factors of 3 and 2 were 179 psi and 269 psi, respectively. A bond-strength-factor of 2.5 (i.e. f_{tb} = 215 psi) was also used in the lift-off - probability computation to provide an additional perspective of the probability envelop.

Table 4.5 presents the required information used in the computation of the probability of lift-off for the overlay project in Houston, TX. Figure 4.29 presents the predicted and the observed probability of lift-off for the overlay project. It may be observed that most of the probability estimations corresponding to the 28-day split tensile bond strength of 245 psi (i.e. with a bond-strength-factor = 2.20) were in close agreement with the field observations. The probability of lift-off for the overlay constructed on 23 February 2011 was the only one that was not in close proximity of the probability estimations associated with the bond-strength-factor of 2.20. However, that observation was within the limits of the probability envelop predicted by the model. Hence, it can be concluded that with reasonable assumption on the strength parameters, the probability of lift-off model predictions were in good agreement with the field observations.

Table 4.5. Compressive, Split Tensile, and Split Tensile Bond Strength Information for the Overlay Construction Project

Compressive Strength (psi)	Split Tensile Strength (psi)	Bond Strength Factor	Split Tensile Bond Strength (psi)
28-day	**28-day**		**28-day**
(1)	(2)	(3)	(4)=(2)/(3)
5245	540	2.2	245
		3.0	179
		2.5	215
		2.0	269

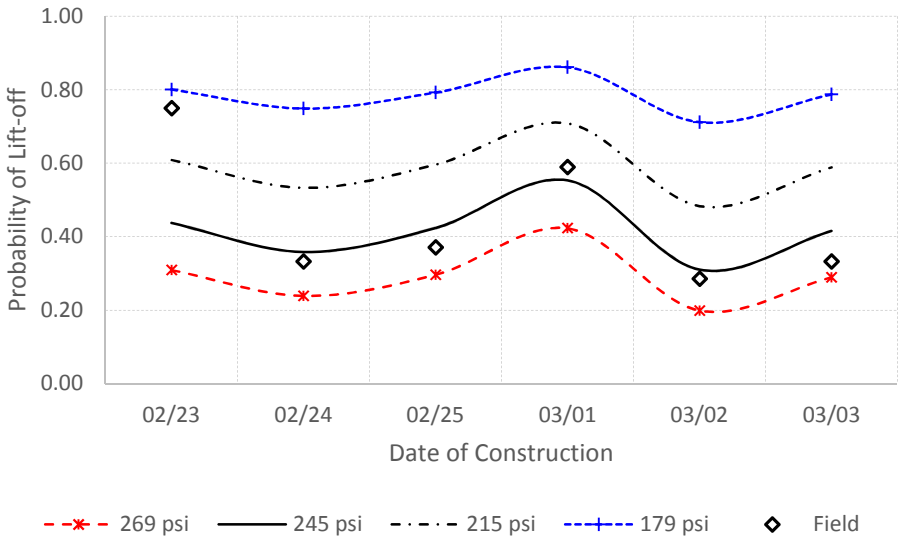

Figure 4.29: Predicted and Observed Probability of Lift-off for Various Split Tensile Bond Strength

4.5 Sensitivity Analysis

In this section, sensitivity analysis was performed to gain insight regarding the constructability of overlay and concrete pavements. Several key parameters considered in the analysis was the slab thickness, the time of concrete placement, the season of construction, and the effect of curing compound. In order to study the effect of time of concrete placement as well as the effect of season of construction, the ambient temperature and relative humidity variations during February and July were taken into consideration for demonstration purpose only. The minimum and maximum temperatures and relative humidity information for the chosen three-day periods covering 72 hours in each month, shown in Table 4.6, were used to fit a sine function to define the hourly ambient temperature and relative humidity variations throughout the 72 hours. The ambient temperature and relative humidity histories for February and July that were used in the sensitivity analysis are shown in Figures 4.30 through 4.33.

Table 4.6. Environmental Information for February and July

Date of Construction	Temperature (°C)		Relative Humidity (%)	
	Min	Max	Min	Max
24 Feb. 2011	20.0	26.1	60	94
25 Feb. 2011	11.7	25.0	32	100
26 Feb. 2011	10.6	22.7	72	93
02 July 2011	23.3	38.9	29	94
03 July 2011	24.4	36.7	35	94
04 July 2011	25.6	36.1	35	85

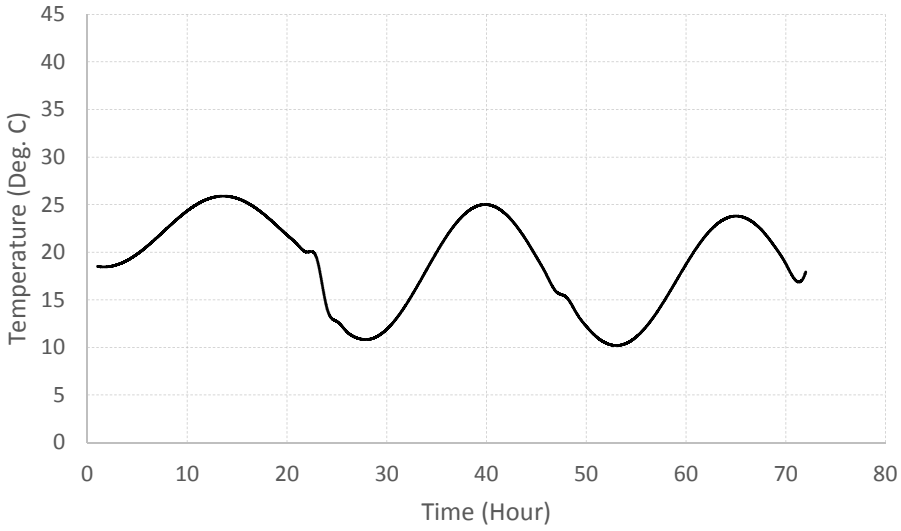

Figure 4.30: Ambient Temperature History Starting from 24 February 2011

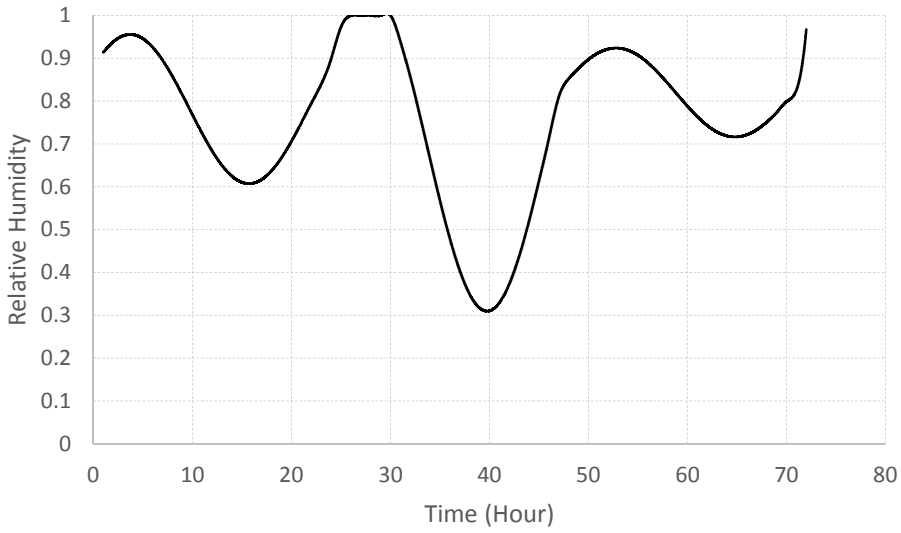

Figure 4.31: Ambient Relative Humidity History Starting from 24 February 2011

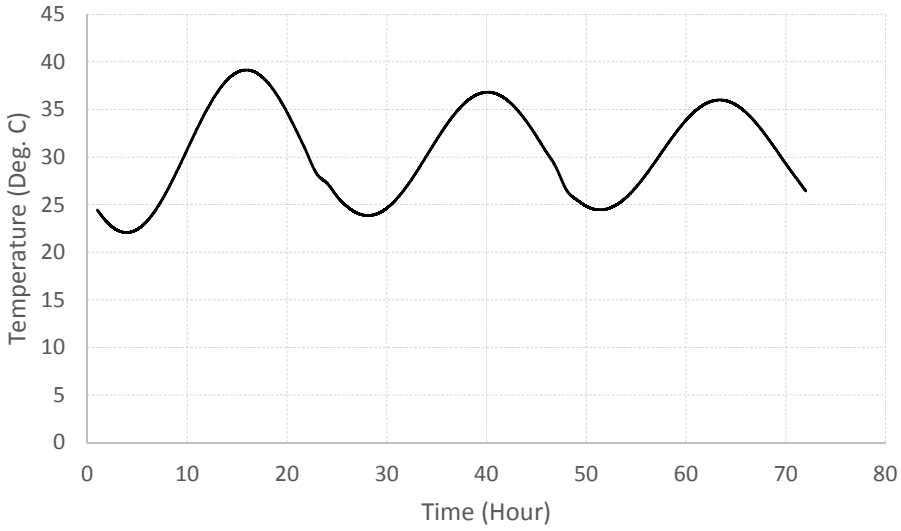

Figure 4.32: Ambient Temperature History Starting from 02 July 2011

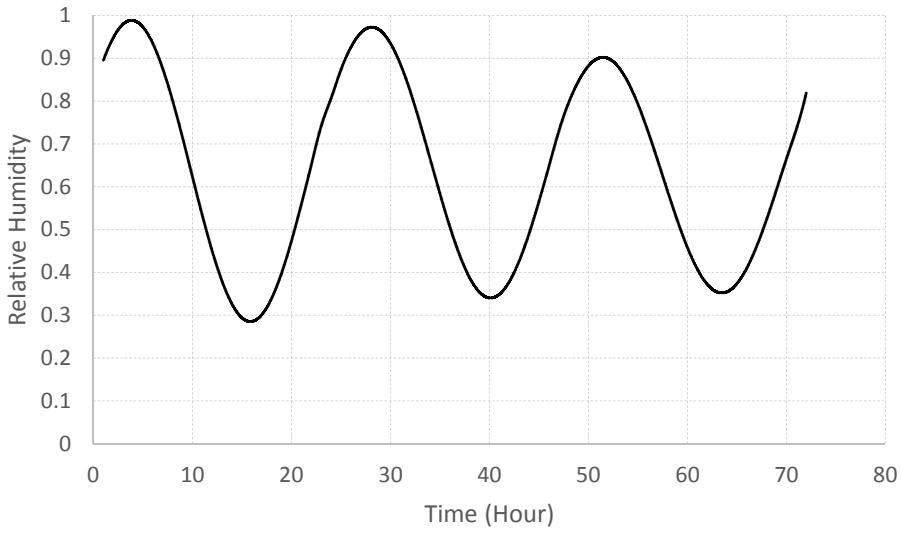

Figure 4.33: Ambient Relative Humidity History Starting from 02 July 2011

4.5.1 The Effect of Time of Construction or Placement

The first parameter of interest was the time of construction or placement to investigate whether there is any effect of time of construction on the potentials for cracking and lift-off. Numerical simulations were performed by placing concrete slab at different times of the day for a given environmental excitation history. While holding all the other parameters constant expect the time of placement, the temperature and the relative humidity gradients within the pavement were simulated up to the 72 hours after placing the concrete. Using the simulated temperature and relative humidity gradients across the slab thickness, the corresponding induced stress in the slab was computed. Then comparing the evolution of stress and strength, the potentials for lift-off as well as cracking were computed. The time of placements or constructions were considered in 2 hour increments starting from hour 2 up to hour 24.

To demonstrate the effect of time of placement, the ambient temperature and relative humidity histories for a three-day period in February, as shown in Figures 4.30 and 4.31, were selected for illustration purpose only. These were used to simulate the temperature and the relative humidity gradients within an 8 inch overlay for different placement hours along the day and the corresponding probabilities of lift-off and cracking were computed. The computed probabilities of lift-off and cracking for an overlay constructed at different times of the day are plotted in Figures 4.34 and 4.35, respectively. Both the figures depict the fact that the time of construction has an impact on the potential for distresses and it can be seen that slabs constructed between hour 17 and hour 21 are less prone to lift-off as well as cracking.

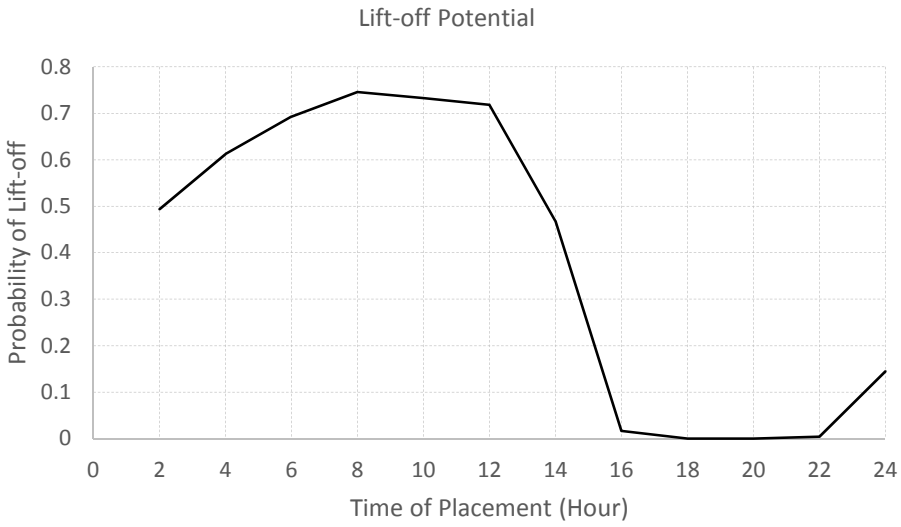

Figure 4.34: The Effect of Time of Placement on Lift-off Potential

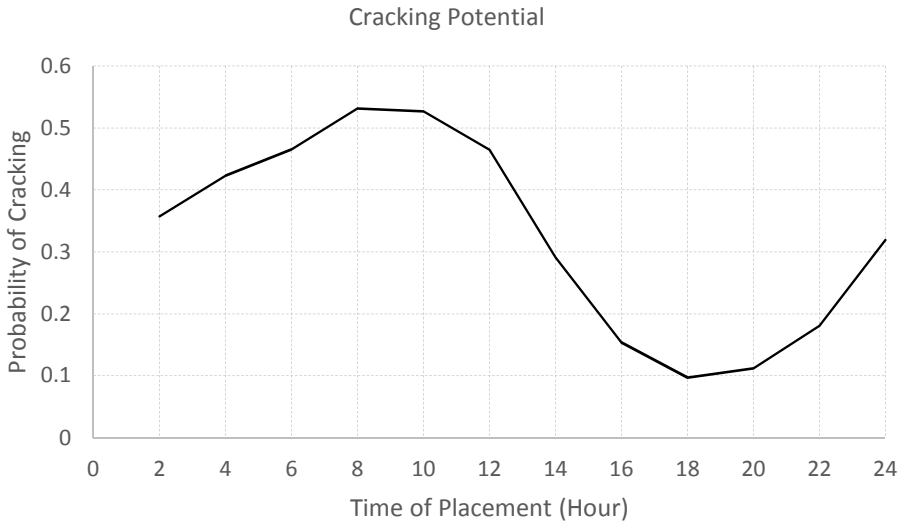

Figure 4.35: The Effect of Time of Placement on Cracking Potential

The interpretation of such a phenomenon is that the after-hours of the time window, i.e. hour 17 to hour 21, has a favorable environment for the pavement for which the temperature and set gradients and the relative humidity gradients induced lower stresses within the pavement and as a result lowered the potentials for lift-off as well as cracking.

4.5.2 The Effect of Thickness

The effect of slab thickness was the second parameter of interest for investigating its impact on the probability of lift-off and cracking. Two different slab thicknesses, such as 4 inch and 8 inch, were considered in the analysis. Numerical simulations were performed with the two different slab thicknesses by placing those at different times of the day at 2 hour time interval starting from 2 am. Simulations were conducted up to 72 hours after concrete placement to obtain the temperature and the relative humidity gradients across the slab thicknesses for a given environmental history and the corresponding potentials for lift-off as well as cracking were computed using those gradients.

To demonstrate the effect of thickness, the temperature and the relative humidity histories for the three-day period in February, as described before, were used for illustration purpose only. The probabilities of lift-off and cracking, computed for the two chosen slab thicknesses are presented in Figures 4.36 and 4.37, respectively.

Comparing the variations of lift-off potential for the two chosen slab thicknesses placed at different times over a 24-hour period, as shown in Figure 4.36, it is evident that a thinner overlay (i.e. 4 in.) performed better than a thicker overlay (i.e. 8 in.) in resisting

lift-off displacement. The thinner structure, constructed at any time throughout the day, exhibited insignificant potential for lift-off. On the other hand, the thicker structure exhibited lift-off potentials ranging from 0% to 55% depending on the time of construction. Thus, thin structures are found to be less prone to lift-off displacement compared to thick structures and the potential for lift-off for the thicker structure showed a variation with the time of construction throughout the day.

The cracking potentials, as shown in Figure 4.37, for the thin and thick structures indicated that the thicker pavement, except few observations, exhibited lower cracking potentials compared to that of the thinner pavement. The cracking potential for the 4 inch pavement varied from about 0.18 to 0.40 whereas the cracking potential for the 8 inch pavement ranged from about 0.04 to 0.50 depending on the time of construction. Compared to the 8 inch pavement, the 4 inch pavement was more prone to cracking between hour 4 and hour 18, and the probability of cracking during that time span did not fall below 0.15. However, during the same time window, the 8 inch pavement exhibited a gradual decline in cracking potentials and the cracking probability went as low as 0.05. There were few exceptions where the 8 inch pavement experienced higher cracking probability compared to the 4 inch pavement as can be seen for the placement hours before hour 4 and after hour 18. The explanation to such phenomenon is that the combined environmental gradients for those construction hours induced a higher strain in the 8 inch structure compared to the 4 inch structure and thus, an 8 inch pavement exhibited a higher cracking potential. Overall, depending on the time of construction, the

thicker pavement was found to perform better in terms of resisting crack formation compared to the thinner pavements.

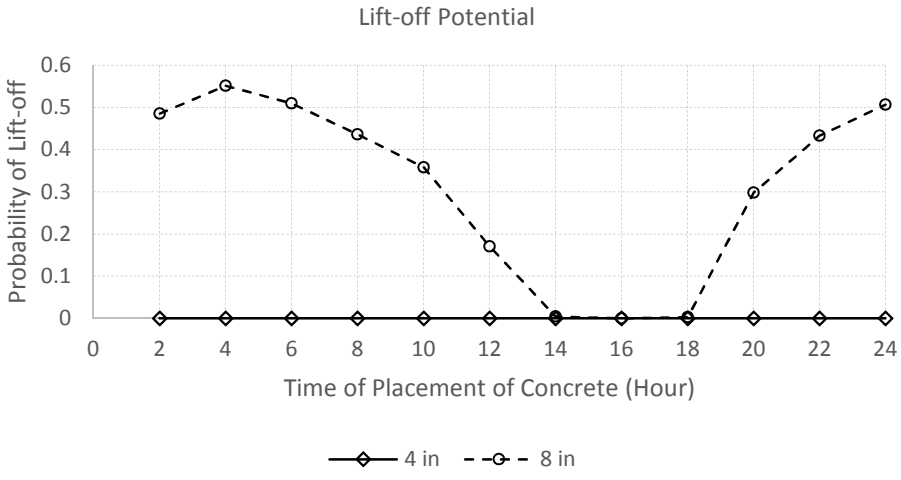

Figure 4.36: The Effect of Slab Thickness and Time of Placement on Lift-off Potential

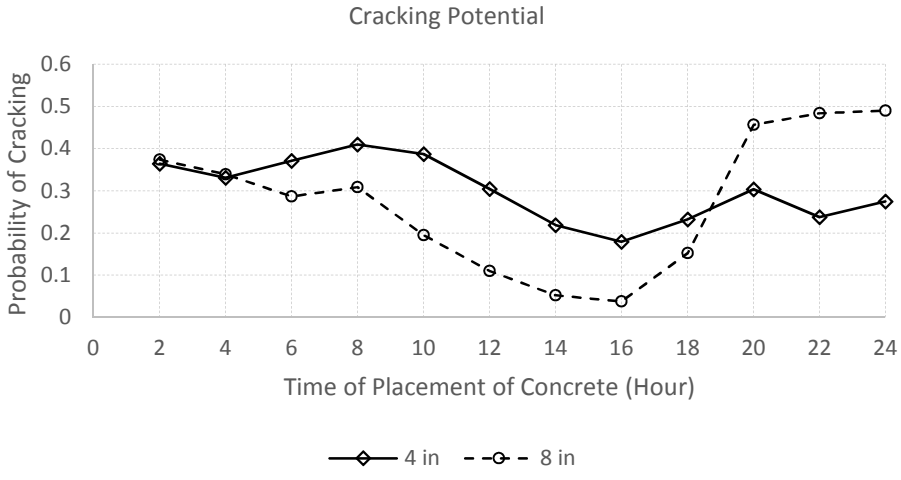

Figure 4.37: The Effect of Slab Thickness and Time of Placement on Cracking Potential

4.5.3 The Effect of Season of Construction

The third parameter of interest was the season of construction and the sensitivity analysis was performed on the season of construction to assess the corresponding effect on the cracking and lift-off potentials. The temperature and the relative humidity gradients in an 8 inch slab was obtained through simulation using the environmental histories for February and July as shown in Figures 4.30 through 4.33 representing the spring and the summer season, respectively. The 8 inch slab thickness was chosen arbitrarily for illustration purpose. The computed probabilities of lift-off and cracking for the spring and the summer are shown in Figures 4.38 and 4.39.

It is seen from Figure 4.38 that the season of construction has an impact on the lift-off potential. The construction during the summer exhibited a noticeably higher lift-off potential compared to that of the spring for the time of construction varying from hour 2 to hour 16. For the rest of the day, the summer construction seemed to have equal or better performance in terms of resisting lift-off.

Figure 4.39 also exhibits similar impact of construction season on the cracking potential. For the time of construction ranging between hour 2 and hour 18, the summer construction again showed a prominently higher cracking potential compared to that of the spring construction. Similar to the lift-off potential trend for the rest of the day, the cracking potential is seen to be lower for the summer construction compared to that of the spring construction.

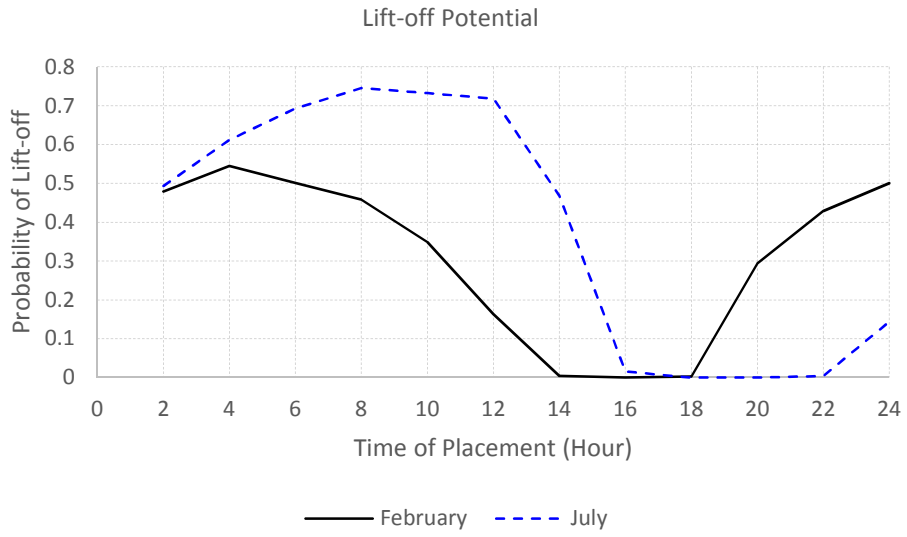

Figure 4.38: The Effect of Season of Construction on Lift-off Potential

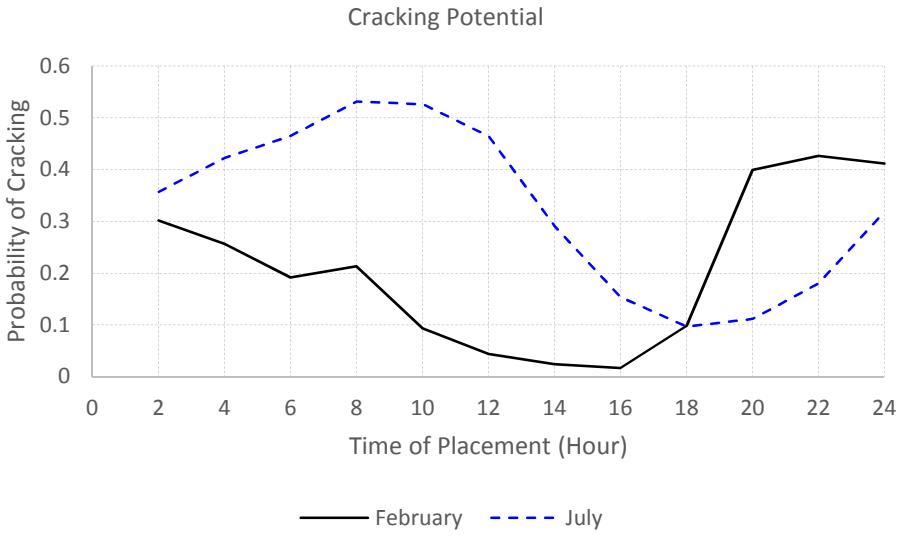

Figure 4.39: The Effect of Season of Construction on Cracking Potential

4.5.4 The Effect of Curing Compound

The last parameter studied was the effect of curing compound on the both types of distress potentials. Keeping the other conditions constant, numerical simulations were performed for an 8 inch slab with two curing methods: base case without any curing application and the other with application of curing compound B for both the spring and the summer construction. The effect of curing compound on the lift-off and the cracking potentials for both the seasons are presented respectively in Figures 4.40 through 4.43. It can be seen that the construction with curing compound B performed better in resisting lift-off displacement compared to the base case representing no curing application. Similarly, while considering the potential for cracking, the construction with curing compound B seemed to have a substantially lower cracking tendency compared to that of the base case. Hence as expected, curing compound can contribute to better construction outcome through minimizing both the lift-off and cracking potentials.

The information regarding the performance of a pavement or an overlay structure obtained from the sensitivity analysis were combined and an index termed as "constructability index" was defined which is discussed in the following subsection.

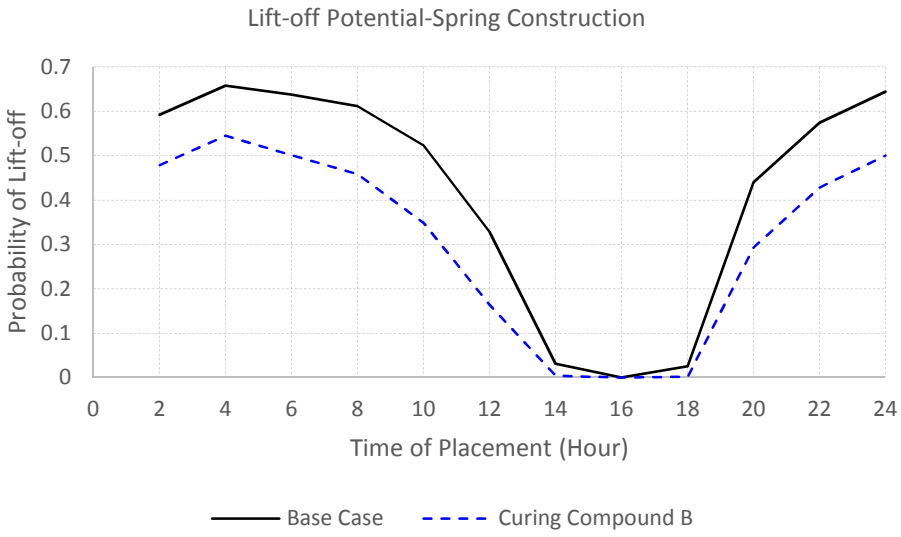

Figure 4.40: Lift-off Potentials with Curing Compound during Spring

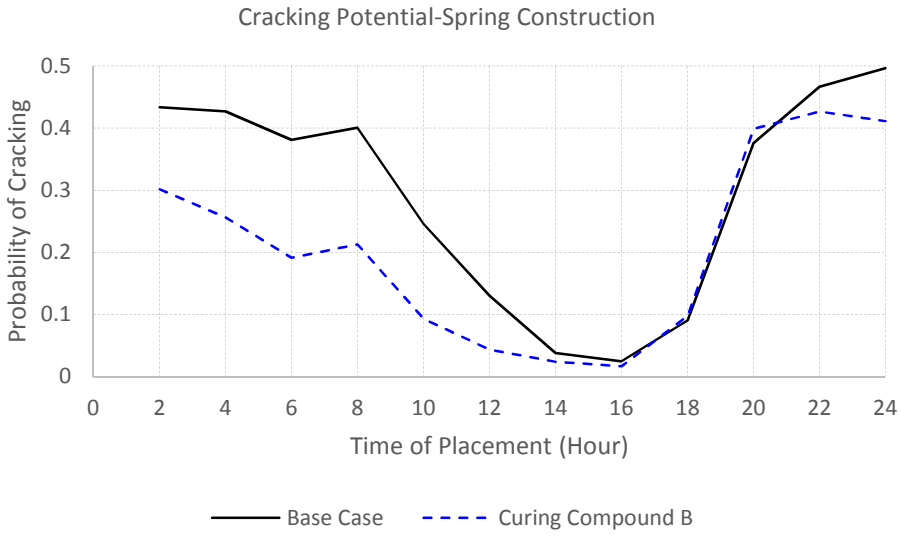

Figure 4.41: Cracking Potentials with Curing Compound during Spring

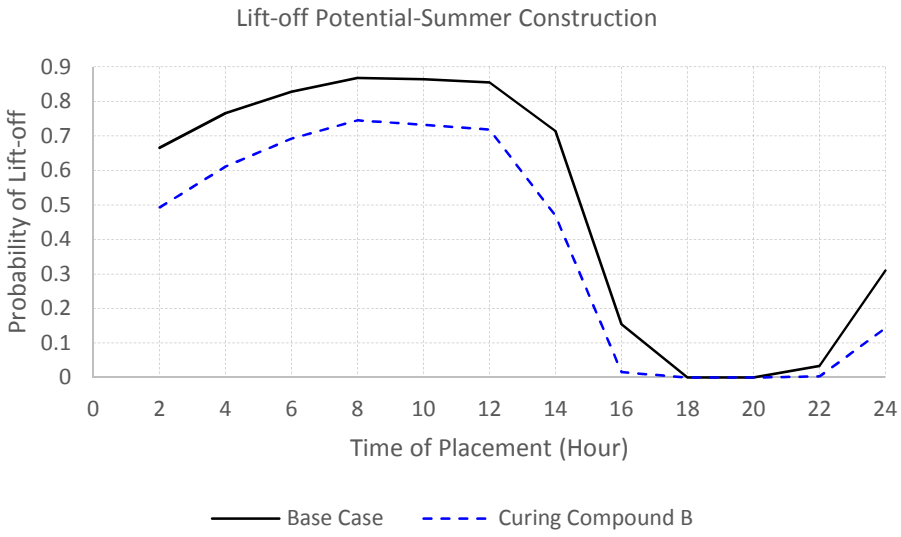

Figure 4.42: Lift-off Potentials with Curing Compound during Summer

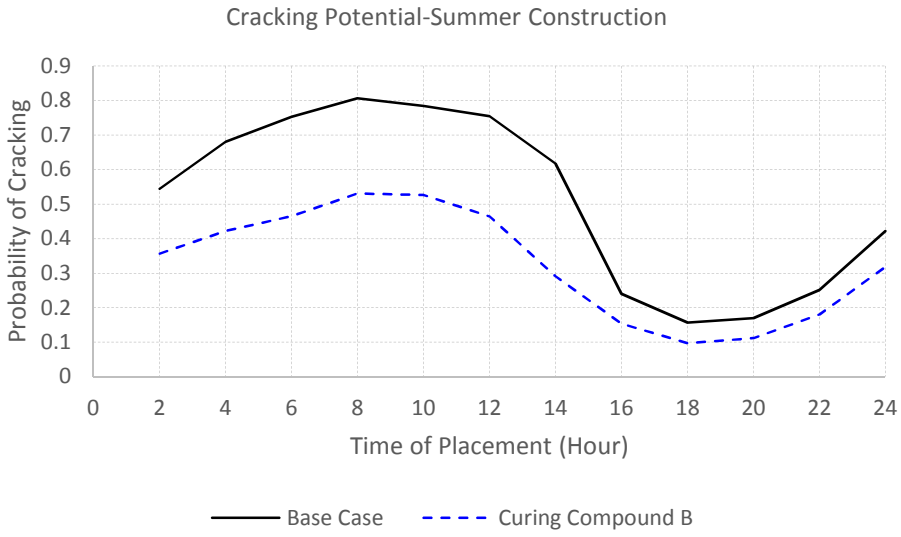

Figure 4.43: Cracking Potentials with Curing Compound during Summer

4.6 Constructability Index

In this section, an index called "constructability index" was proposed with a view to assist the design engineers and construction managers for arriving at an optimal and best construction option. The potentials for two distresses, such as cracking and lift-off displacement, were taken into consideration in formulating the constructability index. The index varies from zero to one, where one indicates the best possible construction option and zero being indicative of the opposite extreme. The constructability index, in this study, was formulated as follows:

$$I_{cons} = 1 - \left(P_{delam} + P_{cr} - P_{cr} \cdot P_{delam} \right) \tag{4.21}$$

where,

$I_{cons} = constructability\ index$

$P_{delam} = probability\ of\ delamination$

$P_{cr} = probability\ of\ cracking$

The constructability index was computed for both the construction seasons of spring and summer for two curing methods: the base case without any curing application and the other with application of curing compound B for the construction time varying from hour 2 to hour 24. The computed indices are presented in Figures 4.44 and 4.45. It can be seen that the proposed constructability index captures the differences in performance between the two curing methods, depicting a performance variation with time of construction. Also the index was capable of manifesting the seasonal effect on

the constructability of the project. Comparing Figures 4.44 and 4.45 for the computed constructability indices, it can be seen that the spring construction was found to be more favorable compared to the summer construction. The design engineers and project managers can benefit from this index through studying the effect of different key elements on the distress potentials, incorporating those estimates in the constructability index for assessing the given design and construction scenario followed by controlling and adjusting those elements to obtain the best possible construction outcome.

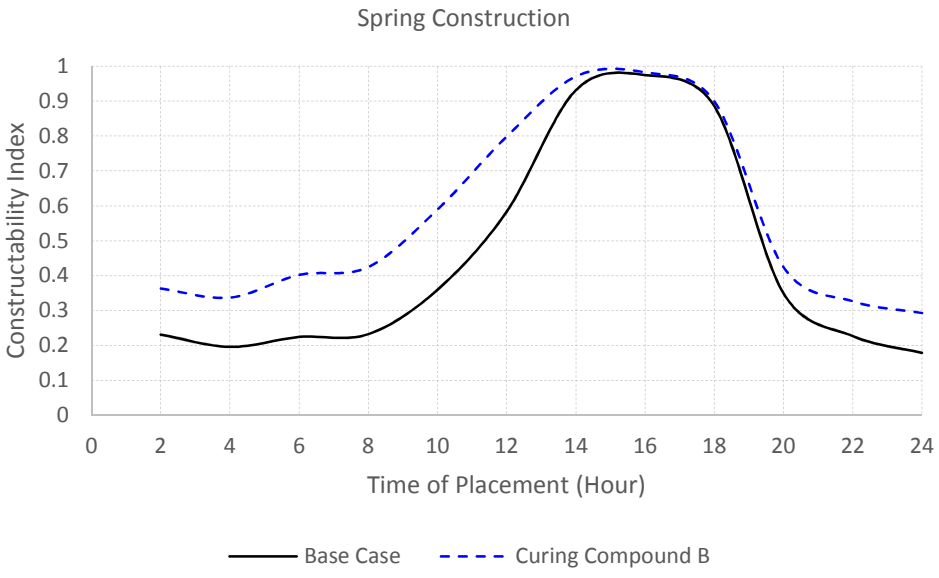

Figure 4.44: Constructability Index for Project Constructed in Spring

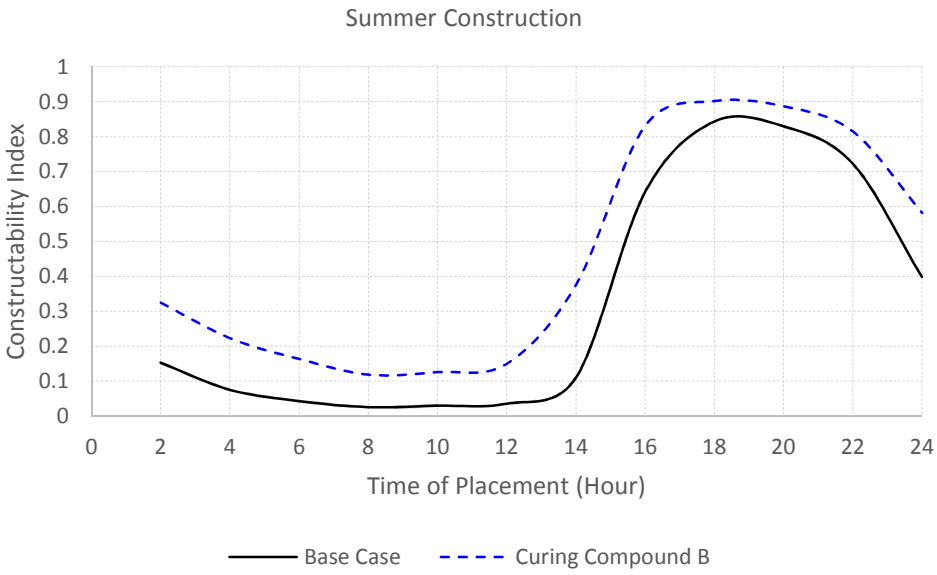

Figure 4.45: Constructability Index for Project Constructed in Summer

5. CONCLUSION AND RECOMMENDATION

5.1 Summary and Conclusion

In this research a methodology was proposed and developed to assess the constructability of concrete pavement and overlay in order to improve the performance as well as to extend the service life of pavement system. The main core of this research was based on incorporating the effect of curing process (i.e. curing compound) as well as modeling the impact of environmental excitations, i.e. temperature and relative humidity histories, into the design analysis in order to assess the distress potentials of concrete pavement and overlay. Curing compound, in effect, influences the relative humidity or the moisture transfer process between the pavement and the ambient environment. Depending on the quality of curing compound applied on the concrete pavement and the overlay, it can control the drying shrinkage taking place during the construction phase to some possible extent. The effect of environmental excitations can also be assessed and minimized by simulating its effect on pavement distresses by adjusting the time and season of construction in a modeling framework.

The results obtained from this study indicated that it is possible to minimize the potential for distresses through applying curing compound during the construction phase as well as by adjusting the time and season of construction. The construction assessment methodology developed in this study involved modeling several elements as stated below:

(i) incorporating the effect of curing process in a design framework through adjusting the diffusion coefficient of concrete and modeling the influence of curing method on the moisture transfer process taking place during the construction phase;

(ii) proposing two indices: (a) curing index and (b) overall curing index to facilitate comparison among the performance of different curing compounds;

(iii) predicting the probability of the pavement and the overlay to experience lift-off displacement as well as cracking due to the stresses induced by environmental excitations; and

(iv) finally incorporating these probabilities of distress into a decision making framework through proposing an index defined as "constructability index".

The effect of curing compound applied during the construction of concrete pavement is manifested in the time dependent diffusion coefficient of concrete. A mathematical model was proposed in this study to back-calculate the diffusion coefficient of concrete that had curing compound applied on its surface. For a concrete sample prepared in the laboratory, three different relative humidity measurements were obtained, such as sealed RH, filtered RH, and ambient RH, in order to back-calculate the time dependent diffusion coefficient of cured concrete. With the three relative humidity measurements and the solution methodology called system identification method, it was possible to back-calculate the diffusion coefficient of cured concrete with time. The back-calculated diffusion coefficients of concrete without any curing compound (i.e. the

base case) as well as with two different curing compounds A and B were illustrated in the study.

An indexing system with the back-calculated time dependent diffusion coefficient $\alpha(t)$ was formulated. Two different indices were proposed in this study: (i) the curing index depicting the time dependent effectiveness of the curing compound and (ii) the overall curing index demonstrating the overall performance of the curing compound for a given time span. The time dependent curing index was formulated by taking into account the two possible theoretical extremes i.e. the lowest (best) and the highest (worst) possible values of the diffusion coefficient and the curing index was defined as follows.

$$Curing\ Index, CI(t) = \frac{\alpha_{highest}(t) - \alpha_{calc}(t)}{\alpha_{highest}(t) - \alpha_{lowest}(t)}$$

The overall curing index was computed by taking the ratios of the area under the CI curve to the area under the ideal CI curve for a given time span - in this study the time span was taken as 72 hours. The ideal curing index curve was considered to have a value of one throughout the considered time span, i.e. 72 hours. The overall curing index in this study was defined as follows.

$$Overall\ Curing\ Index, CI_{overall} = \frac{area\ under\ the\ CI\ curve}{area\ under\ the\ ideal\ CI\ curve}$$

With these two indices, it was possible to capture the difference in performance between the two different curing methods considered in the study, i.e. the base case without any curing application and the other with application of two different curing compounds A and B.

Lift-off displacement model and climatic stress model were formulated for concrete pavement or overlay to predict the lift-off displacement and cracking behavior for a given environmental excitation history. Both these models were validated with the experimental observations obtained by Jeong and Zollinger (2001 and 2005). The temperature and the relative humidity histories, the evolution of strength and elastic modulus reported by Jeong and Zollinger (2001 and 2005) were used as input in the lift-off displacement and climatic stress models. The predictions from both the models indicated that the models were in good agreement with the experimental observation.

Probabilistic models were formulated for predicting the potentials for lift-off and cracking for a given design and construction scenario. Both the probabilistic models were validated with the experimental observations for an overlay project constructed at Houston Intercontinental, TX. Finite difference models were formulated to predict the temperature and the relative humidity distributions within the concrete for the given weather history. The evolution of concrete strength and elastic modulus were computed with the available project specifications. With the computed concrete strength, elastic modulus as well as the temperature and moisture gradients, the probabilities for cracking and lift-off were computed and were compared with the field observations. The

predictions of both the probabilistic models exhibited sufficient agreement with the field observations.

With the validated lift-off and cracking models, sensitivity analysis was performed to compute the potential for lift-off and cracking with a view to gain insight regarding the constructability of a pavement or overlay construction project for a given design and construction scenario. Parameters of interest were the thickness of the structure, the time of placement or construction, the season of construction, and the application curing compound. The results of the sensitivity analysis are briefly discussed below:

- The effect of thickness on the lift-off and cracking potentials indicated that the thicker pavement was less prone to cracking compared to the thinner pavement. On the other hand, the thicker overlay were more prone to lift-off displacement compared to that of the thinner one.
- The effect of time of construction on the lift-off and cracking potentials indicated that both the probability of lift-off and the probability of cracking followed a sinusoidal variations along the day. This revealed that the possibility of lift-off and cracking can be minimized by constructing the pavement and the overlay during a particular time window of the day, such as approximately between 5 pm and 9 pm as found in simulation results of this study;
- The effect of season of construction on the lift-off and cracking potentials revealed that the season of construction has an impact on the probability of lift-

off as well as the probability of cracking. For example, in this study the spring construction exhibited less distress potentials compared to the summer construction for the time of construction taking place between about 2 am and 6 pm.

- The effect of curing compound on the distress potentials was investigated by comparing the construction having no curing application (termed as base case) with the construction having curing application. Simulation results indicated that the lift-off and cracking potentials for the construction projects having curing applications were noticeably less compared to the construction projects without any curing applications.

With the results from the sensitivity analysis, an index called "constructability index" was proposed and demonstrated in this research in order to assist the design and construction managers to study the effect of different key elements of a construction project on the constructability of a pavement and overlay project. The constructability index was formulated by incorporating the probability of lift-off as well as the probability of cracking as shown below.

$$Constructability\ Index, I_{cons} = 1 - \left(P_{delam} + P_{cr} - P_{cr} \cdot P_{delam} \right)$$

The proposed constructability index was able to capture the difference in performance between the two curing method, i.e. with no curing application versus with curing

application, as well as demonstrated a performance variation with the time of construction as well as the season of construction. The design engineers and the construction managers can design and construct better pavements and overlays using this constructability index through controlling and adjusting the different key elements of a construction projects.

5.2 Recommendations for Further Study

This research deals with modeling and incorporating the curing process into design analysis as well as providing a methodology for assessing the constructability of concrete pavement and overlay projects. Based on the outcome of the research, the following needs have been identified for future research that would make logical extensions of this research.

- The result from this research indicated that the quality and duration of curing during the initial phase of construction was important. This initial time window when the pavement construction is vulnerable to environmental excitations needs to be established through experimentation. Close monitoring and inspection regarding the quality and the duration of curing and the corresponding effect on the distress potentials during this time frame will be required.
- Relationship between the quality and the duration of curing (represented by curing index and overall curing index) and the intensity of distress potential needs to be established and validated through laboratory and field experimentations.

- The current code and design guidelines need to be updated with better curing management approach. Current industry practice indicated that curing process is neither paid for nor is specified and inspected during the construction phase. Acceptance criteria regarding the curing process needs to be established in order to minimize the negative impact on the long term durability of the pavement and the overlay.
- This research focused on modeling the effect of curing compound on the constructability of pavement projects. Internal curing, another mitigation strategy for concrete projects, can further be modeled and incorporated in the assessment of constructability of concrete projects to capture the additional benefits manifested through minimizing the risk of cracking and lift-off displacement.
- In the current lift-off displacement model, only split tensile bond strength of concrete was considered as the strength parameter. Suction can also be incorporated as an additional strength parameter to study the effect of suction on the lift-off displacement and the delamination distance of concrete overlay.
- In this research only environmental load induced distresses were considered to assess the constructability of concrete pavement and overlay. The research can be further extended through incorporating the effect of traffic load induced distresses and subsequently simulating the performance of the pavement and overlay after opening to traffic.

- The constructability index proposed in this research needs to be validated with the outcome of construction projects to see if further adjustment or modification of the index is necessary to correlate with the field observations.
- The proposed constructability index in this study incorporated only cracking and delamination potentials. The constructability index can further be extended through incorporating other forms of distress, such as spalling, to better predict the outcome of a design and construction scenario.

It is obvious that there are opportunities for future research in modeling the constructability of both asphalt and concrete pavement projects. The modeling approach proposed in this research can be used as a basis for further development, refinement, and applications of these concepts.

REFERENCES

American Concrete Institute (ACI) Committee 209. (1992). “Prediction of creep, shrinkage and temperature effects in concrete structures.” ACI 209R-92, American Concrete Institute, Detroit.

Al-Gahtani, A. (2010). "Effect of curing methods on the properties of plain and blended cement concretes." *Constr. Build. Mater.*, 24(3), 308-314.

Altoubat, S. A. (2000). "Early age stresses and creep-shrinkage interaction of restrained concrete". Ph.D. dissertation, University of Illinois at Urbana-Champaign.

Ames, W. F. (1992). *Numerical methods for partial differential equations*, Third edition, Academic Press, Inc., Boston.

Ang, A. H-S. , and Tang, W. H. (1984). *Probability concepts in engineering planning and design. Volume II—Decision, risk and reliability*, Wiley, New York.

Arioglu, N., Girgin, Z. C., and Arioglu, E. (2006). “Evaluation of ratio between splitting tensile strength and compressive strength for concretes up to 120 MPa and its application in strength criterion.” *ACI Mater. J.*, 103(1), 18–24.

Armaghani, J. M., Larsen, T. J., and Smith, L. L. (1988). “Temperature response of concrete pavements.” *Transp. Res. Rec. No. 1121*, Transportation Research Board, Washington, D.C., 23–33.

ASHRAE. (1993). *1993 ASHRAE handbook*, American Society of Heating, Refrigerating and Air-Conditioning Engineers, Inc., Atlanta, GA.

ASHRAE. (2005). *2005 ASHRAE handbook*, American Society of Heating, Refrigerating and Air-Conditioning Engineers, Inc., Atlanta, GA.

Atrushi, D. S. (2003). "Tensile and compressive creep of early age concrete: testing and modelling." Doctoral thesis, The Norwegian University of Science and Technology, Trondheim, Norway.

Barcelo, L. (2003). "Chemical shrinkage." *Early age cracking in cementitious systems*, A. Bentur, ed, RILEM Publication S. A. R. L., Bagneux, France.

Baweja, S., Dvorak, G., and Bazant, Z. (1998). “Triaxial composite model for basic creep of concrete.” *J. Eng. Mech.*, 124 (9), 959–965.

Bazant, Z. P. (1977). “Viscoelasticity of porous solidifying material—concrete.” *J. Engrg. Mech. Div., ASCE*, 103 (6), 1049–1067.

Bazant, Z. P. (1979). "Thermodynamics of solidifying or melting viscoelastic material." *J. Engrg. Mech. Div.*, *ASCE*, 105(6), 933-952.

Bazant, Z. P., and Baweja, S. (1995). “Creep and shrinkage prediction model for analysis and design of concrete structures—model B3.” *Mat. and Struct.*, Paris, France, 28, 357–365.

Bazant, Z., and Chern, J. (1985). "Concrete creep at variable humidity: constitutive law and mechanism." *Mater. and Struct.*, 18(1), 1-20.

Bazant, Z. P., Hauggaard, A. B., Baweja, S., and Ulm, F. J. (1997). “Microprestress-solidification theory for concrete creep. I: Aging and drying effects.” *J. Engrg. Mech.*, 123 (11), 1188–1194.

Bazant, Z. P., and L'Hermite, R. (1988). *Mathematical modeling of creep and shrinkage of concrete*, John Wiley and Sons, New York.

Bazant, Z. P., and Panula, L. (1978a). “Practical prediction of time-dependent deformations of concrete. Part III: Drying creep. Part IV: Temperature effect on basic creep.” *Mater. Struct.* , 11 (66), 415–434.

Bazant, Z.P., and Panula, L. (1978b). “A note on amelioration of the creep function for improved Dischinger method.” *Cement and Concrete Research*, 8 (3), 381–386.

Bazant, Z. P., and Prasannan, S. (1989a). “Solidification theory for concrete creep. II: Verification and application.” *J. Engrg. Mech., ASCE*, 115 (8), 1704–1725.

Bazant, Z. P., and Prasannan, S. (1989b). “Solidification theory for concrete creep. I: Formulation.”*J. Engrg. Mech., ASCE*, 115 (8), 1691–1703.

Bazant, Z. P., and Xi, Y. (1994). “Drying creep of concrete: constitutive model and new experiments separating its mechanisms.” *Mater. Struct.*, 27(1), 3–14.

Bentz, D. P., Garboczi, E. J., and Quenard, D. A. (1998). “Modelling drying shrinkage in reconstructed porous materials: application to porous Vycor glass.” *Modell. Simul. Mater. Sci. Eng.*, 6 (3), 211–236.

Berger, F. (1931). "Über den Temperaturverlauf in einem Zylinder von endlicher Länge beim Abkühlen und Erwärmen," *J. App. Math. and Mech./ Z. f. angew. Math. u. Mech.*, 11, 45-58,

Bissonnette, B., Marchand, J., Charron, J., Delagrave, A., and Barcelo, L. (2001). "Early age behavior of cement-based materials." *Materials Science of Concrete VI*, 243-326.

Bogue, R. H. (1947). *The chemistry of Portland cement*, Reinhold Publishing Corporation, New York.

Bolomey, J. (1935). "Granulation et prevision de la resistance probable des betons. " *Travoux*, 19(30), 228–232.

Bolz, R. E., and Tuve, G. L. (1976). *CRC Handbook of tables for applied engineering science (edn)*, 2nd Edition, CRC Press, Cleveland, Ohio.

Bradbury, R. D. (1938). *Reinforced concrete pavements*, Wire Reinforcement Institute, Washington, D.C.

Branco, F. A., Mendes, R. A., and Mirabell, E. H. (1992). "Heat of hydration effects in concrete structures." *ACI Mater. J.*, 89 (2), 139–145.

Brandt, A. M. (1995). *Cement based composites: Materials, mechanical properties and performance*, E & FN Spon, London.

Brandt, A. M. (1998). *Optimization methods for material design of cement-based composites*, E & FN Spon, London.

Branson, D. E. (1977). *Deformation of concrete structures*, McGraw–Hill, New York.

Brutsaert, W. (1975). "On a derivable formula for long-wave radiation from clear skies." *Water Resour. Res*., 11(5), 742–744.

Burden, R., and Faires, J. D. (1997). *Numerical analysis*, Sixth edition, Brooks/Cole Publishing Company, New York.

Byfors, J. (1980). "Plain concrete at early ages." Res. Rep. F3:80, Swedish Cement and Concrete Res. Inst., Stockholm, Sweden.

Carol, I. and Bazant, Z. (1993). "Viscoelasticity with aging caused by solidification of nonaging constituent." *J. of Eng. Mech.*, 119(11), 2252-2259.

Chapman, A. J. (1982). *Fundamentals of heat transfer,* Macmillan Inc, New York.

Choubane, B., and Tia, M. (1992). "Nonlinear temperature gradient effect on maximum warping stresses in rigid pavements." *Transp. Res. Record 1370*, Transp. Res. Board, Washington, D.C., 11–19.

Czubak, G. (2011). "Concrete delamination: its causes and prevention." http://www.goslingczubak.com/UserFiles/File/ConcreteDelamination.pdf, accessed on 10.22.2012.

Dempsey, B.J. "A heat-transfer model for evaluating frost action and temperature related effects in multilayered pavements systems." Ph.D. dissertation, University of Illinois, at Urbana, IL.

D'Ambrosia, M. D., Lange, D., and Grasley, Z. (2004). "Measurement and modeling of concrete tensile creep and shrinkage at early age." *ACI Special Publication*, 220, 99-112.

D'Ambrosia, M. D., and Lange, D. A. (2005). "Modeling early age tensile creep and shrinkage of concrete." *ACI Special Publication*, 227, 349-366.

D'Ambrosia, M. D. (2011). "Early age creep and shrinkage of emerging concrete materials." Ph.D. dissertation, University of Illinois at Urbana-Champaign, Illinois.

de Larrard, F. (1999). *Concrete mixture proportioning: A scientific approach*, E & FN, Spon, London, UK.

De Schutter, G., and Taerwe, L. (1995). "Specific heat and thermal diffusivity of hardening concrete." *Magazine of Concrete Research*, 47(172), 203-208.

Emborg, M. (1989). “Thermal stresses in concrete structures at early ages.” Ph.D. thesis, *Div. of Struct. Engrg.*, Lulea Univ. of Technol., Lulea, Sweden, No. 73D.

Feldman, R. F. (1972). "Mechanism of creep of hydrated Portland cement paste." *Cem. Concr. Res.*, 2(5), 521-540.

Ferraris, C., and Wittmann, F. H. (1987). "Shrinkage mechanisms of hardened cement paste." *Cem. Concr. Res.*, 17(3), 453-464.

Freedman, J. M., Fitzjarrald, D. R., Moore, K. E., and Sakai, R. K. (2001). "Boundary layer clouds and vegetation-atmosphere feedbacks." *J. Clim.*, 14(2), 180-197.

Freiesleben Hansen, P., and Pedersen, E. J. (1977). “Maturity analysis by computer for controlling curing and hardening of concrete.” *Nordisk Betong*, 1, 21–25.

Freiesleben Hansen, P., and Pedersen, E. J. (1985). “Curing of concrete structures.” *Draft DEB—Guide to durable concrete structures*, Appendix 1, Comité Euro-International du Béton, Switzerland.

Gamble, B., and Parrott, L. (1978). "Creep of concrete in compression during drying and wetting." *Magazine of Concrete Research*, 30(104), 129-138.

Goldstein, S. (1932). "The application of Heaviside's operational method to the solution of a problem in heat conduction." *ZAMM-Journal of Applied Mathematics and Mechanics/Zeitschrift für Angewandte Mathematik und Mechanik*, *12*(4), 234-243.

Grasley, Z. C., Lange, D. A., and Matthew, D. (2006). "Internal relative humidity and drying stress gradients in concrete." *Mater. Struct.*, 39(9), 901-909.

Grasley, Z. C. (2006). "Measuring and modeling the time-dependent response of cementitious materials to internal stresses." Ph.D. dissertation, University of Illinois, Urbana-Champaign.

Honsberg, C. and Bowden, S. (2013). "The sun's position." http://pveducation.org/pvcdrom/properties-of-sunlight/suns-position, accessed 08.03.2013.

Hsieh, C. K., Qin, C., and Ryder, E. E. (1989). "Development of computer modeling for prediction of temperature distribution inside concrete pavements." Rep. Number FL/DOT/SMO/90–374, Final Report to Florida Dept. of Transportation.

Huang, Y. H. (2004). *Pavement design and analysis*, Second edition, Pearson/Prentice Hall, Upper Saddle River, NJ.

Imamoto, K., Kanda, T., Momose, H. and Mihashi, H. (2004). "Performance design of shrinkage cracking control – Part 1, 2, and 3." *Proceeding of the 75th Architectural Research Meetings*, Kanto Chapter, Architectural Institute of Japan, 75-I, 41-52 (in Japanese).

Incropera, F. P., and Dewitt, D. P. (2002). *Fundamentals of mass and heat transfer*, John Wiley & Sons, Inc., New York.

Isaacson, E., and Keller, H. B. (1994). *Analysis of numerical methods,* Courier Dover Publications, New York.

Janna, W. S. (2000). *Engineering heat transfer*, Second edition, CRC Press LLC, Boca Raton, Florida.

Janssen, D. J. (1986). "Moisture in Portland cement concrete." *Transp. Res. Rec.*, 1121, Transportation Research Board, Washington, D.C., 40–44.

Jennings, H. M. (2004). "Colloid model of C-S-H and implications to the problem of creep and shrinkage." *Mater. Struct.*, 37(1), 59-70.

Jeong, J., Chapke, N., and Zollinger, D. (2001). "A probabilistic approach to sawcut timing and depth requirements for newly constructed Portland cement concrete pavements." *Seventh International Conference on Concrete Pavements. The Use of Concrete in Developing Long-Lasting Pavement Solutions for the 21st Century*, International Society for Concrete Pavements, Orlando, Florida.

Jeong, J., and Zollinger, D. G. (2005). "Environmental effects on the behavior of jointed plain concrete pavements." *J. Transp. Eng.*, 131(2), 140-148.

Jeong, J. H. (2003). "Characterization of slab behavior and related material properties due to temperature and moisture effects." Ph.D. dissertation, Texas A&M Univ., College Station, Texas.

Jonasson, J.E., Groth, P., and Hedlund, H. (1995). "Modeling of temperature and moisture field in concrete to study early age movements as a basis for stress analysis." *Proceedings of the International RILEM Symposium on Thermal Cracking in Concrete at Early Ages*, Edited by R. Springenschmid, E & EF Spon, London, 45-52.

JSCE. (2002). "Standard specification for concrete structures—2002 'materials and construction'." *JSCE guidelines for concrete*, No. 6, Japan Society of Civil Engineers.

Kanda, T., Momose, H., Imamoto, K., and Mihashi, H. (2008). "Stochastic approach to shrinkage cracking control for reinforced concrete structural elements." *Journal of Advanced Concrete Technology*, 6(1), 121-133.

Khan, A. A., Cook, W. D., and Mitchell, D. (1995). "Early age compressive stress-strain properties of low-medium, and high-strength concretes." *ACI Mat. J.*, 92(6), 617–624.

Kishi, T., and Maekawa, K. (1995). "Thermal and mechanical modeling of young concrete based on hydration process of multi-component cement minerals." *Proceedings of the International RILEM Symposium on Thermal Cracking in Concrete at Early Ages*, Edited by R. Springenschmid, E & EF Spon, London, 11-18.

Korenev, B. G., and Chernigovskaya, E. I. (1962). *Analysis of plates on elastic foundation*. Gosstroiizdat, Moscow, Russia (in Russian).

Kovler, K. (1994). "Testing system for determining the mechanical behaviour of early age concrete under restrained and free uniaxial shrinkage." *Mater. Struct.*, 27(6), 324-330.

Lee, C. J. (2007). "Response of concrete structures subject to material aging and volume instability." Ph.D. dissertation, University of Illinois at Urbana-Champaign, Illinois.

Lee, C. J., Lange, D. A., and Liu, Y. (2011). "Prediction of moisture curling of concrete slab." *Mater. Struct.*, 44(4), 787-803.

Lee, S. I. (2010). "Development of approach to estimate volume fraction of multiphase material using dielectrics." Ph.D. dissertation, Texas A&M University, Texas.

L'Hermite, R. (1959). "What do we know about the plastic deformation and creep of concrete?" *RILEM Bull.*, No. 1, Paris, France, 21–51.

Lytton, R. L., Tsai, F., Lee, S. I., Luo, R., Hu, S., and Zhou, F. (2010). "Models for predicting reflection cracking of hot-mix asphalt overlays." Project 01-41, National Cooperative Highway Research Program, Transportation Research Board National Research Council, Washington, D.C.

Mindess, S., and Young, J. F. (1981). *Concrete*, Prentice-Hall, Englewood Cliffs, N.J.,

Mindess, S., Young, J.F., Darwin, D. (2002). *Concrete*, 2nd Ed., Prentice Hall, Upper Saddle River, NJ.

Mindess, S., Young, J. F., and Darwin, D. (2003). *Concrete*, 2nd Ed., Prentice-Hall, Upper Saddle River, N.J.

Mirambell, E. (1990). "Temperature and stress distributions in plain concrete pavements under thermal and mechanical loads." *Proc., 2nd Int. Workship on Design and Rehabilitation of Concrete Pavements*, Sigüenza, Spain, 121–135.

Mitchell, P. W. (1979). "The structural analysis of footings on expansive soil." *Research Report No. 1*, Kenneth W. G. Smith and Associates, Adelaide, South Australia.

Mohamed, A. R., and Hansen, W. (1996). "Effect of nonlinear temperature gradient on curling stress in concrete pavement." *Transportation Research Record*. 1568 (1), Transportation Research Board, National Research Council, Washington, D.C., 65–71.

Nakamura, H., Hamada, S., Tanimoto, T., and Miyamoto, A. (1999). "Estimation of thermal crack resistance for mass concrete structures with uncertain material properties." *ACI Struct. J.*, 96(4), 509-518.

Natke, H. G. (1982). *Identification of vibrating structures,* Springer-Verlag New York, Inc., N.Y.

Nellis, G., and Klein, S. (2009). "Mass transfer." *Heat transfer*, Cambridge University Press, Cambridge, New York.

Neville, A. (1981). *Properties of concrete*, Third Edition, Pitman Publishing. Ltd., London, England.

Neville, A. M., Dilger, W. H., and Brooks, J. J. (1983). *Creep of plain and structural concrete,* Construction Press, Longman Group Ltd., London, England.

Neville, A. M. (1996). *Properties of concrete*, John Wiley & Sons, New York.

Nguyen, T. K. (2013). "Convective mass transfer (class notes)." http://www.csupomona.edu/~tknguyen/che313/pdf/chap3-1.pdf, accessed 08.19.2013.

Okamoto, P. A., Nussbaum, P. J., Smith, K. D., Darter, M. I., Wilson, T. P., Wu, C. L., and Tayabji, S. D. (1991). "Guidelines for timing contraction joint sawing and earlier loading for concrete pavements." Rep. No. FHWA-RD-91-070, Federal Highway Administration, McLean, Va.

Østergaard, L., Lange, D. A., Altoubat, S. A., and Stang, H. (2001). "Tensile basic creep of early-age concrete under constant load." *Cem. Concr. Res.*, 31(12), 1895-1899.

Pickett, G. (1942). "The effect of change in moisture content on the creep of concrete under a sustained load."*ACI J.*, 38, 333–355.

Portland Cement Association (PCA). (2013). "Concrete pavements." http://www.cement.org/pavements/pv_cp.asp, accessed on 10.12.2012.

Powers, T. C. (1947). "A discussion of cement hydration in relation to the curing of concrete." *Proc., Highway Research Board*, 27, Highway Research Board, Washington, DC, 178–188.

Powers, T. C. (1967). "Study of creep of concrete." *RILEM Bulletin*, 34, 73-85.

Powers, T. C. (1968). “The thermodynamics of volume change and creep.” *Mat. and Struct., Paris, France* , 1 (6), 487–507.

Press, W. H., Teukolsky, S. A., Vetterling, W. T., and Flannery, B. P. (2007). *Numerical recipes: the art of scientific computing*, Third edition, Cambridge University Press, New York.

Radlinska, A. (2008). "Reliability-based analysis of early-age cracking in concrete." Ph.D. dissertation, Purdue University, West Lafayette, Indiana.

Radosavljevic, J., and Djordjevic, A. (2001). “Defining of the intensity of solar radiation on horizontal and oblique surfaces on Earth.” *Series: Working and Living Environmental Protection*, Facta Universitatis, 2 (1), 77–86

Rajamane, N., and Ambily, P. (2012). "Modified Bolomey equation for strengths of lightweight concretes containing fly ash aggregates." *Magazine of Concrete Research*, 64(4), 285.

Rasheeduzzafar, Al-Gahtani, A. S., and Al-Saadoun, S. S. (1989). "Influence of construction practices on concrete durability." *ACI Mater. J.*, 86(6), 566-575.

Riding, K. A., Poole, J. L., Schindler, A. K., Juenger, M. C., and Folliard, K. J. (2007). "Temperature Boundary Condition Models for Concrete Bridge Members." *ACI Mater. J.*, 104(4), 379-387.

Riedel, M. R. (2013). "Implicit methods: the Crank-Nicolson algorithm." http://www.dynamicearth.de/Lectures/FortgGeodyn.WiSe10/Tutorial/Day2/cranknicholson.pdf, accessed on 08.19.2013.

Ruetz, W. (1968). “A hypothesis for the creep of hardened cement paste and the influence of simultaneous shrinkage.” *Proc. Int. Conf. Structure of Concrete*, held in London, England, 1965, Cement and Concrete Assoc., London, England, 365–387.

Ruiz, J. M., Rasmussen, R. O., Chang, G. K., Dick, J. C., and Nelson, P. K. (2005). "Computer-based guidelines for concrete pavements." *Vol. II: Design and Construction Guidelines and HIPERPAV II User's Manual*, Publication No. FHWA-HRT-04-122, Federal Highway Administration, Washington, DC.

Scanlon, J. M. and McDonald, J. E. (1994). "Thermal properties, significance of tests and properties of concrete and concrete-making materials." Edited by Klieger, P. and Lamonds, J. F., ASTM Special Technical Publication No. 169C, 229–239.

Scherer, G. W. (2000). "Measuring permeability of rigid materials by a beam bending method: I, Theory." *J. Am. Ceramic Soc.,* 83(9), 2231-2239.

Schindler, Anton K., Terry Dossey, and B. Frank McCullough (2002). "Temperature control during construction to improve the long term performance of Portland cement concrete pavements." Research Report Number FHWA/TX-05/0-1700-2, Center for Transportation Research, University of Texas at Austin, Austin, TX.

Schindler, A. K. (2004). "Effect of temperature on hydration of cementitious materials." *ACI Mater. J.*, 101(1), 72-81.

Sellevold, E. J., and Richards, C. W. (1972). "Short-time creep transition for hardened cement paste." *J. Am. Ceramic Soc.*, 55(6), 284–289.

Shin, H. (2000). "Early age behavior of bonded concrete overlays due to shrinkage and thermal changes". Ph.D. dissertation, University of Illinois at Urbana-Champaign, Illinois.

Stubbs, N. (1987). "A general theory of non-destructive damage detection in structures." *Structural control*, H. H. H. Leipholz, ed., Springer Netherlands, 694–713.

Sun, P. (2013). "A new protocol for evaluating concrete curing effectiveness". M.S. thesis, Texas A&M University, Texas.

Tang, T., Zollinger, D. G., and Senadheera, S. (1993). "Analysis of concave curling in concrete slabs." *J. Transp. Engrg.*, ASCE, 119 (4), 618–633.

Tamtsia, B., and Beaudoin, J. (2000). "Basic creep of hardened cement paste - A re-examination of the role of water." *Cem. Concr. Res.*, 30 (9), 1465–1475.

Taus, V. L., Villagrán, Y. A., and Di Maio, A. A. (2008). "Influence of curing conditions on transport properties of blended cement concrete." *ACI Special Publication,* 253*,* 25-40.

Thepchatri, T., Johnson, C. F., and Matlock, H. (1977). "Prediction of temperature and stresses in highway bridges by a numerical procedure using daily weather reports." Tech. Report23-1, Texas Univ. at Austin Ctr. for Highway Res., Austin, Texas, 1–145.

The Weather Underground, LLC. (2014). "Welcome to weather underground." http://www.wunderground.com/, accessed on 11.10.2013.

Thomlinson, J. (1940). “Temperature variations and consequent stresses produced by daily and seasonal temperature cycles in concrete slabs.” *Concrete Constructional Engrg.*, 36(6), 298–307; 36(7), 352–360.

Tokumaru, H., Shibata, H., Okamura, H., Hasegawa, T., Soeda, T., Nakamizo, T., Akitsuki, K., and Yamakawa, S. (1987). “Handbook of statistical engineering.” Chapter 12, 547-552 (in Japanese).

Torpunuri, V. S. (1990). "A methodology to identify material properties in layered visoelastic halfspaces." Ph.D. dissertation, Texas A & M University, College, TX.

van Breugel, K.. (1998). “Prediction of temperature development in hardening concrete.” *Prevention of thermal cracking in concrete at early ages*, R. Springenschmid, ed., E & FN Spon, London, 51–75.

van Breugel, K. , and Lokhorst, S. J. (2001). “Stress-based crack criterion as a basis for the prevention of through cracks in concrete structures at early-ages.” *Int. conf. on early-age cracking in cementitous systems (EAC’01)*, K. Kovler and A. Bentur, eds., RILEM Publications S. A. R. L., France, 229–236.

Walker, S., and Bloem, D. L. (1957). "Effects of curing and moisture distribution on measured strength of concrete." *Highway Research Board Proceedings,* Highway Research Board, Washington, D.C., 36, 334-346.

Wang, F., and Lytton, R. L. (1993). “System identification method for back calculating pavement layer properties.” *Transportation Research Record* 1384, Transportation Research Board, Washington, D.C., 1–7.

Wang, L., and Zollinger, D. G. (2000). “A mechanistic design framework for spalling distress.” *Transportation Research Record* 1730, Transportation Research Board, Washington, D.C., 18–24.

Westergaard, H. M. (1926). “Analysis of stresses in concrete pavements due to variations of temperature.” *Proc., Highway Research Board*, 6, 201–215.

Westergaard, H. M. (1927). “Theory of concrete pavement design.” *Proc., Highway Research Board*, Part I, 175–181.

Wittmann, F. H., and Roelfstra, P. E. (1980). “Total deformation of loaded drying concrete.” *Cement and Concrete Res.*, 10(5), 601–610.

Wittmann, F. H. (1993). “On the influence of stress on shrinkage of concrete.” *Creep & shrinkage of concrete*, Z. Bazant and I. Carol, eds., RILEM Proc. No. 22 , E & FN Spoon Publ., London, England, 151–157.

Wojcik, G. S. (2004). "Effects of Atmospheric and Construction Conditions on Concrete Equivalent Ages." *ACI Mater. J.*, 101(5), 376-384.

Ye, D. (2007). "Early-age concrete temperature and moisture relative to curing effectiveness and projected effects on selected aspects of slab behavior". Ph.D. dissertation, Texas A&M University, College Station.

Ye, D., Mukhopadhyay, A. K., and Zollinger, D. G. (2009). "Laboratory and field evaluation of concrete paving curing effectiveness." Rep. No. FHWA/TX-10/0-5106-3*,* Texas Transportation Institute, Texas A&M University System.

Yoder, E., and Witczak, M. (1975). *Principles of pavement design*, Second edition, John Wiley & Sons, New York, 85-86.

Yuan, Y., and Wan, Z. L. (2002). “Prediction of cracking within early-age concrete due to thermal, drying and creep behavior.” *Cem. Concr. Res.*, 32 (7), 1053–1059.

Zhi, P., Xianyu, J., and Nanguo, J. (2010). "Theoretical Modeling of Concrete Moisture Diffusion Surface Factor." *Earth and Space 2010: Engineering, Science, Construction, and Operations in Challenging Environments, ASCE*, 3610-3616.

Zienkiewicz, O. C., Watson, M., and King, I. P. (1968). “A numerical method of viscoelastic stress analysis.” *Int. J. Mech. Sci.*, 10, 807–827.

Zollinger, D. G., Lee, S., Puccinelli, J., and Jackson, N. (2008). "LTPP computed parameter: Moisture content." Report No. FHWA-HRT-08-035, Federal Highway Administration, Washington, D.C.

Zollinger, D. G. (2013). "Evaluation of concrete curing effectiveness." *ACI Spring Convention 2013*. Minneapolis, MN.